Infrastructure exposure to shallow landslides in upper Gudbrandsdalen

Predicting the impact of climate change using the TRIGRS and RAMMS models

Øystein Grasdal

Master Thesis
Geohazards and Geomechanics
60 credits

Department of Geosciences
Faculty of Mathematics and Natural Sciences

UNIVERSITY OF OSLO

May 2022

Infrastructure exposure to shallow landslides in upper Gudbrandsdalen

Predicting the impact of climate change using the TRIGRS and RAMMS models

Master Thesis
Geohazards and Geomechanics
Øystein Grasdal

2022

Infrastructure exposure to shallow landslides in Upper Gudbrandsdalen; Predicting the impact of climate change using the TRIGRS and RAMMS models

Front: E6 and railway (right) in Rosten, Upper Gudbrandsdalen (photo: Øystein Grasdal)

Øystein Grasdal

http://www.duo.uio.no/

Print: Reprosentralen, Universitetet i Oslo

Abstract

Linear infrastructure networks, such as roads and railways, are of great social and economic importance in connecting the different regions of Norway. Landslides are cause of unexpected traffic flow disruptions of significant societal cost every year, costs which are expected to increase in the future with climatic and demographic changes. This study presents a combination of the two physically based models TRIGRS and RAMMS to produce a hazard chain from intense rainfall to subsequent landslide initiation and runout for a case study site in upper Gudbrandsdalen in South-Eastern Norway. By implementing a climate factor to the precipitation intensity, the climatic effect is traced through the hazard chain, successfully illustrating future change in infrastructure exposure to landslides. A significant increase of unstable slope areas with response to climate induced increase in precipitation intensity is observed for extreme rainfall events of 20-, 50-, 100- and 200-year return period. Similar results are observed for the runout simulations, where the climatic effect is seen as an increase in both runout volume and spatial distribution of flow. The runout analysis outlines the historically most active parts of the study area, with six out of seven documented landslides occurring within the modelled sections of exposed road and railway. The uncertainty of the model is well illustrated by a poor match to both release areas and runout footprint of the landslide events subject to calibration of the model. Model accuracy is limited due to shortcomings of data for the calibration event, input detail of physical characteristics of surface and sub-surface, as well as uncertainty related to the landslide release mechanisms. Although the practical utility of the coupled model is thereby limited in terms of accurate landslide prediction, the results illustrate how it may be utilized in remotely based assessments of hazard hot-spots and assist in selection of sites suitable for risk-reducing measures.

Preface

A sudden sense of déjà vu…

This master thesis is the final product of my Master's Degree in Geohazards and Geomechanics at the University of Oslo. It is written in collaboration with the Norwegian Geotechnical Institute (NGI) as a part of the NordicLink project.

First, I would like to thank my main supervisor, Graham Gilbert at NGI for guidance, help and feedback through this project. Thank you for guiding me in setting the framework for my project, for following up on my results, and for your feedback on my thesis. I also very much appreciate your effort in facilitating my stay at NGI. Although Covid worked against us, it worked out in the end, and it has been a great environment to finish my thesis in. Many thanks also to Anders Solheim at NGI for your genuine interest and follow-up on my project despite not having any official supervisory role. Thank you also for your feedback on my thesis, and for including me in the NordicLink project in the first place. I am also grateful to you both for giving me the opportunity to join the project field trip to Otta.

Thanks to Luca Piciullo at NGI for your helpful input on the TRIGRS model.

Thanks also to Jose Cepeda and the Department of Geosciences for engaging and interesting courses during the last two years. Thank you also to my co-students, especially Ole, Jørgen and Lars Haakon. The last two years would be much less memorable if it wasn't for the beers, coffee breaks and the disc golf.

Finally, thanks to my family and friends, and to Linda Williamsen in particular, for your encouragement, patience, and support through the last two years. This is my last Master's thesis, I promise.

Øystein Grasdal

Oslo, May 2022

Contents

List of figures

1 Introduction

Topographic and meteorological conditions make landslides one of the most challenging geohazards affecting societal infrastructure in Norway. Periods of extensive or intense rainfall often act as release mechanisms for landslides (NVE, 2013). Data from the Norwegian meteorological station network shows increasing trends for both intensity, duration and frequency of extreme precipitation events (Dyrrdal et al., 2011). With climate change, these trends are projected to continue in the future, thus also causing an increase in flood- and landslide events (Dyrrdal et al., 2012; Frauenfelder et al., 2017; Hanssen-Bauer et al., 2017). In addition to a greater number of hazard events, urban growth and expanding development of transportation networks cause an increased societal vulnerability to this natural hazard (NGI, 2014).

Linear infrastructure networks, such as roads and railways, are of great social and economic importance in connecting the different regions of Norway. In mountainous areas, this type of infrastructure is often located at the valley floor margin, running parallel to areas of both flood and landslide hazard. Consequently, on a national level, these hazards cause unexpected traffic flow disruptions of significant societal cost every year (Frauenfelder et al., 2017).

The transportation network, as most infrastructure, is designed in accordance with governing building regulations to ensure adequate safety against natural hazards (e.g. Frekhaug, 2020). Despite the prospect of a greater number of flood- and landslide events in the future, most new infrastructure are still designed based on hazard scenarios of present-day climate, mainly due to lack of climate adjusted hazard maps (Riksrevisjonen, 2022). Infrastructure designed for a given security class in today's climate may thus not meet the requirements for the same security class in the future.

Studies on natural hazards is crucial to understand the complex interplay of different factors controlling spatial and temporal distribution of hazards. A better understanding of hazard response to different climatic scenarios thus enables appropriate development and safeguarding measures to reduce the societal cost related to network disruptions by increasing the infrastructure reliability and safety of network users.

1.1 The NordicLink project

The research activities and outcomes of this study contribute to the NordicLink project. NordicLink is a collaborative research project between the Norwegian Geotechnical institute (NGI), the Finnish Meteorological Institute (FMI) and Chalmers Institute of Technology (Sweden). By studying effects from extreme weather and the Nordic geohazards towards linear infrastructure, the project aims to improve security and resilience along the Nordic infrastructure network. In addition to the research institutions, organizing and ensuring operation of the project, several stakeholders are involved in identification of problem areas, research needs and the ultimate implementation of the project outcome. These user partners oversee development and maintenance of transportation networks such as roads and railway. The project is funded by NordForsk under the Nordic Societal Security Program.

With differences in topographic and climatic conditions, the relevant geohazards vary greatly across the Nordic countries. With these differences in relevant hazards, different regions will also see different hazard responses to climate change and see the need of uniquely adapted mitigative measures. To capture the multidisciplinary aspects of the research problem, the project is organized in a set of work packages, each assessing topics such as hazard identification, active mitigation, risk reduction and use of nature-based solutions. Relevant case study sites are selected to capture the variation in climate- and hazard scenarios across the Nordic countries. In Norway, the selected case study sites are Eidsvoll, Trollstigen and Gudbrandsdalen North (Otta region), each with their own sets of site-specific objectives. For the Otta region, the case-site objectives are:

1. Identification of challenges and locations where linear infrastructure is most frequently exposed to hazards
2. Assess the hazard and estimate probability of occurrence affecting the transportation network
3. Assess risk through quantification of consequences from different hazards. Including both direct damage and repair cost as well as societal cost caused by infrastructure down-time and possible detour routes.
4. Development of sustainable mitigation strategies, with special focus on nature-based solutions and early warning systems.
5. Assess change in hazard- and risk scenarios with climate change and demographic change.

More information on the NordicLink project, the different work packages and case sites can be found on the project home page: nordiclink.no.

1.2 Thesis aim and objectives

The NordicLink project is of both multidisciplinary and multiscale nature. This thesis is one of two parallel studies (Holt, 2022) which assess different geohazard issues for the Otta case study site and contributes to the NordicLink work package 2 . This work package has the overall objective of improving hazard identification and assess how hazard and risk will change in response to future climate and demographic conditions. More specifically, this project is aimed towards case specific objectives 1, 2 and 5 described above, with focus on shallow landslide hazards on a local scale.

This study presents a combination of two physically based models TRIGRS and RAMMS to evaluate both slope stability and possible run-out, thus addressing both hazard and possible consequence scenarios. The TRIGRS model allows for dynamic change in slope stability from hourly changes in rainfall intensity, and the subsequent transport and deposition of the failed slope material is then simulated in RAMMS.

Currently, Zhou et al. (2022) is the only published study using a similar coupling of TRIGRS and RAMMS. With a 76.77% accuracy in simulating debris flows for a case study in the Gansu Province of China, they demonstrated how this coupled model is a useful contribution to the established prediction methods for landslide and debris flow modelling with its remote implementation and the practical value of hour-by-hour scenario development. In contrast to Zhou et al. (2022), this study intends to utilize the coupled model to investigate landslide scenario development of a multi-decadal scale by implementing a climate factor to the precipitation intensity of events with specific statistical return periods (Figure 1.1).

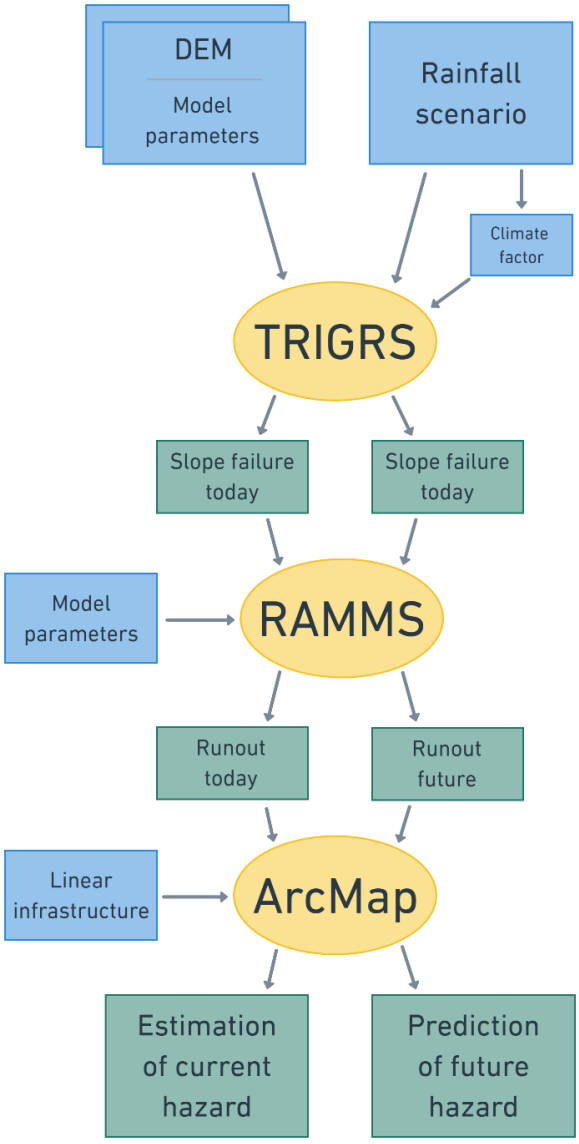

Figure 1.1 - Streamlined workflow for the coupling of hazard models in the present study

With this new approach to a relatively unestablished method, the main objectives of this thesis are to:

1. Produce a realistic hazard chain from intense rainfall scenarios to subsequent landslide initiation and runout.
2. Evaluate the development in infrastructure vulnerability to landslide hazard towards the end of the 21st century.
3. Assess the TRIGRS-RAMMS coupled model's performance in hazard prediction.

In addition to the primary objectives above, there are several sub-questions which will also be assessed:

- What are the specific limitations to TRIGRS, RAMMS and the coupled model?
- What is the quality of the data-coverage in Otta - Is the TRIGRS-RAMMS coupled method suitable in this area?
- What are the general uncertainties related to physically based modelling?
- What level of accuracy is feasible for a remotely based hazard analysis based on open access data?
- How does this type of hazard assessment contribute to the improvement of safety and reliability along the transportation network?

1.3 Otta area description

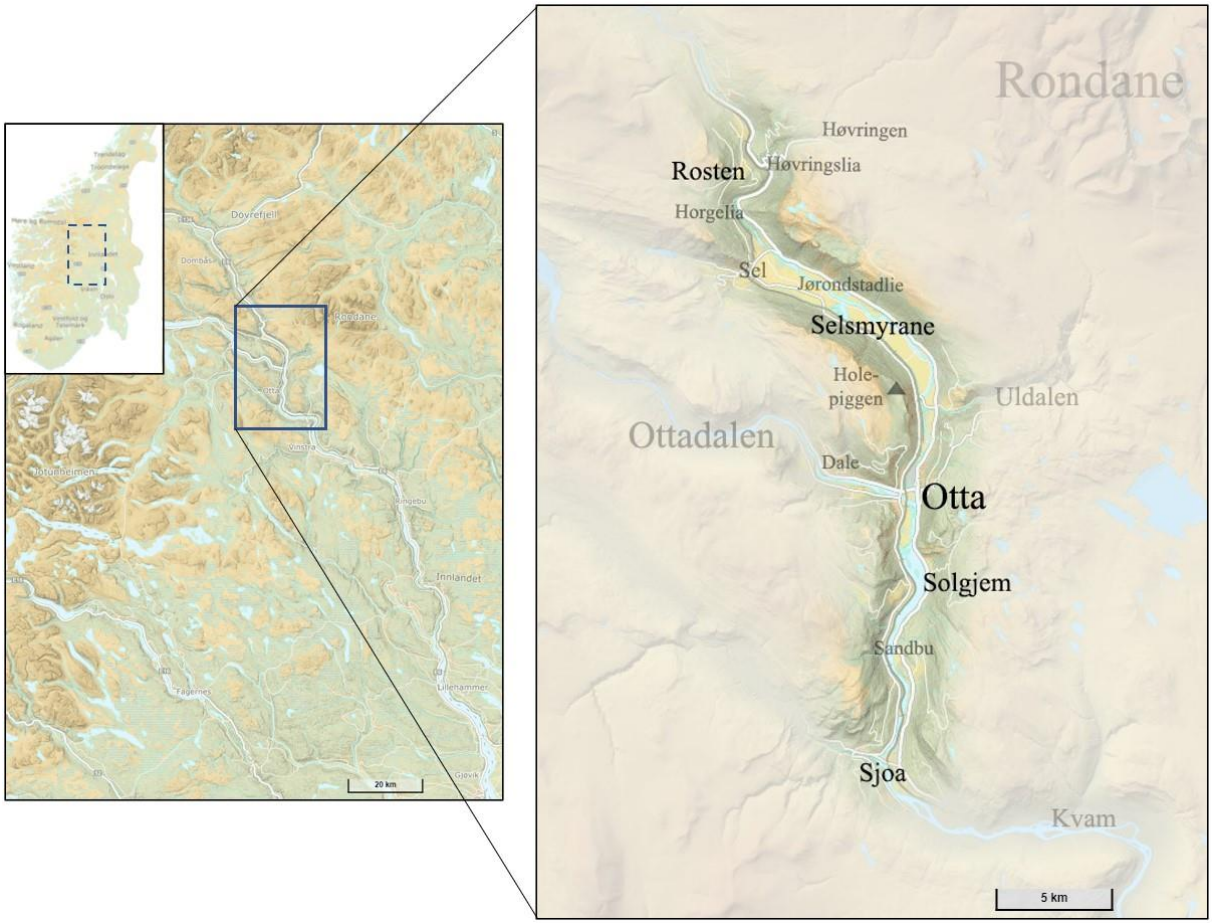

Figure 1.2 - NordicLink study area. The Otta area sits in northern Gudbrandsdalen in central eastern Norway

The NordicLink study area in Otta is situated in the northern part of Gudbrandsdalen, a northwest-southeast trending valley in the center of southern Norway (Figure 1.2). The area consists of several large glacial-cut valleys in an otherwise plateau-like mountainous area. This mountain plateau has a gently undulating topography with both glacially polished terrain features and regional alpine terrain such as in Rondane mountain area. The valley floor of Gudbrandsdalen is relatively flat with only 20 meters of elevation difference in the 23km distance from Sjoa to Rosten. The town of Otta lies in the middle of the study area, at 290 m.a.s.l. The town sits on the floodplain in the junction between Otta and Gudbrandsdalslågen rivers (henceforth Ottaelva and Lågen).

The region of Innlandet and former Oppdal county has a continental climate with dry and warm summers, and cold winters (Figure 1.3). The temperatures in the valley range from -40°C in cold winter days, to >30°C in summer. The part of the region in which northern Gudbrandsdalen is situated is one of the driest parts of Norway with approximately 500 mm of yearly average precipitation (Hisdal et al., 2017; MET., 2022a).

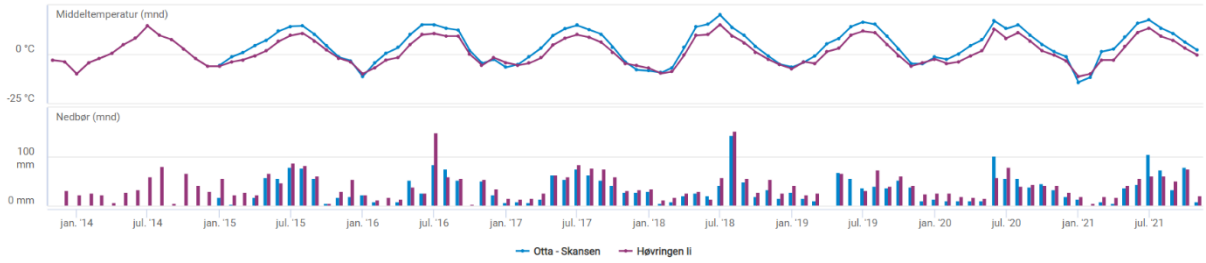

Figure 1.3 - Air temperature and precipitation history for Otta - Skansen and Høvringen weather stations from 2014 to September 2021 (MET., 2022a)

Except for the town of Otta, the valleys in the study area are dominantly farmland and forests. There are also long traditions of mining phyllite- and mica slates in and around Otta, due to the vast abundance of phyllite bedrock (Bryhni & Askheim, 2021). In addition to arkosic sandstone, this is the dominant rock type within the study area (NGU, 2022). The area has also grown to be a popular recreational destination with several areas regulated for cabin developments at the foot of the Rondane mountain region.

Slopes are covered in till of varying thickness and compaction. The till composition is controlled by upslope rock types as well as the rock type in the area where the till rests. Due to the abundant phyllites in the area, the tills in the area are also rich in clay, which may again affect slope stability (further described in 3.1.3 – Controlling factors: Material properties of

soil). The lower parts of the slopes are dominated by fans (Follestad & Bergstrøm, 2004). Gudbrandsdalen saw a major terrain changing event in 1789. Late spring rapid snowmelt accompanied by multiple days of heavy rainfall caused the Storofsen flood and initiated extensive sliding in the mountain slopes (Roald, 2013). Many ravines seen in the terrain today is likely to originate from this event.

1.3.1 ROSTEN Study area

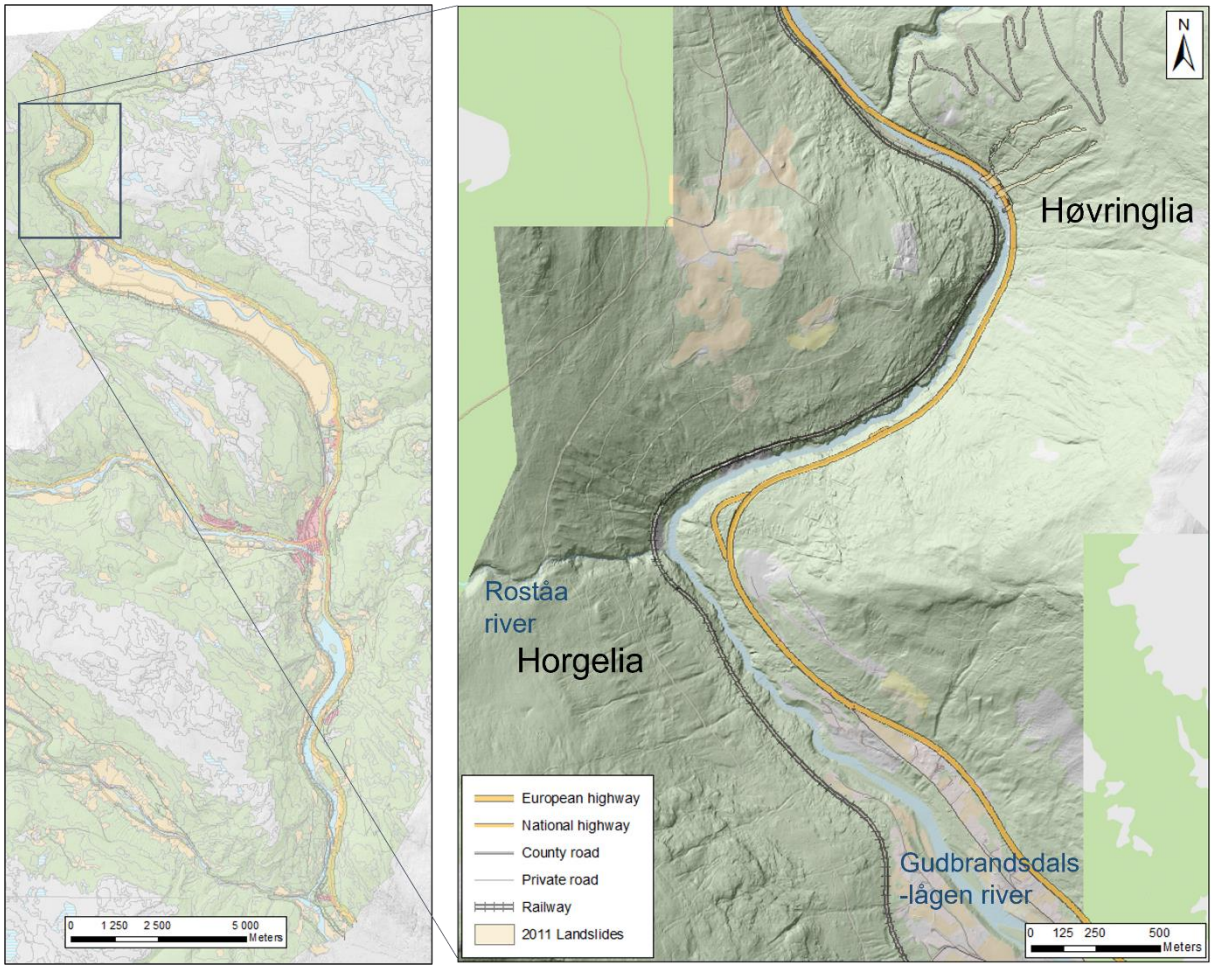

Figure 1.4 - The Rosten case study site sits in the northernmost part of the Otta area which is subject to the NordicLink study.

To model the climate induced changes in landslide hazard in the Otta area, it is necessary to first calibrate the model parameters to realistically simulate a documented landslide event in the area. 2011 and 2013 saw several landslide problem areas around Otta as consequence of extreme precipitation events. One specific area which proved problematic for both road and

Figure 1.5 - Runout tracks from the three landslides in Høvringslia, June 10th, 2011. Photo from Walberg & Devoli (2014).

railway in these events is Rosten (Figure 1.4). The national landslide database (henceforth NLDB) shows landslides on both sides of the valley in this area, and especially on the slopes Høvringslia and Horgelia. This has been identified as a problem area by road authorities, not only because its active slope processes, but also because of the great consequences of road closure in this section of E6. Unlike other parts of the Otta area, Rosten is a particularly vulnerable road section due to its absolute lack of alternative local routes. This could potentially cause rerouting of more than hundred kilometers and several hours detour in some cases.

In June 2011, locally intense rainfall led to several debris flows on both sides of the valley in Rosten. Of these, the most extensive debris flows occurred in Høvringslia. Within a small area, three separate slope failures caused debris flows which crossed E6 at the intersection point with county road fv437 to Høvringen (Figure 1.5). These are not registered in the NLDB, and little information can be found of the exact timing of the three failures (Figure 1.6). These are, however, well documented in digital map data in terms of spatial extent and consequences at the road and are therefore well suited as reference landslides for model calibration. Due to the recent landslide activity in the area and the relatively severe consequences in case of an event, Rosten is a particularly interesting area for a study on potential climate induced change in landslide hazard scenario. Rosten is therefore selected as a sub-site for the slope stability analysis and landslide runout simulation in this study.

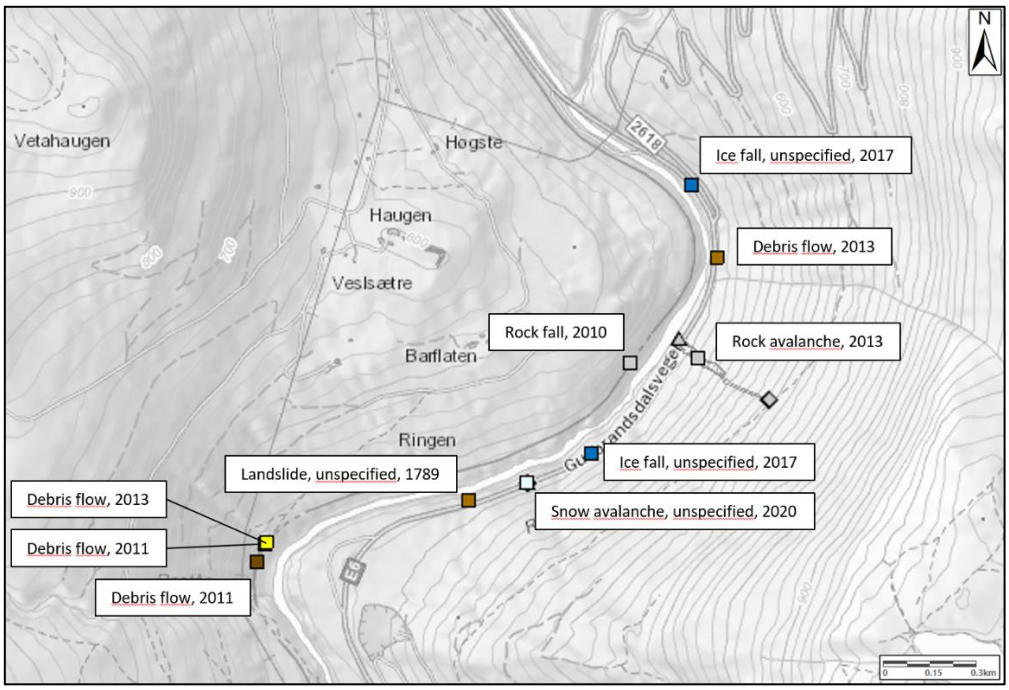

Figure 1.6 - Map of currently registered events in Rosten from the National Landslide Data Base (NLDB). Data from NVE (2022).

1.4 Linear Infrastructure in Sel Municipality

The term ‘linear infrastructure’ refers to the part of the infrastructure serving a purpose for transportation and/or distribution of goods, and power. In and around Otta, this applies to the road network, railway, and power grid, of which particularly the two former are of interest in this study (Figure 1.7).

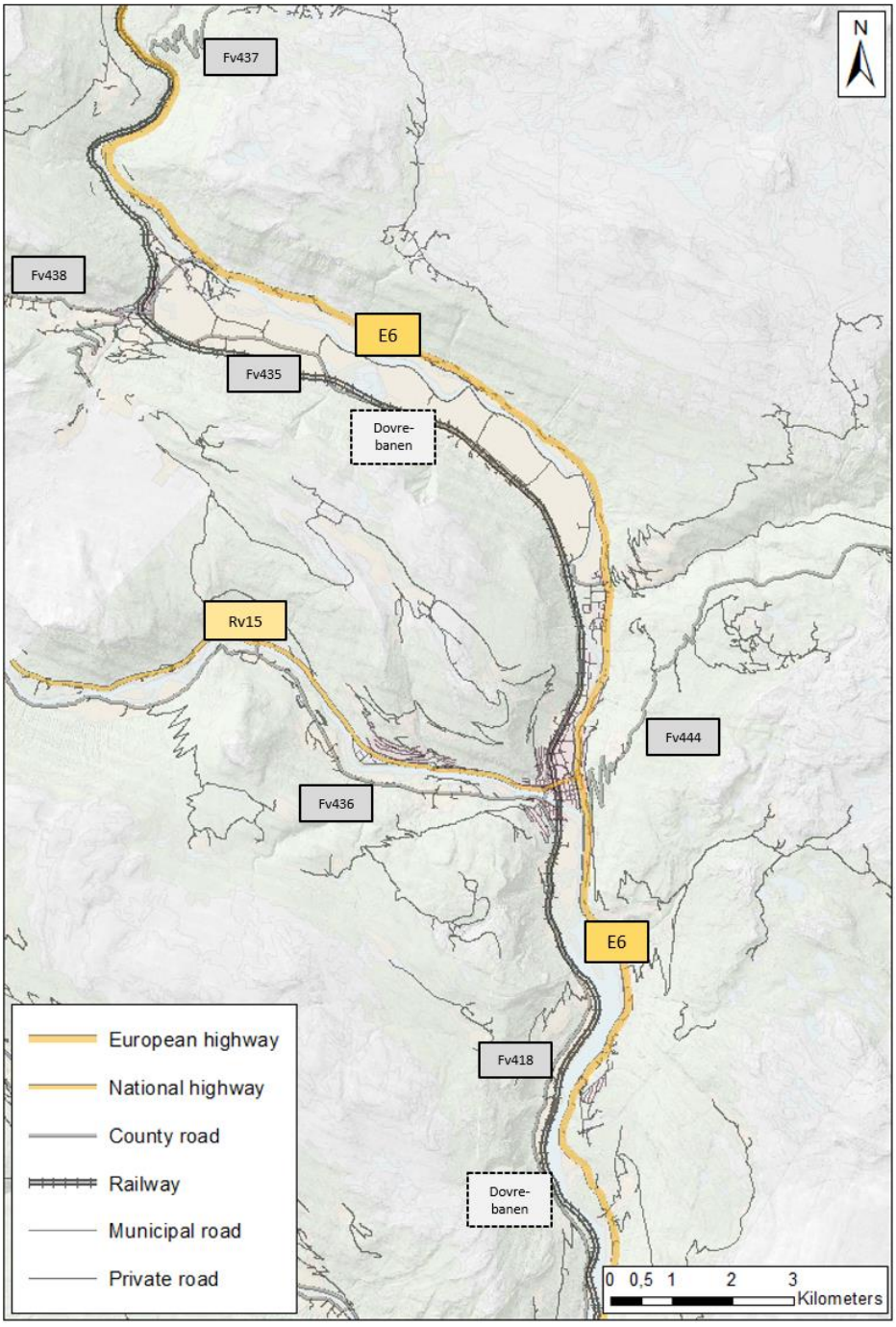

Figure 1.7 - Map view of the transportation network of the Otta area. Roads below county road level is not tagged with their ID.

1.4.1 Road network

The road network can be sub-divided into a hierarchy based on their relative importance to the national transportation network. European highway E6 is the most important road in the valley in terms of closure consequences. Running almost the entire length of Norway and passing into the south of Sweden, this is one of the most important traffic routes connecting Scandinavia to Europe.

E6 meets National highway 15 (Rv15) in the town of Otta. Rv15 is a major east-west connection running up the Otta valley and over Strynefjellet, ending up in Stryn in the northern part of west Norway.

County roads runs on the opposite side of the valley in both Gudbrandsdalen- and the Otta valley. As E6 and Rv15 are the common routes for transportation of goods, the county roads are scaled to support less traffic capacity and are primarily for smaller vehicles. During local traffic flow disruptions on E6 and RV15, these roads can to a certain extent be used as detour routes.

European highways and national highways are operated and maintained by the state through the national road authorities (Statens Vegvesen) and the state-owned enterprise Nye Veier. In addition to the highways, roads of a local character are separated into county roads, municipal roads, private roads, and forest roads. These are operated and maintained below a national level by the county administration, municipalities, or private operators, respectively.

Currently, plans for a new E6 in northern Gudbrandsdalen is under development by Nye Veier, aiming to facilitate an increase in traffic, better road safety and reduce travel time (Nye Veier, 2021). Currently, the northernmost section of the new E6 is planned between Sjoa and Otta. There are no current plans for improvement of E6 through Rosten.

1.4.2 Railway

The railway running through Otta and the northern Gudbrandsdalen is a part of the national railway connecting the north and south of Norway. The stretch of railway from Eidsvoll to Trondheim is called Dovrebanen, named from the mountain pass of Dovrefjell just north of the

Otta study area. The railway was opened in 1921 and electrified in 1970, and now serves as the main route by train for both passenger and goods transport between Trondheim and Oslo. The railway crosses from the east side of Lågen close to Sjoa and run on the west side of the river through the study area. The railway track is raised on a gravel embankment to limit the disruption and damage from floods. Frequent culverts within the embankment are designed to drain streams, rivers, and surface runoff from the upslope terrain to the river. In the narrow part of Rosten, the railway runs in a cliff-cut with bolts and nets mitigating rockfall onto the tracks. Most registered landslide events are located in the southern part of the study area, between Otta and Sjoa. These are almost exclusively categorized as debris flows (chapter ??,??), leaving water, rock, and debris on the tracks, and occasionally causing wash-out of the railway embankment (Figure 1.8).

Figure 1.8 - Railway prone to flooding and debris flow in Sandbu, south of Otta. White gravel in the middle of the picture indicates a repaired section after embankment washout in 2013. (Photo: Øystein Grasdal)

The Norwegian railway network is run and maintained by the state-owned enterprise Bane Nor. The southern part of Dovrebanen is integrated in a Bane Nor project Intercity, a track network on which they aim to provide a better core structure between the central cities in eastern Norway and meet the demand from the increased population in these areas (Bane Nor, 2015). As a part of this investment, and to facilitate an increase in transportation of goods and passengers to Trondheim, several parts of Dovrebanen will see upgrades and improvements during the next decade (Bane Nor, 2016). Disruptions to railway traffic from natural hazards in Gudbrandsdalen leads to large extra costs for Bane Nor, freight operators and passengers. Estimations of societal cost for the 2013 flood and landslide events for the railway alone was calculated to 380MNOK (Siedler, 2015). During such events, with prolonged periods of closure and delays, most cargo is re-distributed to the road network by trailers. Not only is this less effective and more costly for the freight operators, but it also has repercussions in form of additional load to the road network as well as increased emissions and local air pollution. An

alternative track between Hamar and Trondheim is Rørosbanen. This track runs through less challenging terrain, but has restricted capacity due to few stations, shortened sections of double track where trains can pass each other, and manual operation system in parts of its length. Rørosbanen is also diesel run, and re-routing of traffic from Dovrebanen would therefore cause an increase in CO2 emissions for the transport. Electrification of Rørosbanen is currently under assessment by the parliament (BaneNor, 2013).

1.4.3 Power grid

Power grid is the third important feature of linear infrastructure in northern Gudbrandsdalen. However, except for a short regional connection between two transformation stations in Otta center, the power grid in the study area consists exclusively of local distribution lines. The grid has powerlines running on both sides of the valley, with distribution lines to residential outliers and side valleys. The power lines are elevated, supported by 8-10-meter-high poles with variable spacing (typically 50-150m). This limits the contact points between the power grid and the ground, thus also reducing the vulnerability to landslides significantly (Figure 1.9). Vulnerability can be even further reduced by placing the support poles on topographic highs with natural deflection to debris flows.

Figure 1.9 - Powerlines of the distribution network in Solhjem. Lines are carried by wooden poles 8-10 meters above ground, limiting the power line vulnerability from landslide hazards (Photo: Øystein Grasdal).

With its limited vulnerability to landslides and its relatively low consequence in terms of damage related cost and societal cost, the power grid is paid no further attention in this study.

The regional and distribution power grid in Sel municipality is owned and maintained by the system operator AS Eidefoss.

2 Geohazards in the Otta region

The following chapter sets the framework of this thesis in terms of understanding the different geohazards in the study area and how they interact with linear infrastructure. A presentation of past studies in the area is also given, with emphasis on relevant work with focus on shallow landslides.

2.1 Geohazards in the study area

To fully understand the challenges and vulnerability of the linear infrastructure in this area, it is necessary to have a closer look at the different hazards which pose a threat to its functionality. There are some considerable differences in Norwegian- and commonly used international terminology. The following section will describe the relevant geohazards as they will be referred to in this study, and their occurrence in and around the Otta area.

2.1.1 Landslides

Landslides is one of the hazards which pose the largest threat for loss of life, property and functionality of infrastructure in upper Gudbrandsdalen, and is thus also the hazard in focus in this study. Landslide is a general term used to describe the movement of soil, rock and organic debris under the effects of gravity (Highland & Bobrowsky, 2008). Sub-types of landslides are often defined from the type of movement and the material involved.

Debris slide / debris flow

Due to the steep valley slopes with extensive till cover, shallow landslides are the most occurring type of landslides in the Otta area. Such landslides are classified as debris slides (norsk; jordskred) and debris flows (norsk; flomskred). These are similar in that a failure in the soil occur in steep terrain, resulting in a transportation of debris down a slope. It is common to differentiate the two by the conditions in their initiation zone, as well in the characteristics of their depositional morphologies (Figure 2.1). Whereas debris slides occur in slopes with no defined rivers and waterways, debris flows are channelized, occurring in well-defined rivers and gullies (Kristensen et al., 2015). Due to its great water content, a debris flow will have a longer runout zone where the coarsest debris is deposited at the base of the slope and finer

material is carried far out on the valley floor. A debris slide can have varying water content, and thus often have a steeper depositional fan and shorter runout zone than the debris flows (NVE, 2013). Both have the potential to cause devastation along their paths.

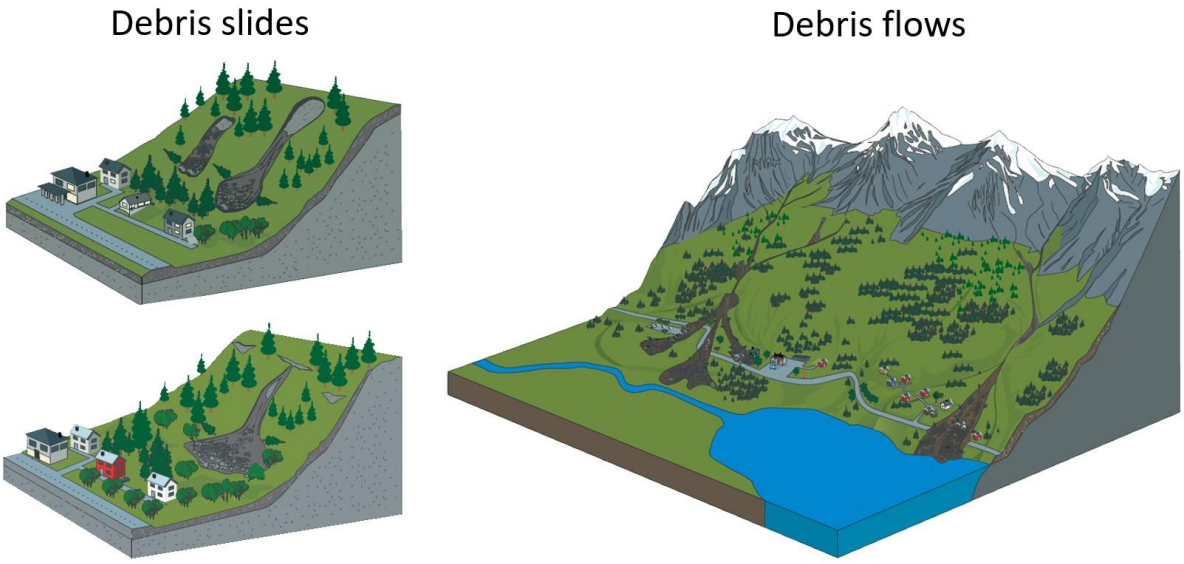

Figure 2.1 - Idealized conceptual morphology of debris slides and debris flows. Debris slide morphology include both regular straight runout (upper) and cone shaped runout (lower). Slightly modified from NVE (2013).

Sletten and Blikra (2007) investigated stratigraphic evolution of the colluvial fans in upper Gudbrandsdalen to study the landslide activity through the Holocene. With use of radiocarbon dating, they found a great amount of activity at different distinct periods with more than 60% of the stratigraphic landslide beds older than 5000 cal yr BP. The youngest laterally extensive landslide event they identified is known as the Storofsen event. This occurred in 1789 and is an important geohazard event in eastern Norway, not only as the greatest known flood and landslide event, but also because it was documented in historical sources. The event was caused by a combination of abnormally great amounts of snow in the winter, an unusually late spring thaw, and following warm weather accompanied by three extensive days of extreme rainfall (Roald, 2013). Extensive landslide activity caused great devastation, and the of the 155 farms in Vågå/Sel municipal area, 120 either had damage or was destroyed by landslides (Furseth, 2006; Walberg & Devoli, 2014). One particularly large landslide in Rosten caused damming of Lågen. When the dam eventually broke, a slurry of water, mud and debris caused devastation in the upper part of Selsmyrane (Roald, 2013).

During the last two decades, several events of significant snowmelt and/or heavy rainfall has caused multiple-landslide events, of which debris flows has been most common.

Spring/summer landslide events of 2008, 2011 and 2013 are especially noteworthy due to their well-documented respective hydrometeorological conditions, spatial and temporal occurrence, and their impact on infrastructure.

Rock avalanche

A rock avalanche (norsk; steinskred) differs from a debris slide in that the moving mass consists predominantly of rock. In Norwegian terminology, a rock avalanche is classified based on the total volume of material. For the landslide to be defined as a rock avalanche, it must originate from failure in bedrock and result in transportation of a rock and debris volume of between 100 and 100 000 cubic meters (Devoli et al., 2011). Considering commonly used international classification by movement from Varnes (1978), these rock avalanches typically start out as rock fall, topple or slides, and develops into an avalanche of more complex motion as it incorporate more material during transportation downslope (Kristensen et al., 2015).

Not many rock avalanches are registered in the Otta area. However, this type of landslide has a large potential of devastation, and a few events with large impacts to infrastructure has been seen in Otta during the last century. A few mentionable events happened in 1905, 1972, 1984 and 2013. Furseth (2006) describes how in 1905, a rock avalanche hit in the northern part of what is today the northern part of Otta town centre, wrecking a farmhouse and causing minor damage to a few other houses. Both events of 1972 and 1984 occurred in Blekalia, the west facing valley slope south-east of Otta Town center. Both reached the E6 highway, and the latter destroyed a house in its track, luckily without causing any fatalities (Furseth, 2006). The most recent event happened in 2013 in Rosten, a few kilometers north of Otta (Figure 2.2). A major block came loose, triggering more rocks and debris downslope. The avalanche travelled across E6, killing one person in his car. The avalanche happened during a dry period in summer, and field investigations by NGI and the road authorities concluded that the avalanche was caused by weakening due to lasting frost weathering (Beyer-Olsen & Johansen, 2013).

Figure 2.2 - 2013 fatal rock avalanche in Rosten (Nordby et al., 2013)

Rockfall

A rockfall, like a rock avalanche, is caused by failure and following transportation of rocks from bedrock outcrops. This often describe the falling motion of the rocks in international literature following Varnes (1978). In Norwegian terminology, however, this is regarded as transportation of a total volume of rock less than 100 m^3 (Devoli et al., 2011). The cause of rockfall is related to the mechanical weathering of bedrock by frost, vegetation (e.g., root growth) and water. When the rocks are loosened, their stability depends on the slope and other rocks holding them in place. Rockfall often occur during heavy precipitation, or in periods when temperature fluctuates around 0°C, triggering failure due to repeated frost wedging (NGI, 2014). Slopes with repetitive rockfall tend to form talus cones - a steep, cone-shaped fan. (Blikra & Nemec, 1998).

In some parts of Gudbrandsdalen where cliffs of bedrock are exposed in steep areas, fresh weathering surfaces and talus fans with little or no vegetation indicate sites of active rockfall. Rock fall is a considerable hazard in the Otta region, especially Jørondstadlia north of Selsmyrene, and the slope beneath Holepiggen 3 kilometers north of Otta (Figure 2.3). From the latter, several rocks have been registered reaching Selsvegen, an alternative local route to E6.

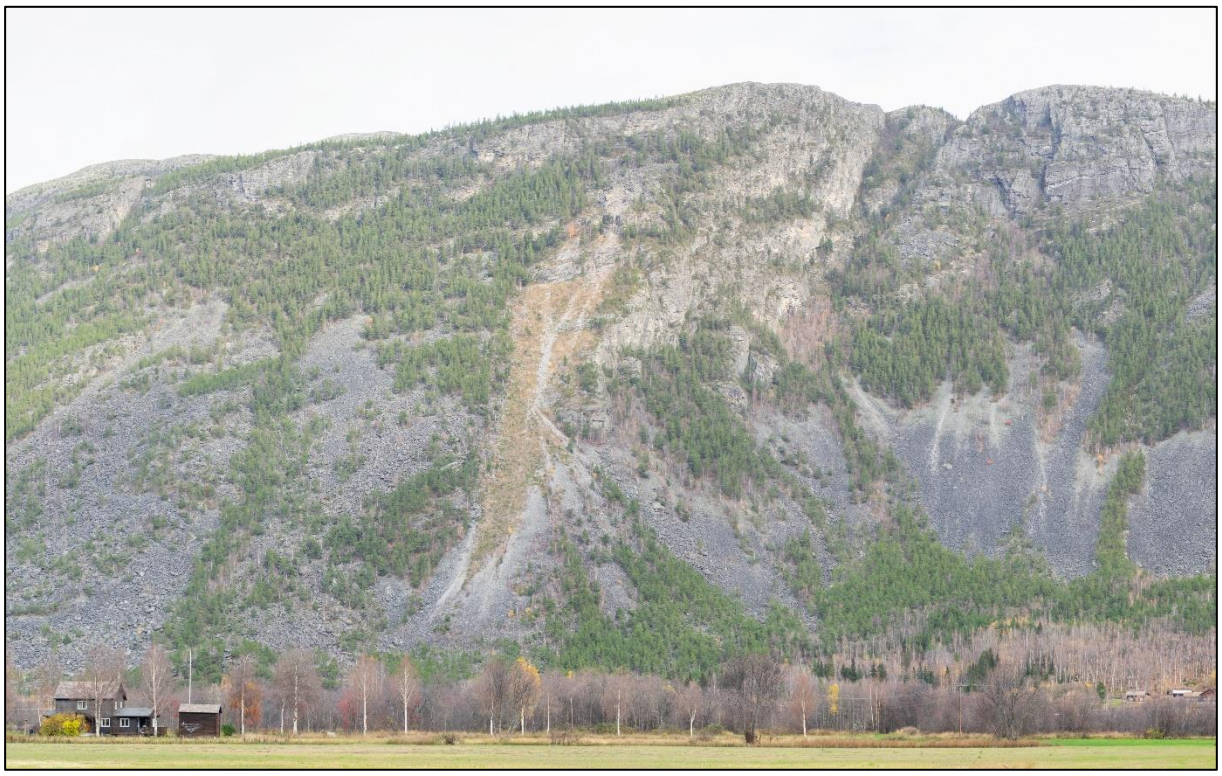

Figure 2.3 - Rockfall is the dominant slope process in Jørondstadlia, the north-eastern valley side of Selsmyrane (Photo: Øystein Grasdal).

2.1.2 Floods

Flood is a significant hydrometeorological hazard in eastern Norway. Even though Otta lies in one of the driest parts of Norway, the Lågen and Ottaelva rivers drains large catchments of which large parts have significantly more precipitation. As much of the catchments also lies at relatively high altitude, a primary cause of major floods in these rivers is snowmelt during the spring. The catchment area of Ottaelva lies to the west of Gudbrandsdalen, reaching into parts of western Norway which receives significantly more precipitation compared to the areas surrounding Otta. Of the two rivers in the study area, Ottaelva is therefore the one with the greatest water discharge during peak flood. This catchment is also at higher elevation compared to the eastern and northern catchments of Lågen, resulting in a somewhat later melt season and a later flood peak. Whereas Lågen usually flood in early June, Ottaelva usually floods in late June (Høydal, 2002).

During the event of Storofsen, the eastern tributary river Ula between Otta and Selsmyrane was flooded as well, and due to extensive debris slides in this catchment, Ula brought great amounts of sediments into Gudbrandsdalen. So much in fact, that the deposition of the sediments shifted

Lågen from the east to the western margin of the fluvial plain. As the farmlands of Selsmyrane lies up-stream of this alluvial fan, these farmlands often became fully submerged during floods during the 19th century. To prevent the deposition of sediments from Ula to raise the water level of the river and cause a permanent lake in Selsmyrane, a catch dam was built in Uldalen in 1879 (Norsk Skogmuseum, n.d.). Even though the riverbed of Lågen was later lowered to enable more consistent conditions for farming again, large flood events still put significant parts of Selsmyrane under water (Figure 2.4).

Figure 2.4 - Selsmyrane between Otta and Rosten after flooding in 1995 (Norsk Skogmuseum, n.d.)

2.1.3 Snow avalanches

The term snow avalanche describes a mass of wet or dry snow, with a rapid movement down a slope (Kristensen et al., 2015). This can further be subdivided into powder avalanches and slab avalanches dependent on their characteristics at failure and motion during transport. Powder avalanches typically start in a point and spreads out downslope in a turbulent cloud. Slab avalanches typically originate from a failure in a weak layer, resulting in a well-defined fracture line in the release area, and an initial sliding motion of the slab. The slab may then gradually break up down-slope and transition into a flow like motion dependent on the size of avalanche and the terrain it moves trough.

In general, registrations in NLDB suggests that snow avalanches cause few problems in and around Otta (NVE, 2022). Of registered events in the main study area, most of the avalanche

events have occurred in a small area in the southern margin of Selsmyrane. At least four different events are registered of which three have reached Selsvegen and one have reached the railway. The database also shows a few instances close to Dale in 2008, 2009 and 2015, but these registrations lack information, and from field inspection in the area, these registrations seem misplaced. The explanation for relative few avalanche events in the study area could be related to the low amounts of precipitation in the area and thus not enough snow to produce significant avalanches, and that the snow is well stabilized by the vegetation in the slopes.

2.2 Past studies and research projects in the Otta area

The first important work within landslide hazard problematics which should be mentioned is the comprehensive overview on historic landslides by Furseth (2006). This work is not so much a study as it is a register, but nevertheless serve an important purpose as a source on historic events, their location, time of occurrence and registered damage to infrastructure.

Quaternary deposit map of Otta reveals the high landslide activity during the Holocene (Follestad & Bergstrøm, 2004). When Sletten and Blikra (2007) investigated the age of beds in colluviums in upper Gudbrandsdalen, they found that there has been alternating periods of relatively high and low landslide activity. They concluded that this is likely due to different climatic conditions during the Holocene, and thus a varying relative importance of rapid snowmelt from solar radiation and heavy precipitation as triggering cause of landslides.

2.2.1 GeoExtreme

The first comprehensive study to link climate change to landslide activity in the northern Gudbrandsdalen area was the multidisciplinary GeoExtreme collaboration between the leading instances in climate- and geohazard studies in Norway (Jaedicke et al., 2008). Although this study aimed to cover entire Norway, four case study sites were chosen for modelling climatic effects on different geohazards as proof of concept. To model the climatic effect on stability conditions for shallow landslides, Otta was chosen as case study site. By coupling hydrological modelling with infinite slope stability analysis for present and future climate scenarios, they aimed to identify the relative change in stability conditions. Jaedicke et al., (2008) modelled an

increase of 20% in the precipitation intensity for 1-day extreme precipitation events according to NVE's precipitation estimates of Skaugen et al. (2002). Preliminary results from this showed statistically significant change in stability and increased probability of failure of up to 25% in certain areas (Figure 2.5).

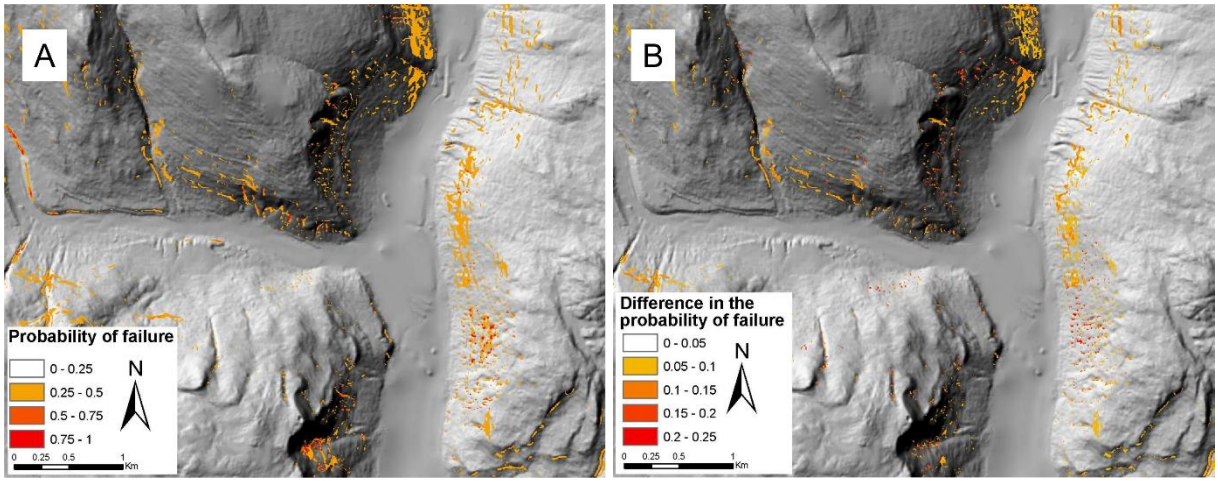

Figure 2.5 - Stability assessment for present and future climate for slopes surrounding the town of Otta. Figure A show present day probability of failure while figure B indicate the increase in probability of failure as response to a 20% increase in precipitation intensity (Slightly modified from Jaedicke et al., 2008)

However, Melchiorre and Frattini (2012), also as part of the GeoExtreme project, concluded that an accurate quantification of change in stability conditions was not feasible. In this study, new precipitation thresholds were derived at fixed return periods by assessing 11 different climate scenarios. They also accounted for antecedent conditions by adding appropriate levels of 4-day precipitation prior to the extreme event. Although the models showed changes in stability when comparing present vs future models, the total uncertainty related to the hydrological modelling and slope stability model parameters exceeded the effect of the climate change. Especially, they found that the topographic data such as hydraulic contributing area and slope angle, as well as the amount of precipitation was the main contributors to the total uncertainty. Factors such as soil cohesion, friction angle, hydraulic conductivity and diffusivity was less influential. The GeoExtreme project suggested a better adaption of infrastructure to present and future landslide risk in Norway. In the Otta case study, however, it concluded with somewhat ambiguous results on the quantified change in slope stability.

2.2.2 InfraRisk 2010-2013

In 2010 to 2013, NGI with partners carried out an interdisciplinary project called “Impact of extreme weather events on infrastructure in Norway (InfraRisk)” (Frauenfelder et al., 2017). The main goal of the project was to investigate the relationship between climate change and the occurrence, distribution, and intensity of extreme weather events in order to evaluate risk of landslide- and avalanche hazards to the Norwegian transportation network.

Of weather variables controlling triggering of landslides and avalanches in Norway, intense and/or periods of prolonged precipitation was given most focus in this study. Trend analysis of historic data with respect to frequency and intensity was carried out to assess likely future development of these variables. Much in accordance with the conclusions from the GeoExtreme project the results showed great spatial variability, with most pronounced trends in the western and northern parts of Norway, and less pronounced to insignificant trends for parts of central- and eastern Norway. In general, however, the trends showed how moderate to heavy precipitation events have occurred more and more often and with increasing intensity during the last fifty years. Projecting these trends to the future, an increase in frequency and intensity of heavy precipitation events in the next fifty to hundred years can be expected, although there are large uncertainties to the spatial distribution related to different climate scenarios (Frauenfelder et al., 2017).

The other aspect of this project aimed to quantify the risk of landslides related to these extreme weather events based on vulnerability and socio-economic impact of different elements at risk in the transportation network. To do this, a tool was developed to capture frequency of road and railway closure, the durability and cost of closure, clean-up and reparation of damages, combined with conventional hazard map data describing type of hazard and expected recurrence interval. The infrastructure elements at risk were given attributes describing type of object, amount of traffic and expected detour transportation time in case of closure. This tool is applicable at multiple scales, and to prove its functionality the model was used to quantify the total risk of Norway, as well as in small scale for a case study site in Otta.

For the case study, the area around Otta town center was analyzed (Figure 2.6). The result showed how this area can expect in average 2.2 events, causing 1 closure of 10.2 hours every 3 years. Based on the probability of impact at different types of roads and railway with different respective cost of traffic delay, traffic flow and potential reparations, the yearly cost related to

landslide risk was estimated at 280 000 NOK each year in 2005. Debris flow was found to be the most frequent event to the infrastructure network, causing most of the network disruptions and account for approximately 75% of the total cost. The event frequency was found to be largest in municipal- and private roads. As there are no data for traffic flow on these roads, the cost related to events in these roads only include clean-up and reparations. The greatest economic consequences were however not related to these direct costs of clean-up and damage, but to closure of the main transportation routes E6 and RV 15, as well as the railway. Uncertainty to the risk estimates is +/-50% due to the separate uncertainties related to both event frequency and vulnerability estimates.

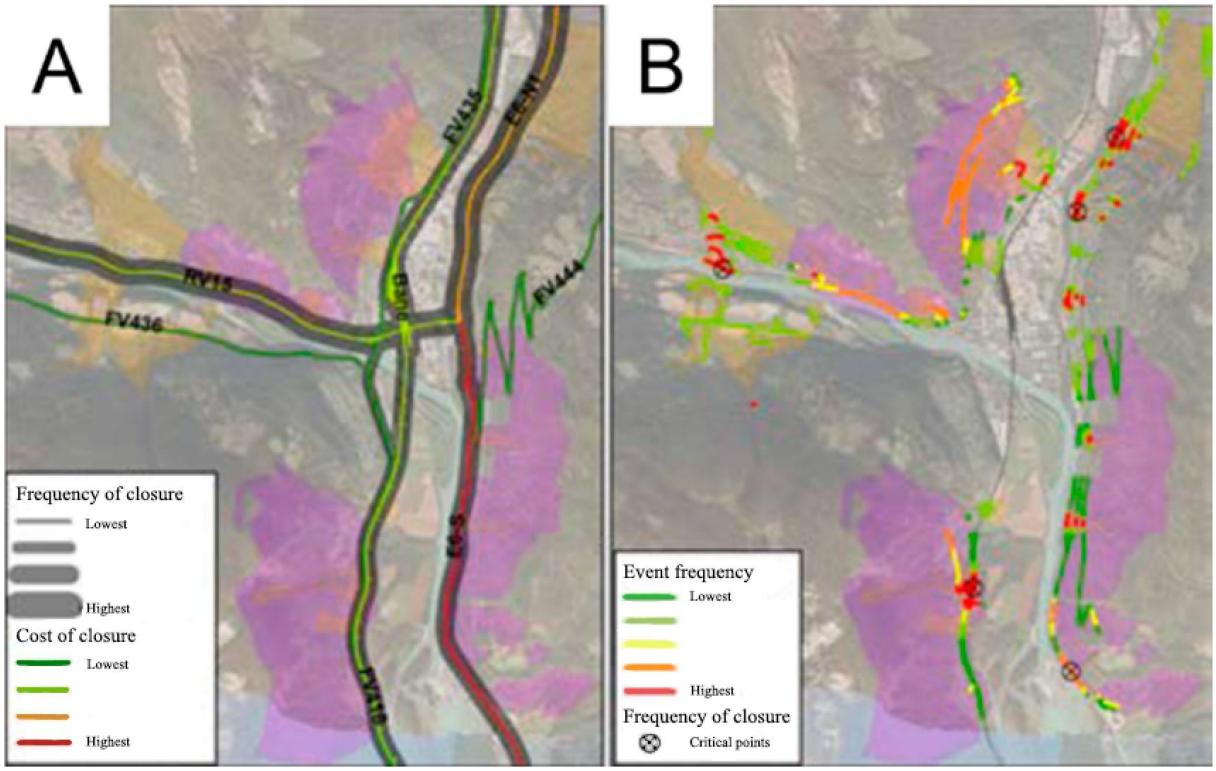

Figure 2.6 - A: Expected annual closing frequency and closing cost for the most important stretches in the area around Otta town center; B: Expected event frequency for each single element at risk. Slightly modified from Frauenfelder et al., (2017).

Although one of the main conclusions from the first part of this study was a projected increase in landslide event frequency, they did not include this projection in their landslide risk model. The model is therefore useful to quantify risk in present conditions, but how to adapt these risk estimates to project the future risk development is still not fully understood. This remains one of the important research questions on the agenda in the ongoing Klima 2050 and NordicLink projects.

2.2.3 Klima 2050 and other projects

Coincidently, during the span of the GeoExtreme and InfraRisk projects, Otta and northern Gudbrandsdalen saw three extreme event situations in 2008, 2011 and 2013. Spatial and temporal data from these events provided a basis for further studies on the conditions and triggers of shallow landslides, ultimately aiming to reduce uncertainty and improve prediction of 'when and where'. Several of these studies spring out from the centre of research-based innovation, Klima 2050. This is a collaborative initiative between public and private sectors, as well as educational purposes, to reduce the societal risks associated with climate change by adaption of buildings and infrastructure.

The hydrometeorological conditions during the 2008, 2011 and 2013 events are well documented and described in the official NVE reports of Kleivane (2011), Walberg and Devoli (2014) and Roald (2015), as well as in Heyerdahl and Høydal (2017). In 2011 and 2013, the landslides triggered during periods of extreme precipitation, whereas in 2008, slides were triggered in relatively dry periods due to groundwater flow from mountainous areas with rapid snowmelt. The total societal cost of the 2013 flood and landslide events was estimated to exceed 1100 MNOK, of which the costs related to linear infrastructure networks amounts to approximately 550 MNOK (Siedler, 2015). As these events followed decades of relatively low landslide activity in the area, inland eastern Norway now received much more attention to the landslide problem.

Walberg and Devoli (2014) assessed the regional forecasting of landslides with respect to the match between regional landslide susceptibility maps and landslide tracks of the events, as well as the performance of a preliminary forecast model issued to selected users and public authorities (later to be used in beta version of varsom.no). New landslide susceptibility maps on a scale of 1:50 000 had just been prepared by NGU (Fischer et al., 2014) aiming to cover all areas where the terrain allows possible occurrence of landslides. Walberg and Devoli tested these maps against landslides in a slope close to Kvam, 15 kilometers southeast of Otta. Although the initiation- and runout zone for many of the observed landslides fell within the modelled susceptible areas, several of the observed events were not captured by the susceptibility map. This is likely attributed to the coarse resolution of the model inputs , thus not capturing smaller ravines and depressions (Walberg & Devoli, 2014).

The forecast model issued warnings of raised landslide susceptibility at three different instances during the spring and summer of 2013, of which the first was raised to the highest level on 22nd of May. This proved accurate, as many landslides were triggered in Gudbrandsdalen, causing large damage to property and infrastructure. A few weeks later, a moderate warning was issued, once again accurate as four shallow landslides in northern Gudbrandsdalen were reported during the period. The third warning was issued for Oppland and Trøndelag in August, this time without any significant events during the warning period. However, shortly after the landslide susceptibility was lowered to the lowest level, several slope failures occurred in Trøndelag. Overall, the study illustrated the uncertainty related to spatial and temporal prediction of events from both susceptibility maps and forecasts, encouraging further work on the landslide early warning system (Krøgli et al., 2018). One aspect introducing additional uncertainty to the models, and which is not possible to include in the forecast, is the man-made modification to terrain and natural waterways. This type of modification is proved to be significant in northern Gudbrandsdalen. The MSc projects of Yao (2012) and Edvardsen (2013) show how several of the 2011 landslides close to Otta and Kvam were caused by slope alteration and redirection of runoff from forest roads, by poor maintenance of culverts and by deforestation. These factors are also emphasized in Heyerdahl and Høydal (2017) as direct causes for several landslides in the area.

As Kvam experienced a great number of landslides in 2011 and 2013 (Figure 2.7), this area has been subject to several studies aiming to reduce uncertainty and improve model accuracy of landslide detection and prediction (Depina et al., 2020; Liu et al., 2021; Schilirò et al., 2021; Østgren, 2017). Schilirò et al. (2021) used the numerical model for rainfall-induced landslide prediction TRIGRS, to reproduce the 2011 and 2013 landslides in Kvam. A different approach was used by Liu et al., (2021) for the same area. This study demonstrated the performance of different machine learning techniques in modelling spatial extent of landslides. By training the model with 70% of the data in the area, the models were able to predict landslides in the remaining 30% of data points, outscoring the reference TRIGRS model significantly both in terms of accuracy and efficiency. All recent studies have however, focused on back modeling of landslides, and neither method has yet been used in forward modelling of future possible landslide areas.

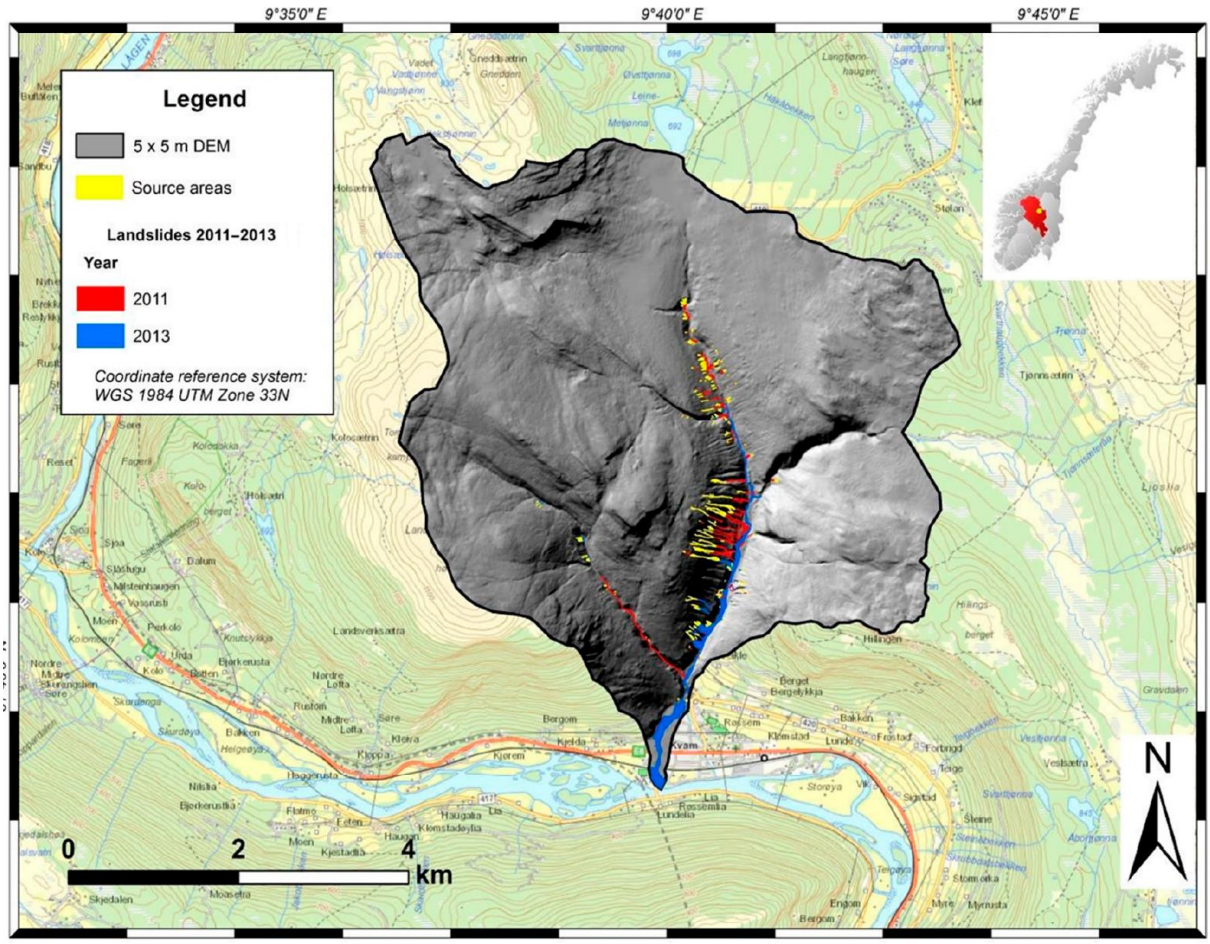

Figure 2.7 - Mapped landslides of 2011 and 2013 in Kvam, subject to studies of Edvardsen (2013), Liu et al., (2021) and Schilirò et al. (2021). Figure from Schilirò et al. (2021).

3 Theory

3.1 Slope stability

The general concept of slope stability describes the stress on an inclined surface from differences in potential energy and can be applied to all types of ground material. As this study focus on shallow landslides, a few key concepts of slope stability in soil should be introduced.

3.1.1 Factor of Safety

Factor of safety (FS) is a commonly used measure of slope stability and describe the relationship between the moments resisting slip failure, and the forces working towards failure (Taylor, 1948). FS is calculated as the sum of resisting forces divided by sum of driving forces acting on the slope:

$$FS = \frac{\sum F_r}{\sum F_d} \quad (1)$$

If sum of resisting moments ($\sum F_r$) is greater than the sum of driving moments ($\sum F_d$), The factor of safety is greater than 1, and the slope is stable. If the driving moments exceed the resisting moments, FS is smaller than 1, the slope will have failed. When the sum of the two force regimes is equal, FS = 1, and the slope is at limit equilibrium.

3.1.2 Stress, strength, and effect of pore pressure

The main driving moment is the gravitational acceleration of the slope mass. This force can be subdivided into two vectors, a normal force perpendicular to the slope, and a shear force parallel to the slope. Of these two, the shear force is a motion driving component, whereas the normal force is a resisting component keeping the soil in place. This normal force is, however, canceled out by a normal force of similar magnitude and opposite direction, exceeded from deeper soil and bedrock. The most important moment resisting motion is therefore the soil shear strength. The effective stress components on the soil are thus the slope parallel driving component of the

gravitational acceleration and the motion-resisting soil strength (Figure 3.1). The relative magnitude of these decides the slope stability.

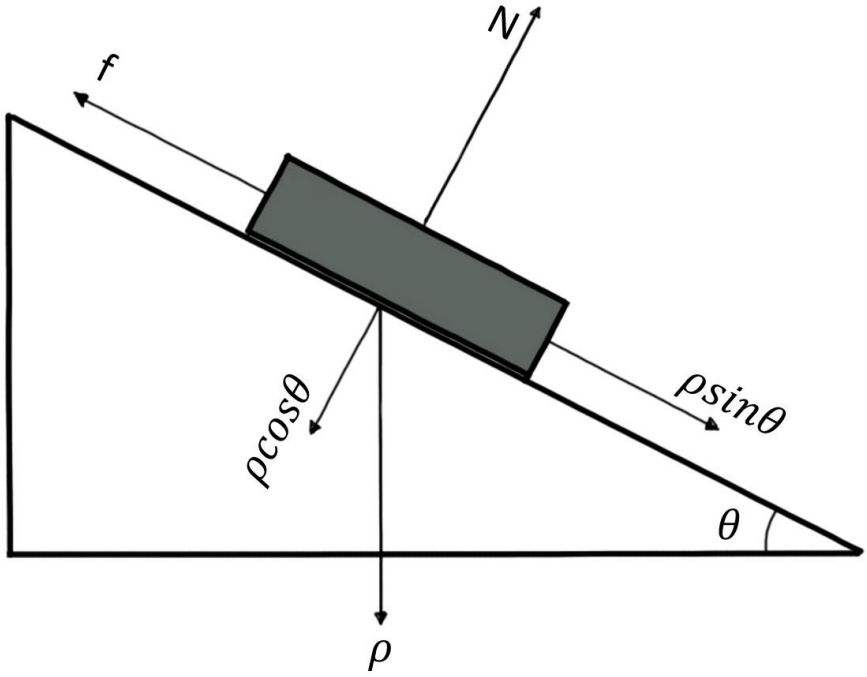

Figure 3.1 - Simplified force regime of a free body on a slope where ρ is unit weight of the body, θ is slope angle, N is the normal force from the slope, and f is the frictional resisting force.

The magnitude of the driving moment is dependent on the unit weight of the soil, as well as the slope angle. The soil strength, however, is controlled by the two components cohesion and angle of internal friction. Mature and well compacted soils with a clay fraction or some sort of cementation will have cohesion, a factor increasing the strength between soil grains by chemical precipitation of minerals in pore spaces, electrostatic and electromagnetic attraction, and adhesion (Mitchell & Soga, 2005). The angle of internal friction is largely determined by the shape of grains in the soil and their distribution. Together with the effective normal force, this determines the frictional resistance along the slip surface (NGI, 2014).

The failure criterion (Figure 3.2) is defined by the linear relationship of the shear strength parameters of the soil and the maximum differential normal stress the soil can withstand:

$$\tau = c' + \sigma \, tan\varphi' \tag{2}$$

where τ is the soil shear strength, c' is the soil cohesion, σ is total normal stress on the failure surface and φ' is the internal friction angle.

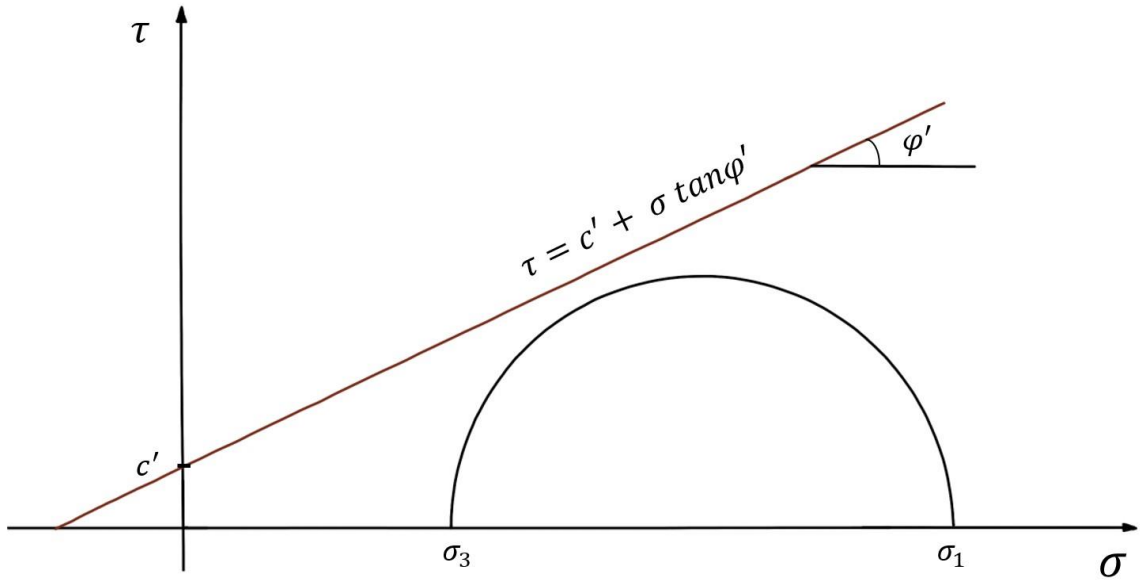

Figure 3.2 - Mohr-Coloumb failure criterion describes the stress space of which the relationship between soil shear strength parameters and the maximum differential normal stress allows stable slope conditions. If the differential stress indicated by the semicircle touch the failure curve, the slope fails.

When soil pore spaces are filled with water, an additional force is added to the equation from pore pressure. As this pressure acts outward from the pore spaces, and with similar magnitude in all directions, each total principal stress acting on the soil block will be reduced by this magnitude of pore pressure. It is thus necessary to introduce the term effective stress, which is defined as the total principal stress minus pore pressure (Terzaghi, 1936):

$$\sigma' = \sigma - u_p \tag{3}$$

Considering the effect of pore pressure to the Mohr circle diagram, the reduction of total stresses results in a leftward translation of the normal stresses, potentially pushing the Mohr's circle over the defined failure criterion (Figure 3.3).

Considering both driving and resisting momentums, and placing the block within the soil profile and not on top, the factor of safety can now be found by:

$$FS = \frac{c' + \left(\rho z \cos^2\theta - u_p\right) \tan\varphi'}{\rho z \cos\theta \sin\theta} \tag{4}$$

where θ is the slope angle, ρ is the unit weight of soil, z is the depth of failure and u_p is the soil pore pressure.

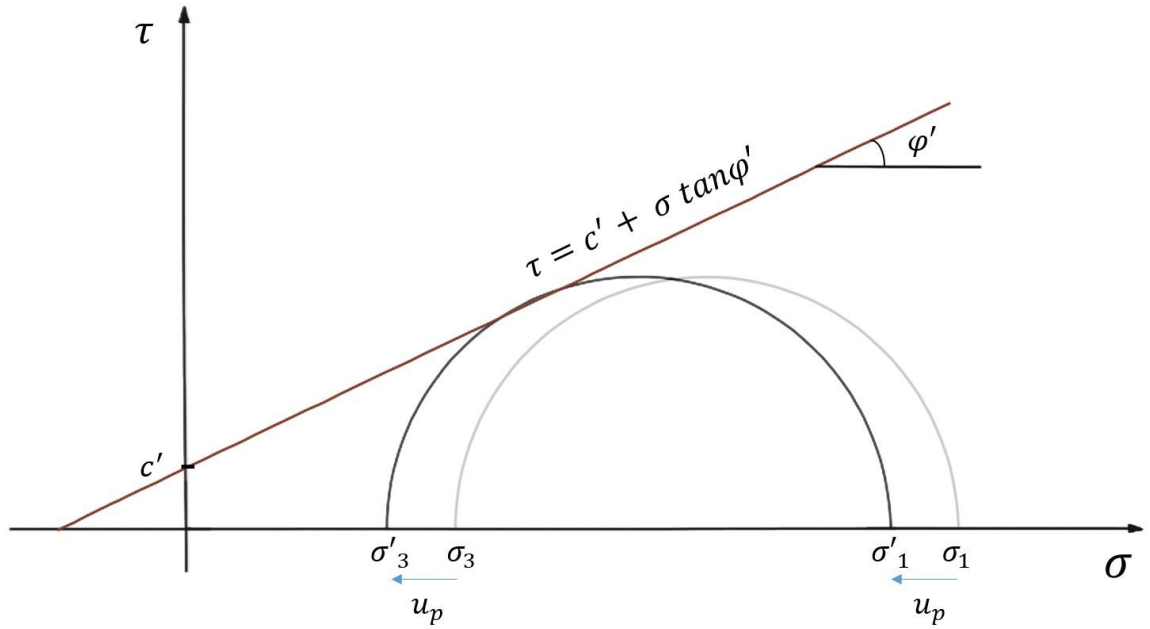

Figure 3.3 – Effect of pore pressure on the slope stress regime. Effective normal stresses are equally reduced, thus maintaining maximum differential normal stress, but at lower stress values. This may effectively force the differential stress beyond the shear strength limit indicated by the Mohr-Coloumb failure criterion.

Infinite slope model

A common way of calculating FS is through the infinite slope stability model. As the name implies, this model assumes a slope with infinite dimensions to calculate planar slip surfaces. This simplifies calculation as one can then assume that the same forces acting on each vertical block of the slope. Thus, by calculating safety factor for a single typical block, one finds the safety factor for the entire slope (NGI, 2014).

3.1.3 Controlling factors

Climate

Soil cover in large parts of eastern Norway is relatively young and immature in a geological perspective, and many slopes thus have relatively low natural stability. During the Holocene, the soil cover has adapted to the existing climatic conditions (Fergus et al., 2011; Sandersen et al., 1997). Thus, at times of extreme weather events with abnormal precipitation and/or snowmelt, slope stability may become critical and result in failure. With the range of different climatic zones in Norway, there are also large differences in the levels of precipitation needed

to cause soil instability and initiate landslides. Large parts of west- and northern Norway have a marine climate and is thus adapted to the relative high amounts of precipitation and runoff.

To relate critical precipitation intensity necessary for slope failure to the governing climatic conditions in a specific area, Sandersen et al., (1997) suggested the following equation:

$$P = 1.2\ D^{0.6} \tag{5}$$

where P is the percentage of yearly precipitation in the area within a given duration D (hours). There are in general two types of hydro-meteorological conditions acting as triggers for shallow landslides in continental Norway: over-saturation of soil due to spring snowmelt and convective extreme precipitation events during summer (Heyerdahl & Høydal, 2017; Sletten & Blikra, 2007). In coastal areas of western Norway, most landslides occur during fall or early winter, during extreme precipitation of a 1–3-day span and often in combination with snowmelt. This typically corresponds to 120-160 mm water supply per day. In continental parts of Norway, the threshold is likely around 40-80 mm during a 2–4-hour span (NGI, 2014). These are, however, only estimations. Exact thresholds depend greatly on the intensity distribution during the precipitation event, as well as initial hydrologic soil conditions.

Material properties of soil

Several of the soil material properties affecting stability are determined by the grain size and grain sorting within the soil. Grain size range from clay fraction to boulders, and the sorting determine the distribution of the different sizes within the soil. A well sorted deposit with similar grain size such as eolian sand dunes can thus described as homogenous, whereas poorly sorted deposits with a wide range of grain sizes is described as heterogenous. Sorting and grain size is largely determined by the depositional agent, and the least sorting agent thus producing the most heterogenous soil are glaciers. Glacial tills, such as the ones that are found in the valley sides of Gudbrandsdalen, consist of all grain sizes with poorly sorted, random distribution in the soil (Jørgensen et al., 2013). Grain size and sorting largely determine porosity and permeability in soils, which are important factors for stability. Porosity is a measure of total pore space in-between grains, whereas permeability describes the connectivity of these pore spaces, and thus the ability for a fluid to flow through the soil. A soil with high permeability

will not build significant pore pressure from seepage and will therefore maintain stability in high slope gradients in events of increased water infiltration (NGI, 2014). This is typical for homogenous soils with sand or coarser grains. In heterogeneous soils, small grain fractions tend to fill the pore spaces and connective pathways between larger grains, reducing both porosity and permeability (Figure 3.4). This will cause pore water pressure to build in events of increased infiltration, resulting in lower stability.

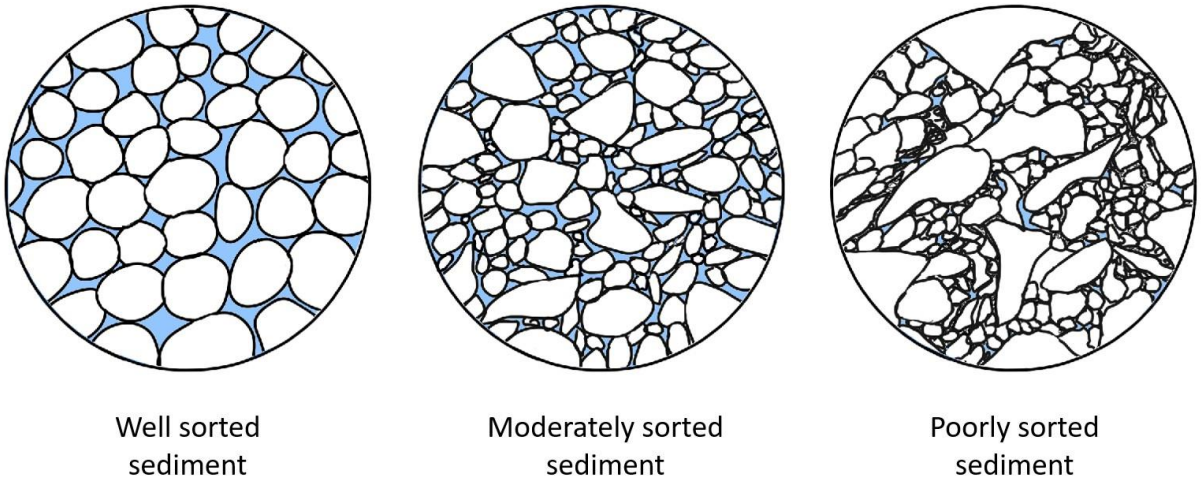

Figure 3.4 - Different degree of grain sorting and its effect on porosity and permeability.

The portion of clay fraction in the soil play an important part in stability, not only in terms of porosity and permeability, but by introducing cohesion between soil particles. When calculating stability, this can be seen as a combination of grain cementation and capillary forces binding grains together and having a positive effect on soil strength (NGI, 2014).

Soil properties varies laterally and within the vertical soil profile. A mature soil will typically have developed layering from leaching in the upper soil profile and cementation in the lower part. The relative difference in permeability of these layers can cause a horizon of increased pore pressure and act as a critical plane during great water infiltration. Other critical planes could be the soil-bedrock boundary, or on top of a horizon of frozen soil. (NGI, 2014)

Vegetation

Vegetation is a complex factor with several positive and negative effects on slope stability. The root system of trees and large plant growth have a binding effect which increase soil strength. The vegetation also removes water from the soil by evapotranspiration, reducing pore water pressure. This effect is especially pronounced in growth season. As growth season coincide

with snow melt season, this is an important stabilizing factor in the spring. The tree canopy can also act as a rain interceptor, reducing erosion and stress on the soil from direct impact of precipitation (Breien et al., 2015). Additional load of vegetation may have either stabilizing or destabilizing effects, dependent on its placement in the slope. In general, this has a positive effect on stability if the growth occurs in lower part of a slope, and negative effect if the load is placed in the upper slope. The magnitude of this effect depends on tree type, size and forest density and may have up to 10% effect on slope factor of safety (Greenwood et al., 2004). Size of trees also affects the windthrow loading on the soil. Heavy wind may cause such motion in a tree that the soil in which it stands is loosened. This reduces the anchoring effect of the roots and thus decrease stability. When trees fall due to wind, their roots are often pulled up from the ground, leaving a scar of loose soil in the slope and increasing the exposure to surface erosion (NVE/NGI, 2015). The effect of windthrow is significantly lower in forests as trees are sheltered from the wind from the ones at the cluster edge (Greenwood et al., 2004).

Topography

Slope angle in which failure may occur largely depend on soil water pressure. In general, shallow landslides release areas typically occur in slopes angle > 25°, but with significant soil water pressure, failure may also occur in gentler slopes. When characterizing release areas from the landslide event of 2011 in Kvam, Edvardsen (2013) found that all release areas occurred in the transition from moderate slope angles to 30°. Curvature of the terrain is important in build-up of pore pressure, and depressions in the slope are typically subject to failure. Release zones also often occurs near streams or rivers. In defined gullies, streams may be fed by smaller slides from the ravine margins, resulting in a debris flood (NGI, 2014).

Alterations of slope (manmade)

As mentioned, the natural stability of a slope will adapt to climate over a longer time. Abrupt changes to the slope conditions may therefore have significant impact on the stability. The two most common alterations of slopes are construction of forest roads, and forestry. Roads in slopes may lead runoff away from its course and along its path. If this is not drained properly it may result in the water running uncontrolled into the slope below the road with significant erosional force and initiate a debris flow (Figure 3.5). Culverts in these roads are often poorly dimensioned and maintained, and are often clogged by rocks, leaves and other debris. The construction design of the road may also affect the stability of a slope. If the road profile is cut

into the slope, the part of the slope that is removed will no longer support the slope above, and this unloading of mass could lower the stability significantly. Similarly, if the road runs on a fundament placed on top of the natural slope, the extra load could destabilize the slope below it. Road construction must thus be carefully adapted to the surrounding conditions such as slope angle, slope material and natural drainage (Fergus et al., 2011).

Figure 3.5 - Inspection of a landslide release area in Solhjem from 2011. A forest road acted as drainage path for the surface runoff. A topographic low along the road caused accumulation of water to a pond, causing a slope failure at its spill point (Photo: Øystein Grasdal).

Forestry has a destabilizing effect on by subtracting the natural net stabilizing effects by vegetation in the slope. The most important effect is the removal of slope support from tree roots. Trees are seldom removed with their roots but cut at some height leaving a stump. This will cause its roots to rot and have the same effect over time as removing them. Ground water level may also rise in a forest field after removal of trees, as the evapotranspiration effect is lost. Surface tracks from forestry machines may also alter the surface runoff pattern and locally enhance slope erosion (NGI, 2014).

3.1.4 Triggers

Figure 3.6 illustrates how shallow landslides and debris flows are usually initiated either due to increased pore water pressure and resulting failure, or due to erosion by running surface runoff (Norem & Sandersen, 2012). These are the two types of failure with focus in this study, and

thus the ones that will be further described. Other triggers could for instance be initiation from rock fall / rock avalanche, volcanic eruptions or by ground shaking from earthquakes.

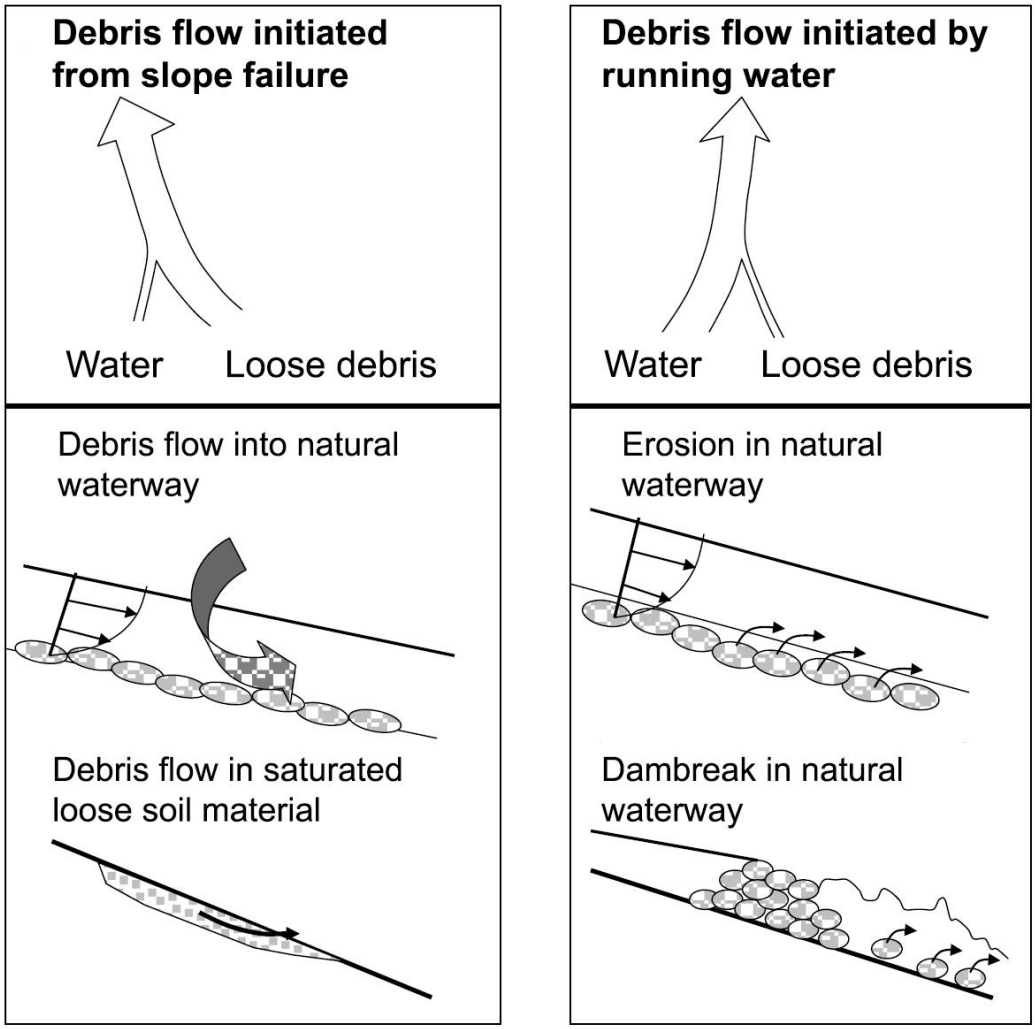

Figure 3.6 - Conceptual illustration of the relative role of water and loose debris in common debris flows triggering processes. Slightly modified from Norem and Sandersen (2012).

As described in chapter 3.1.2, the process of slope failure from increased groundwater content is due to increase in pore pressure and related decrease in stabilizing normal forces. A prerequisite for increase in ground water content is a larger inflow of water than outflow from the soil. The inflow of water in a block of soil is through one of three sources:

- Infiltration from upper soil layer by precipitation and snow melt.
- Groundwater flow within the soil from upslope area or from the side.
- Infiltration from below through cracks in bedrock or bottom soil layer with artesian water pressure.

Factors such as watershed area, thickness and permeability of soil layers and topographic channeling of groundwater largely determine the rate of pore pressure response, and thus also the timing of potential slope failure with respect to a given rainfall or snowmelt scenario (Norem & Sandersen, 2012). In cases when slope failure occurs and the slide is carried into an existing stream, the flow may be further saturated with water, resulting in a more turbulent flow of increased velocity. This may further increase erosion in the stream, incorporating more and more debris to the flow downstream.

In streams or other natural waterways, the surface will be adapted to normal-weather water runoff. During extreme events of significantly higher runoff, however, the shear force in the flow increase, and thus its erosional potential increases. The relationship between critical flow velocity and grain size for surface erosion is well described by the Hjulstrøm curve (Figure 3.7).

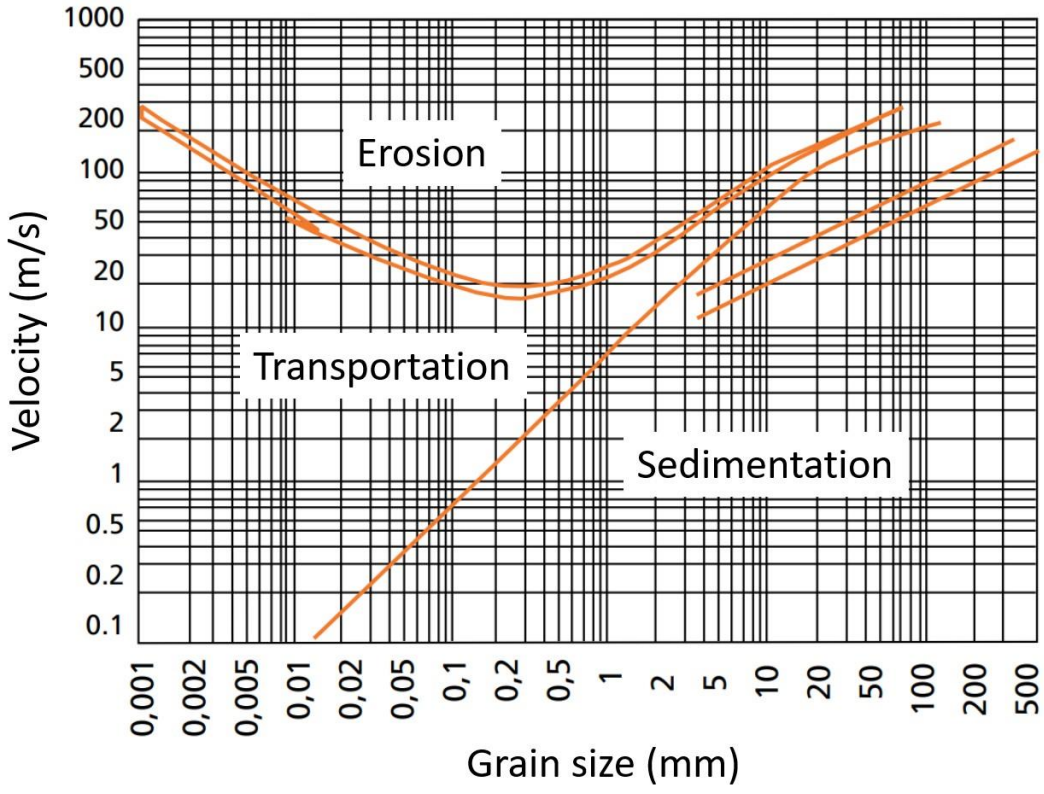

Figure 3.7 - Hjulstrøm curve describing critical flow velocities for erosion, transportation, and sedimentation of different grain size particles. Slightly modified from Fergus et al. (2010).

Seen from right to left, the diagram curve shows how potential erosion occur at ever lower flow velocity for decreasing grain size. This trend culminates at 0.2 – 0.3 mm grain size at approximately 0.2 m/s flow velocity, and from this point ever higher velocities are required to initiate erosion in surfaces of decreasing grain size. For grain size larger than 0.2 mm, the

transferred shear force required to initiate motion in individual grains increase due to greater unit weight and following increase in friction to the underlying surface and neighboring grains. For grain size lower than 0.2mm, the effect from cohesion contribute to the soil shear strength and thus require higher flow velocity to initiate erosion. When material is set in motion, the shear force of the surface flow will further increase, thus also increasing the erosional potential of the flow. This process may trigger a large viscous debris flow. A debris flow may also occur in situations where increase in runoff and enhanced erosion cause the dam break of previously deposited sediments, or artificial dams such as forest roads.

3.2 TRIGRS

The **T**ransient **R**ainfall **I**nfiltration and **G**rid-based **R**egional **S**lope-stability model TRIGRS is a physically based modelling tool from USGS, designed to illustrate the temporal development of slope stability from rainfall infiltration. The program lets the user define soil parameters, rainfall scenario and grid files for topographic conditions through a command-line user interface. When running the prompt, the program computes a cell-by-cell factor of safety for either saturated or unsaturated initial conditions.

For saturated initial conditions, TRIGRS is based on Iverson's (2000) solution of the Richards equation consisting of one steady- and one transient infiltration component. The steady component is determined by the steady background infiltration rate, saturated hydraulic conductivity, slope angle and depth to water table. The transient component is largely controlled by short term response to precipitation, resulting in pressure diffusion. Thus, the two components decide the hydraulic pressure head (ψ) at initial conditions t0 and the change in pressure head response over a specified time. Excess water is modelled as runoff until it potentially reaches more permeable downslope zones.

The safety factor at depth Z is then calculated following Iverson (2000):

$$FS(Z,t) = \frac{\tan\varphi'}{tan\theta} + \frac{c' - (\psi(Z,t)\,\rho_w \tan\varphi')}{\rho\, Z \sin\theta \cos\theta} \quad (6)$$

where φ' is the internal friction angle of the soil, θ is slope angle, c' is the effective soil cohesion, ρ_w is the unit weight of water, and ρ is the total unit weight of soil.

A comprehensive description of functionality, stability calculations and user operation of the TRIGRS model is presented in Baum et al. (2008).

3.2.1 TopoGrid

A few of the files used as input in TRIGRS, is obtained by running the integrated TopoIndex program. This program uses grid files of elevation (DEM) and flow direction generated by the user as input to generate a surface runoff routing scheme. If TRIGRS is run without these files, no surface runoff will be included in the calculation of FS. TopoIndex is dependent on a hydrologically consistent DEM to successfully generate its output files. It does not include potential artificial drainage such as culverts into the runoff routing calculation (Baum et al., 2008).

3.3 RAMMS

RAMMS is a tool developed for **Ra**pid **M**ass **M**ovement **S**imulation in Switzerland at the WSL Institute for Snow and Avalanche Research SLF. By numerical modelling, RAMMS performs a runout simulation of a landslide, predicting flow speed, flow pressure and flow height, as well reach. The model was developed as a tool for geotechnical engineers as an aid in practical landslide problems and development of mitigation measures. The software consists of three modules, RAMMS Avalanche, RAMMS Rockfall, and RAMMS Debrisflow. Of these, RAMMS Debrisflow is the appropriate module to assess the runout of shallow landslides in Gudbrandsdalen.

RAMMS Debrisflow uses a Voellmy-fluid friction model with gravitational driven flow and frictional resistance to flow divided into a dry-Coloumb type friction and a viscous turbulent friction. The total frictional resistance S (Pa) is calculated as

$$S = \mu N + \frac{\rho g v^2}{\xi} \quad , \qquad with \ N = \rho h g \cos(\theta) \quad and \ v = \left(v_x, v_y\right)^T \tag{7}$$

where ρ is flow density, g is the gravitational acceleration, N is the normal stress on the running surface and u is the time dependent vector v consisting of flow velocity in two directions. The

frictional coefficient μ (Mu) and turbulent coefficient ξ (Xi) determine the resistance to flow in solid and turbulent fluid state, and their relationship determine the behavior of the flow. The choice of frictional coefficients is up to the user, and it is recommended these are selected after careful calibration to runout from documented events. In addition, the user can specify cohesion, which is added as a yield stress. The total frictional resistance is then given as:

$$S = \mu N + \frac{\rho g v^2}{\xi} + (1 - \mu) N_0 - (1 - \mu) N_0 \, e^{\frac{N}{N_0}} \quad (8)$$

where N_0 is the yield stress of the flowing material. It is however, recommended to calibrate the model to the frictional parameters before including yield stress to the flow simulation.

The soil susceptibility to erosion can be specified by defining erosional rate, potential depth of erosion as well as critical shear stress and maximum erosional depth for a given area. Magnitude of erosion is then spatially dependent on the normal stress to the running surface as described by $N = \rho h g \cos(\theta)$, at the rate and depth as determined by the input boundaries set by the user.

RAMMS is highly compatible to GIS software. Input data such as elevation model, erosional properties and release areas are either prepared as polygons in GIS or drawn directly in RAMMS. Output files such as maximum flow height, velocity and pressure, as well as topographic changes to the input elevation model can be exported either as shapefiles or as ASCII grid files back to GIS for further analysis.

For a more detailed summary of application, model calculation and software operations, the reader is referred to the user manual of Bartelt et al. (2017).

4 Data and methods

4.1 ArcMap

A large portion of input data to both TRIGRS and RAMMS is based on the representation of elevation data in a digital elevation model (Figure 4.1). Elevation models from multiple data acquisitions are available for download from the online service hoydedata.no provided by Kartverket. For this study, portions of three different datasets have been selected based on their spatial coverage and year of acquisition (Table 4.1). These are imported to ArcMap and resampled to a cell size of 5x5 meters. This resolution is commonly used with TRIGRS, and significantly reduces the time of runout simulation computations in RAMMS compared to running 1m DEMs over larger areas. These DEMs provide the basis for generation of slope maps and hydrological modelling such as flow direction, flow accumulation and visualization of individual watersheds using functions in the ArcMap toolbox. These data sets, as well as the DEM file itself, are exported as either .tif or .asc files for use as inputs in both stability modelling and runout simulations.

Table 4.1 - Digital elevation datasets from Kartverket, extracted from https://hoydedata.no/LaserInnsyn/

Project name + year	Project number	Point density (pt./m)	Resolution (m)
Nord-Gudbrandsdalen 2008	LACGOP81	1	1
Nord-Gudbrandsdalen Flom Ras 2011	LACGOP91	5	0.25
Nord-Gudbrandsdalen 2013	LACHOP33	5	0.25

The most important use of ArcMap is to reference different datasets to a common datum, thus enabling analysis and visualization of relationships between different map layers. Datasets of road- and railway, land use, quaternary deposits and landslide susceptibility maps are some of the datasets which are imported to ArcMap to carry out the hazard assessment of this study. A complete list of used data and their sources is presented in Table 4.2. Finally, ArcMap has been used to visualize results from TRIGRS and RAMMS, and to evaluate the exposure of the infrastructure to different present and future landslide scenarios.

Table 4.2 – ArcMap map data input overview

Map data	Dataset	Data source	Data type	Scale	Retrieved from	Date of download
Digital elevation model*	Multiple sets	Kartverket	Raster	-	hoydedata.no	20.09.2021
Road network	Vbase	Kartverket	Polyline	-	geonorge.no	20.09.2021
Railway network	Jernbane - banenettverk	Bane Nor SF	Polyline	-	geonorge.no	20.09.2021
Power grid network	Nettanlegg	NVE	Point / Polyline	-	nedlasting.nve.no	20.09.2021
Quaternary deposits	Løsmasser	NGU	Raster	50 000	geonorge.no	25.09.2021
Landslide susceptibility	Aktsomhets-områder	NVE	Polygon	-	nedlasting.nve.no	25.09.2021
Historic landslide events	Skredhendelser	NVE	Point	-	nedlasting.nve.no	25.09.2021
Area resource map	AR5 Arealtyper	NIBIO	Polygon	5 000	wms.nibio.no	-

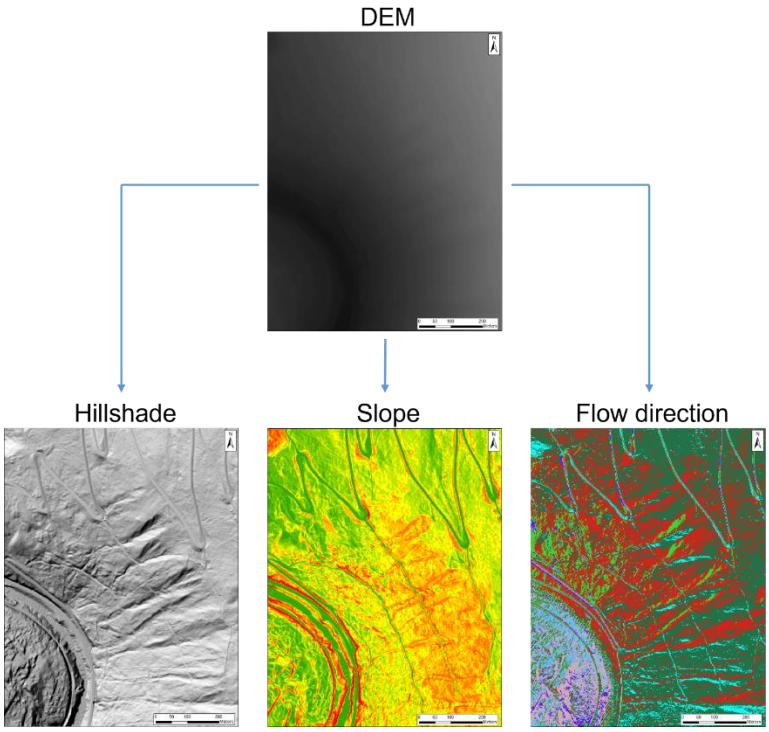

Figure 4.1 – Digital Elevation Model (DEM) provides the basis for several illustrative and functional map layers in ArcMap

4.2 TRIGRS

The confidence in the results is closely related to the uncertainty of the input data, and thus TRIGRS should normally be run in an area with well-known soil properties and field measurements for accurate and precise results. For this study, the model is run with limited geo-mechanical data from the field area, and without field measurements. The result of this is low accuracy modelling of past events, and similarly high uncertainty to future scenario projections. The upside of running a model based on digital open-source geographic data is the possibility of calibration and up-scaling to larger areas without costly, time-consuming field investigations. In this study, TRIGRS is used to investigate possible climate induced changes in landslide release area to be able to identify potential future problem areas in the infrastructure. Thus, TRIGRS is run with focus on investigating changes in slope stability in response to different levels of precipitation.

4.2.1 Calibration to 2011 Rosten landslide event.

The selected event occurred on the 10th of June in Rosten, the northernmost part of the study area. Three separate debris flows were triggered in a south-west facing hillside from intense precipitation. The first and only report of debris flow was at 10:51 am on the 10th of June. All three debris flows crossed E6 in the intersection point with county road fv437 to Høvringen (Figure 4.2).

The spatial data coverage for this event is good with respect to the elevation model from which slope and flow direction can be derived. Precipitation data is restricted to daily grid from radar, limiting both temporal resolution of precipitation intensity, as well as the precision of background rainfall intensity. As no field data is obtained from the area, different geotechnical parameters, as well as soil depth estimations rely on estimations and previous studies in the area.

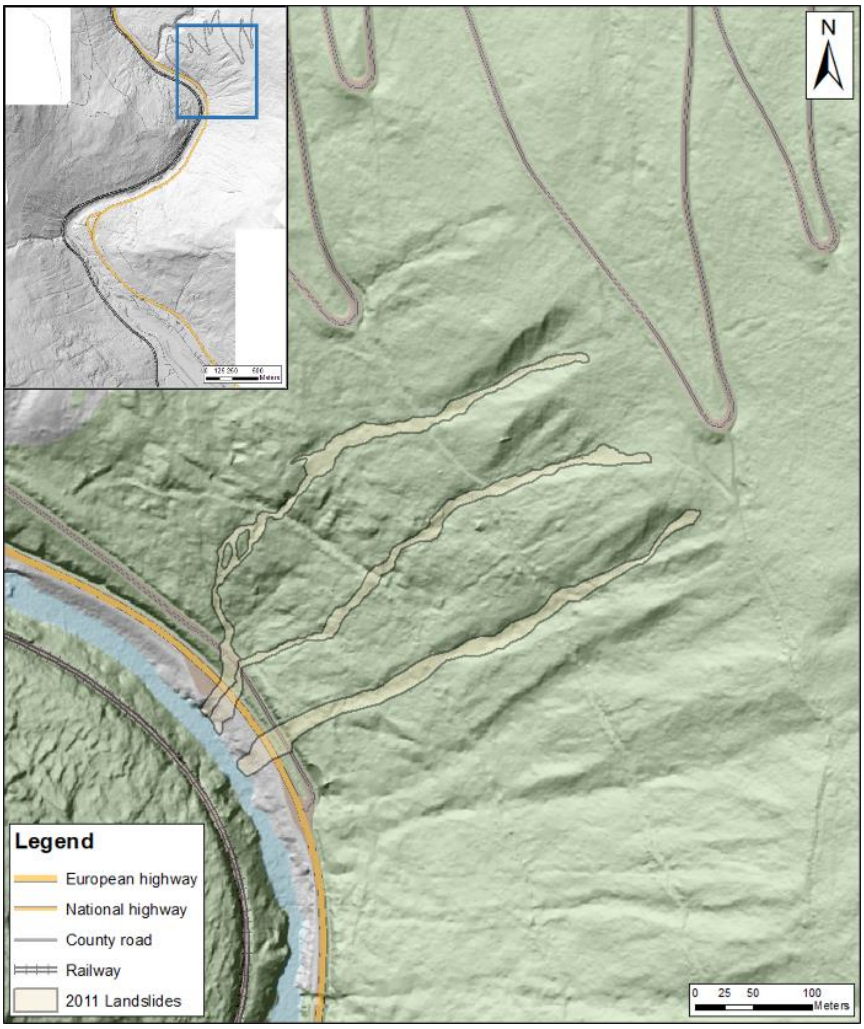

Figure 4.2 - Extent of 2011 landslides in Rosten as interpreted from aerial photographs.

When back modeling the landslide event, the goal is to obtain the best possible match in stability results to the landslide event using the TRIGRS model. Thus, there are two very important stages during the event, which the simulation should be fitted to. The two stages are the initial soil conditions at t_0, and the time of failure t_f. The first step in the process is to calibrate model parameters to minimize areas of unstable slope conditions at t_0 when only background precipitation has been introduced to the soil. To adjust the model to stability at t_0, cohesion, and friction angle are the parameters subject to calibration, as these have the most impact on slope stability, together with soil thickness (Schilirò et al., 2021).

TopoIndex

To have a hydrologically consistent DEM as input for the calculation of runoff routing, the ArcMap *Fill* tool has been used to fill data cells with no drainage direction. These cells are depressions in the terrain, and effectively acts as sinks. By filling these to the elevation of the

lowest adjacent cell, the water entering this cell will continue its flow downhill as if the depression spills over from being filled with water. To assess the effect of *Fill* on the runoff in the slope, the *Minus* tool can be used. By subtracting the original DEM from the filled DEM, the position and amount of fill can be found. Figure 4.3 show the distribution of fill effect on the DEM in the case site of Rosten. In this case, the fill tool contributes to a consistent DEM without compromising the actual terrain in the slope of focus.

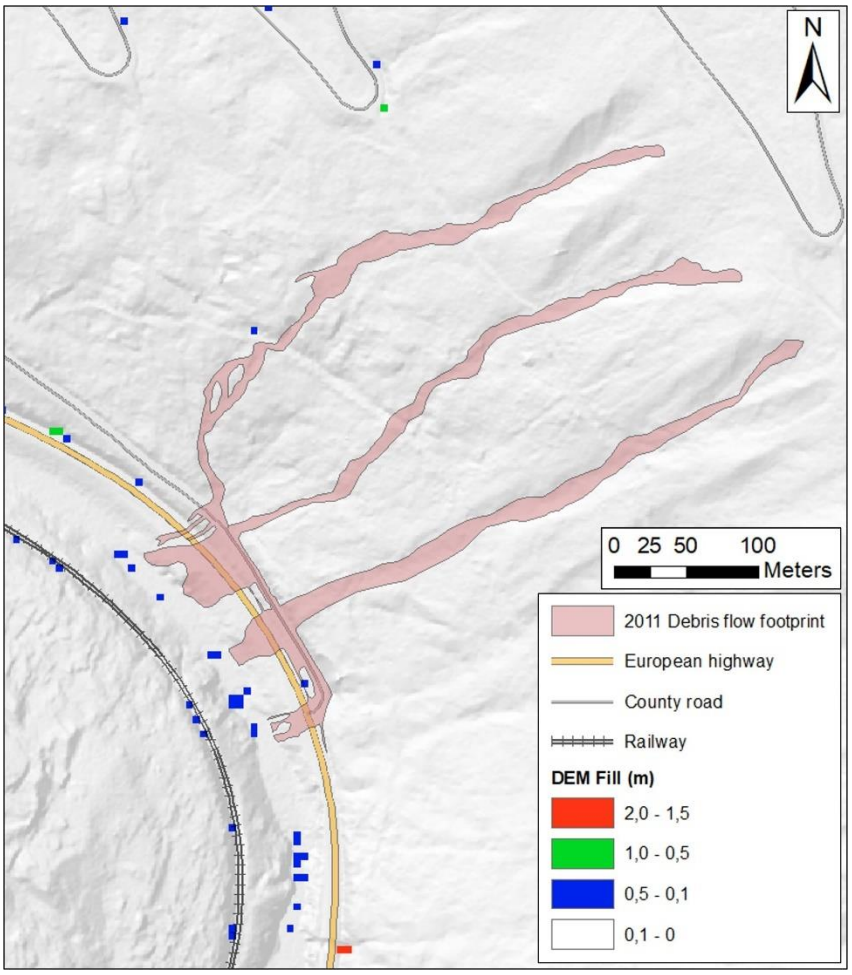

Figure 4.3 – Adjustments to the DEM using ArcMap fill tool.

Estimation of soil thickness

Soil thickness is spatially variable and difficult to model due to the natural variation in till morphology and the underlying bedrock. With no field measurements, data is limited to Quaternary deposits map from Norwegian Geological Survey (NGU). In the northern part of the study area, this is based on the 1:50 000 resolution mapping by Follestad and Bergstrøm (2004). The slope of focus is dominantly covered by till (Figure 4.4). This till is separated into

two types, till with continuous cover of locally great thickness, and till of discontinuous or thin cover. From distinct landslide tracks in the deposits map, it is evident how most landslides in the area are initiated from these two types of deposits. From product specification of the digital Quaternary deposits map, thickness of the two till cover types are suggested as normally less than 0.5 m with locally thicker patches for the thin, discontinuous till. For the continuous till type, thickness range from 0.5 m to tens of meters. Saulnier et al. (1997) proposed a formula to estimate soil thickness based on observed slope angle, maximum and minimum observed soil thickness in the area. This approach has been modified by Schilirò et al. (2021) for modelling the soil thickness in Kvam in the same type of till covers as in Rosten:

$$h_i = h_{max}\left[1-\left(\left[\frac{tan\alpha_i - tan\alpha_{min}}{tan\alpha_{max} - tan\alpha_{min}}\right]\left[1-\left(\frac{h_{min}}{h_{\max}}\right)\right]\right)\right] \quad (9)$$

where h_i is the soil thickness in pixel i, h_{max} and h_{min} are maximum and minimum observed thickness, α_i is the slope value in pixel i from DEM-derived slope angle map (Figure 4.4), and α_{max}, α_{min} are maximum and minimum observed slope values in the modelled area.

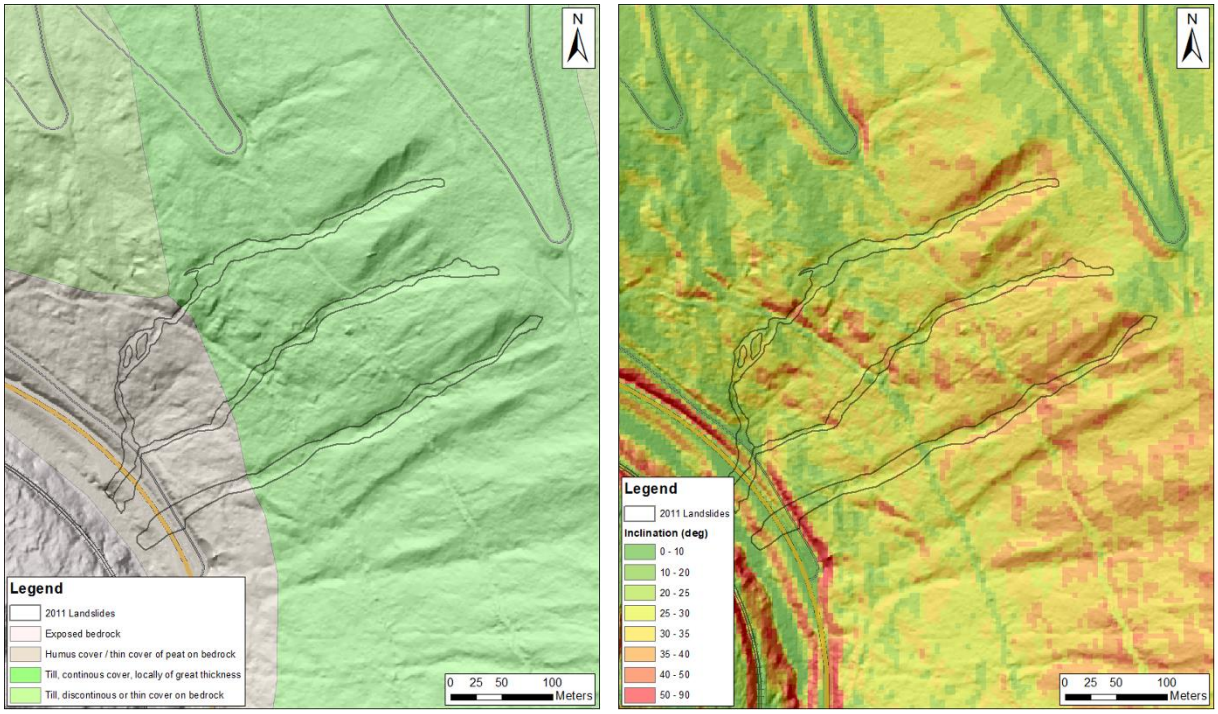

Figure 4.4 - Left: Quaternary deposits overlay on the 2008 DEM hillshade map and polygons indicating position of the 2011 landslides. Right: Slope inclination map derived from 2008 DEM.

As soil depth has not been measured in the field, maximum and minimum soil thickness is estimated from two high resolution DEM's from 2008 and 2011. By subtracting the DEM prior

to the landslides from the one after the event, the thickness of removed soil has been estimated (Figure 4.5). This thickness is then compared to high resolution post-event aerial photographs. In areas where exposed bedrock can be seen in the landslide scars, the soil depth prior to the landslide can be estimated with confidence. These values are used to estimate h_{max} and h_{min}. Together with the slope inclination raster, and its maximum and minimum values, these are used in equation ?? to calculate a soil thickness map using python code (Appendix D). To incorporate the thickness differentiations for the till types as they are defined in the Quaternary deposits map, a soil type scale factor is multiplied with the soil depth map to constrain the final thickness to appropriate ranges of the respective till type. As the continuous till cover in Rosten varies in the range of ±2m, this scale factor is set to 0.25 for the areas mapped as discontinuous thin till cover to adjust these areas to approximately 0.5m thickness. The result is a soil cover thickness map with spatial variation dependent on slope angle, within the defined thickness range of the respective mapped soil covers (Figure 4.5).

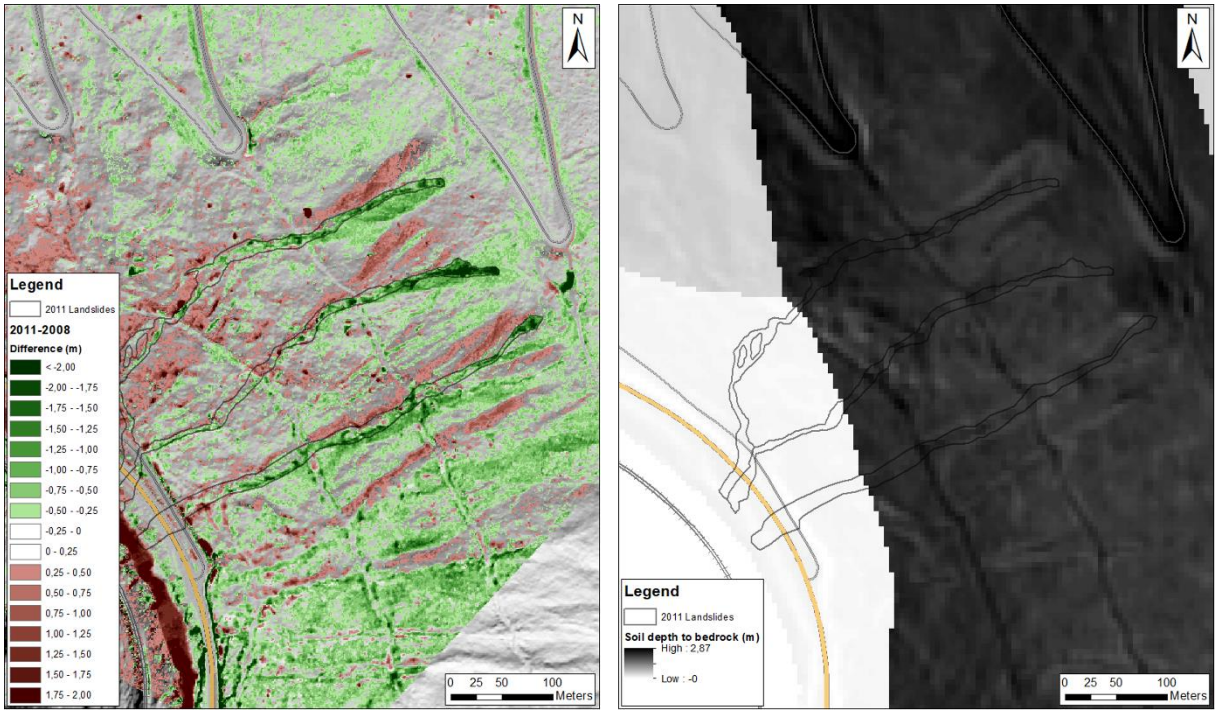

Figure 4.5 - Left: difference in DEM from 2008 to 2011 used to assess the removed thickness of soil during the landslides of 2011. Right: Soil thickness map derived from DEM difference, definitions from quaternary deposit map and fitted soil thickness equation of Schiliro et. al, 2021)

Precipitation scenario

June 10th, 2011, saw plumes of extreme precipitation in multiple parts of eastern Norway, one of which occurred in northern Gudbrandsdalen (Figure 4.6). The precipitation scenario for the

event is reconstructed from available data in the interpolated gridded data series from SeNorge, available through xgeo.no (MET., 2022b). This data series comprise historical precipitation from 1957 to current date, with a 1x1 km spatial- and 24h temporal resolution (Lussana, 2020). Although each 24h registration is assigned to a date, the 24h data contain the sum of precipitation in a cell from 08.00 of the specified date to 08.00 the following day (07.00 to 07.00 in winter).

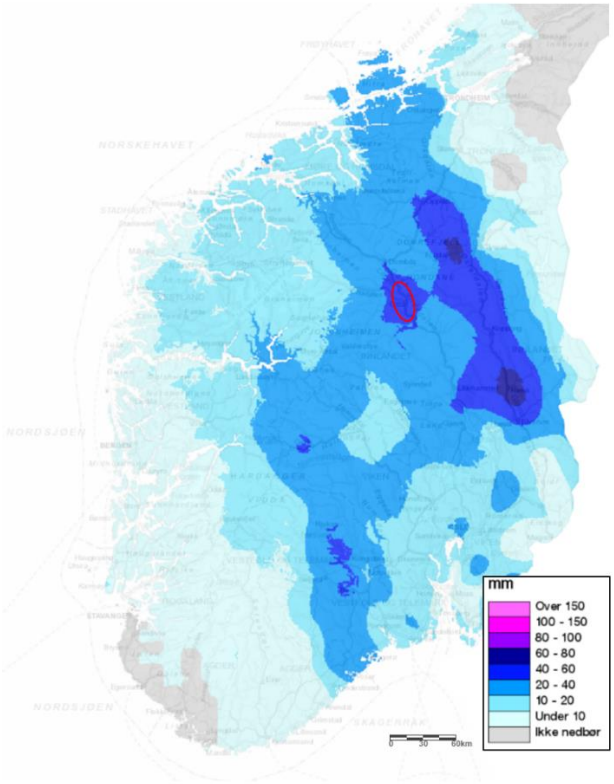

Figure 4.6 - Precipitation for southern Norway from June 10th of 2011. Red ellipsoid indicate the position of the Otta area in northern Gudbrandsdalen. Modified from MET. (2022b)

As no information about the landslide development exist between 10.51 on the 10th of June, until E6 was opened again on the 12th, it is assumed that two of the three landslides could have happened either on the 10th or the 11th. For model calibration for the 2011 events, a 48h precipitation scenario with 24h of 50.6mm from the 10th to 11th, followed by 24h of 25.2mm from 11th to 12th was tested. Saturated initial conditions are assumed from the amount of precipitation the two weeks prior to the landslides, and from snowmelt related to the high air temperature of the preceding week (Kleivane, 2011). Output for minimum factor of safety from TRIGRS suggest that the lowest slope stability occur by the end of the first 24h of heavy rainfall. It is likely that all three landslides were triggered in this interval, and further model calibration was therefore carried out with a 24h precipitation scenario of 2.11mm/h.

Soil mechanical properties

Unit weight of soil, hydraulic diffusivity and hydraulic conductivity is set similar to Schilirò et al. (2021) and Melchiorre and Frattini (2012), at 20kN/m3, 1.0 x 10^{-5} m/s and 1.0 x 10^{-4} m^2/s, respectively. No data is available for the depth of initial groundwater table. Thus, this is assumed uniformly at intersection of soil and bedrock as this is a frequently used approach in other studies using TRIGRS (Larsen, 2021). Input for the initial ground water table is therefore set using the same file as for the soil depth in the TRIGRS input command text. Background infiltration rate is calculated as average precipitation from the two antecedent weeks prior to the landslide event (Baum et al., 2008).

12 simulations of the slope stability are run in TRIGRS with different cohesion and friction angle in order to calibrate the model to stable slope conditions prior to rainfall, and an approximate amount of failing cells compared to the landslide scenario of 2011 (Figure 4.7 and Figure 4.8). The evaluated range is from 32 to 38 degrees friction angle, and from 4 to 8 kPa cohesion. For both parameters, larger values increase stability. Commonly used values for these parameters in glacial deposits has been 32 degrees friction angle and 4 kPa (Melchiorre & Frattini, 2012; Schilirò et al., 2021). As shown in Figure 4.7, these values result in FS<1 for large parts of the slope, indicating unrealistic slope conditions. To reflect stable initial conditions, friction angle of 35 degrees and cohesion of 7.25 kPa is used for the further analysis. These high values could potentially be caused by a relatively large portion of clay grain size fraction, high degree of cementation, and the stabilizing effect of densely spaced, large spruce trees in the slope.

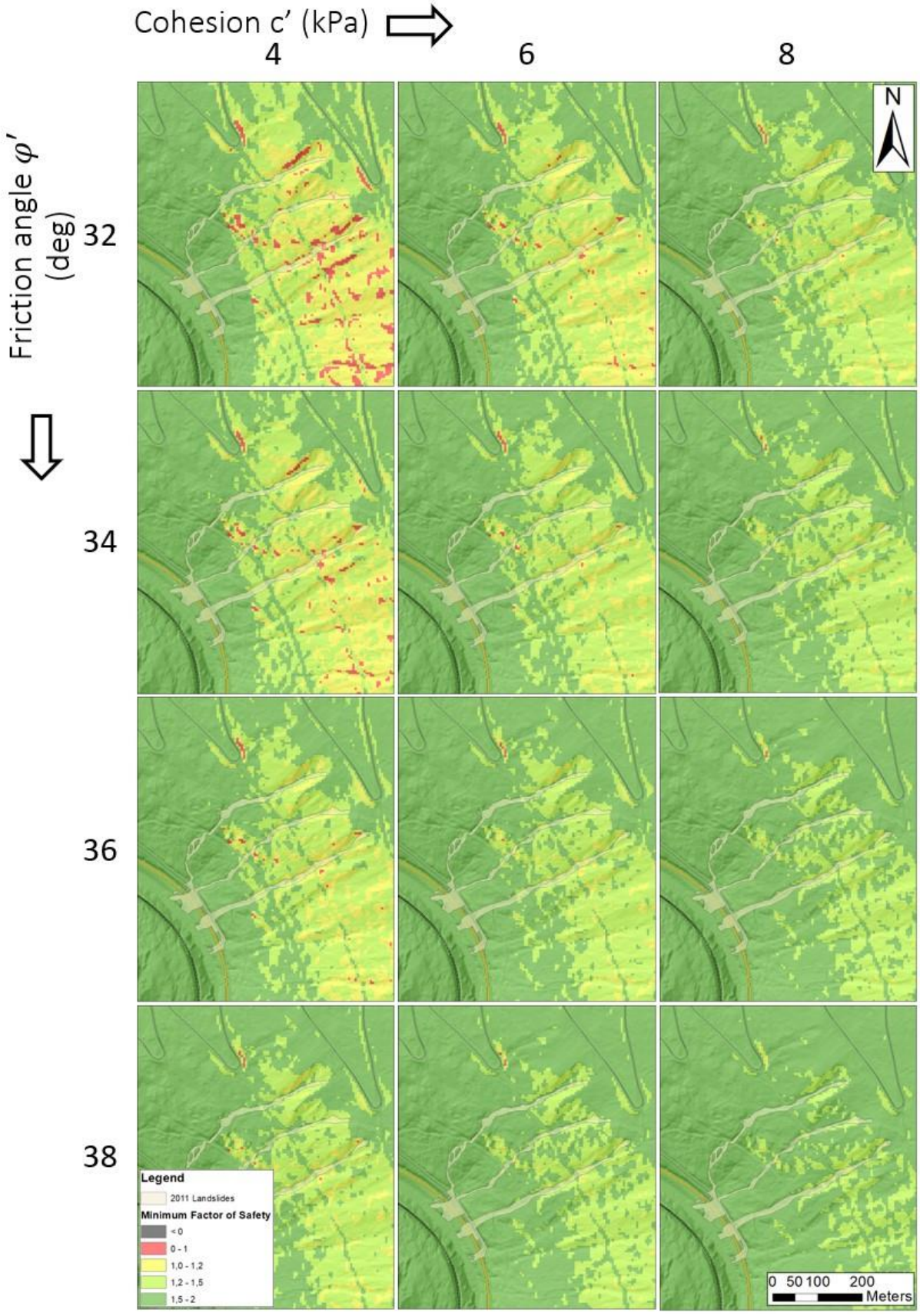

Figure 4.7 - Effect of cohesion c' and friction angle φ' on slope stability at t_0 for saturated initial conditions

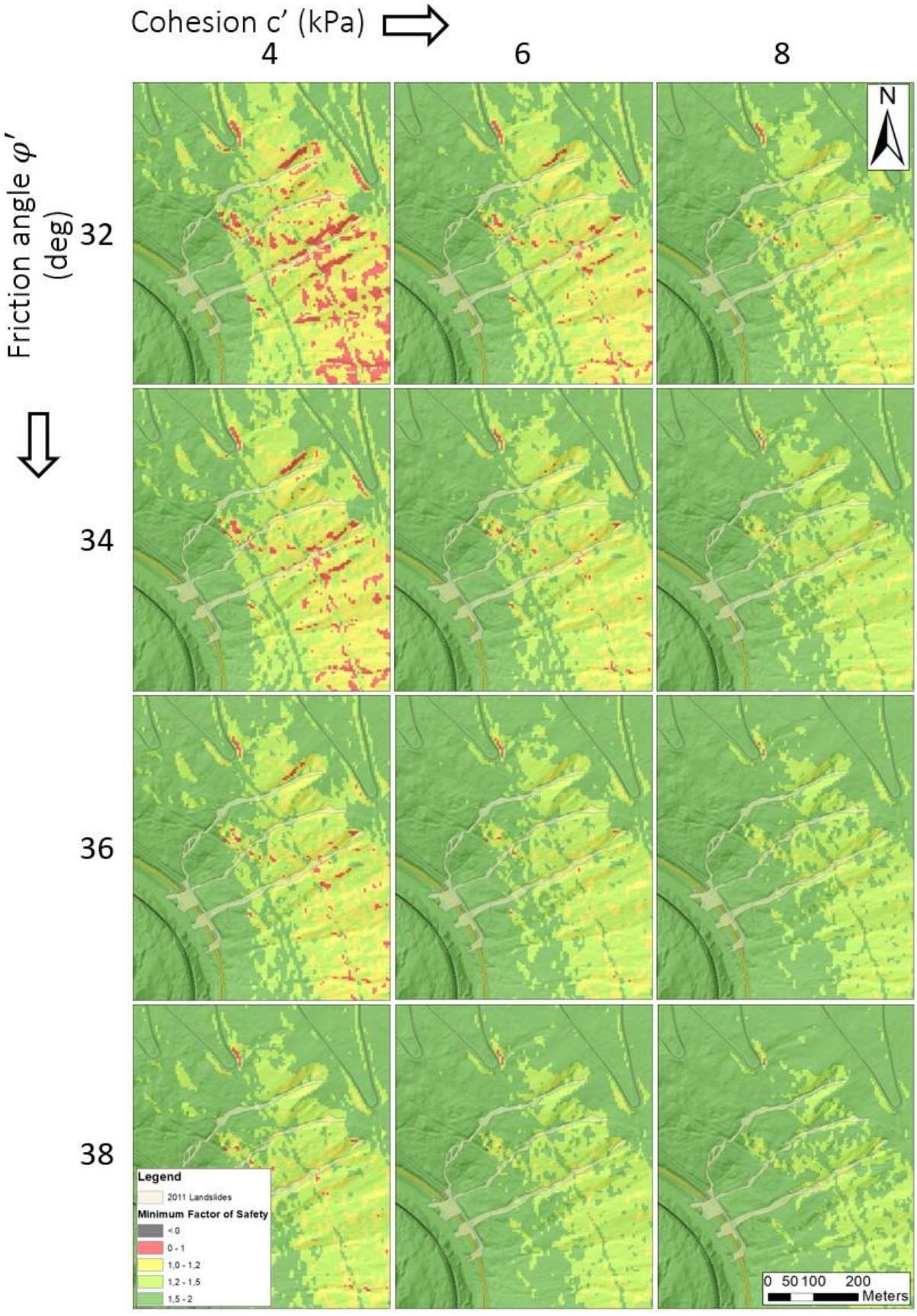

Figure 4.8 - Effect of cohesion c' and friction angle φ' on slope stability at t_f for saturated initial conditions

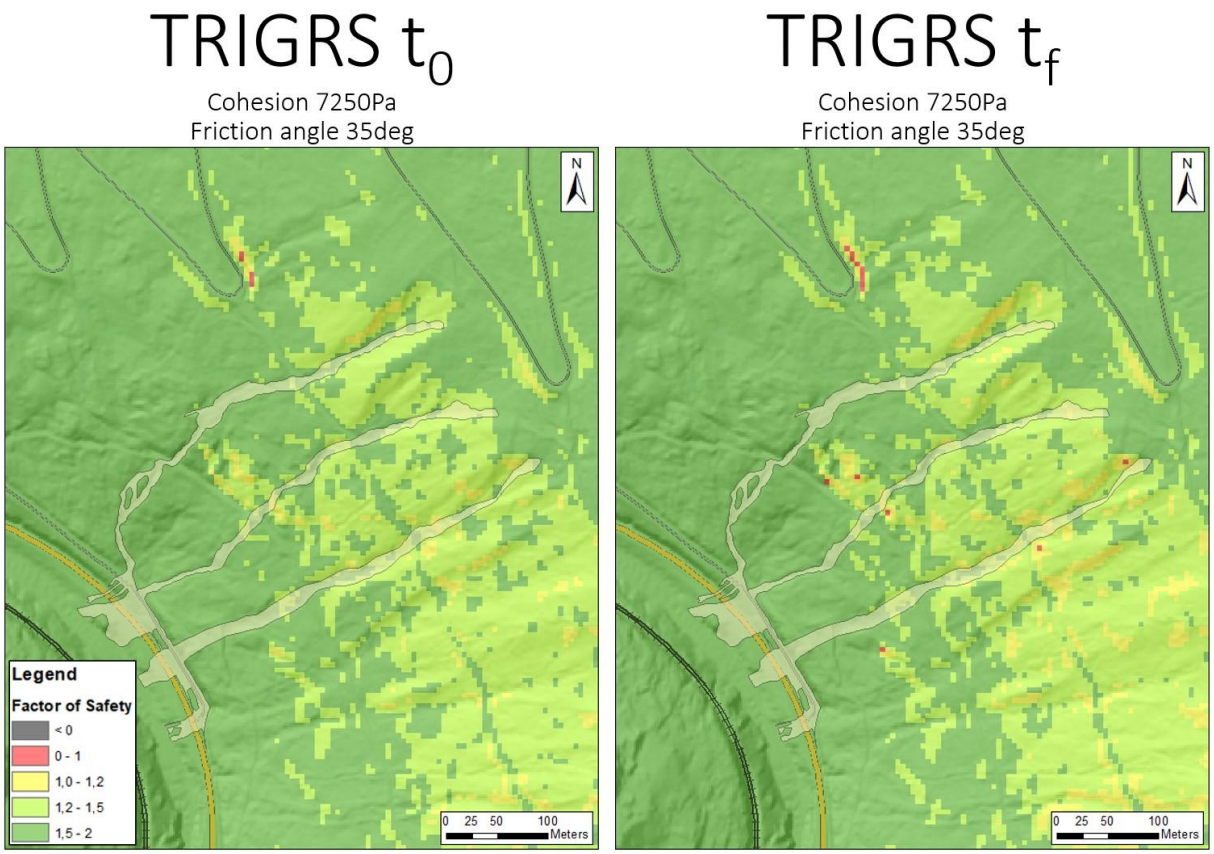

Figure 4.9 – Slope stability response to TRIGRS modelling of the 2011 event at t_0 and t_f with calibrated values.

As shown in Figure 4.9, none of the unstable cells calculated by TRIGRS at t_f match the slope failures from the landslides in 2011, illustrating the many uncertainties related to this method when high resolution input data is absent. This severe mismatch must be kept in mind for the further analysis as it represents the uncertainty of results from TRIGRS in this study. It is also worth mentioning that the failing grid cells computed from TRIGRS represent only one of two of the trigger mechanisms involved in landslide initiation. Surface erosion from streams which is likely to have had influence on the 2011 landslide scenario in Rosten, is not included in this computation. However, the desired outcome from using TRIGRS is ultimately to assess relative change in slope stability from one precipitation scenario to another. Running TRIGRS with similar saturated conditions and geotechnical parameters for different scenarios thus limits the differences from one simulation to the next to the rain-induced effect on slope stability. The uncertainties related to TRIGRS results are further addressed in chapter 6.1.1.

4.2.2 Rainfall IDF scenario modelling

To study the effect of the different precipitation scenarios with respect to the landslide scenario towards both road and railway, the study is increased from the calibrated section of Høvringslia to cover the wider section of Rosten (Figure 4.10). For these simulations, a 0.25m resolution DEM from the airborne acquisition of Nord-Gudbrandsdalen 2013 was clipped to the area of interest. It was resampled in ArcMap with bilinear interpolation to a 5x5m cell size to maintain an appropriate resolution in the TRIGRS simulation and stay consistent with the calibration inputs of the 2011 landslides. A summary of data and calibrated inputs used for the further TRIGRS stability modelling is presented in Table 4.3.

Table 4.3 - Input parameters used for the stability modelling of design value precipitation scenarios in Rosten.

Input Parameter	Symbol	Input value	Unit	Source
Slope		Spatially variable	°	5 x 5 m DEM – Nord-Gudbrandsdalen 2013
Soil Thickness	z	Spatially variable	m	Equation (9)
Friction angle		35	°	Model calibration
Cohesion	c'	7.25	kPa	Model calibration
Soil unit weight		20	kN m^{-3}	Melchiorre & Frattini (2008)
Hydraulic conductivity	K_s	1.0 x 10^{-5}	m s^{-1}	Melchiorre & Frattini (2008)
Hydraulic diffusivity	D_0	4.0 x 10^{-4}	m^2 s^{-1}	Melchiorre & Frattini (2008)
Saturated water content		0.45	-	Luca Piciullo, pers com.
Residual water content		0.05	-	Luca Piciullo, pers com.
Initial water table depth	d_{wt}	Spatially variable	m	Equation (9)
Background rainfall rate	I_{ZLT}	4.85 x 10^{-8}	m s^{-1}	SeNorge
Rainfall rate	I_Z	Variable	m s^{-1}	SeNorge

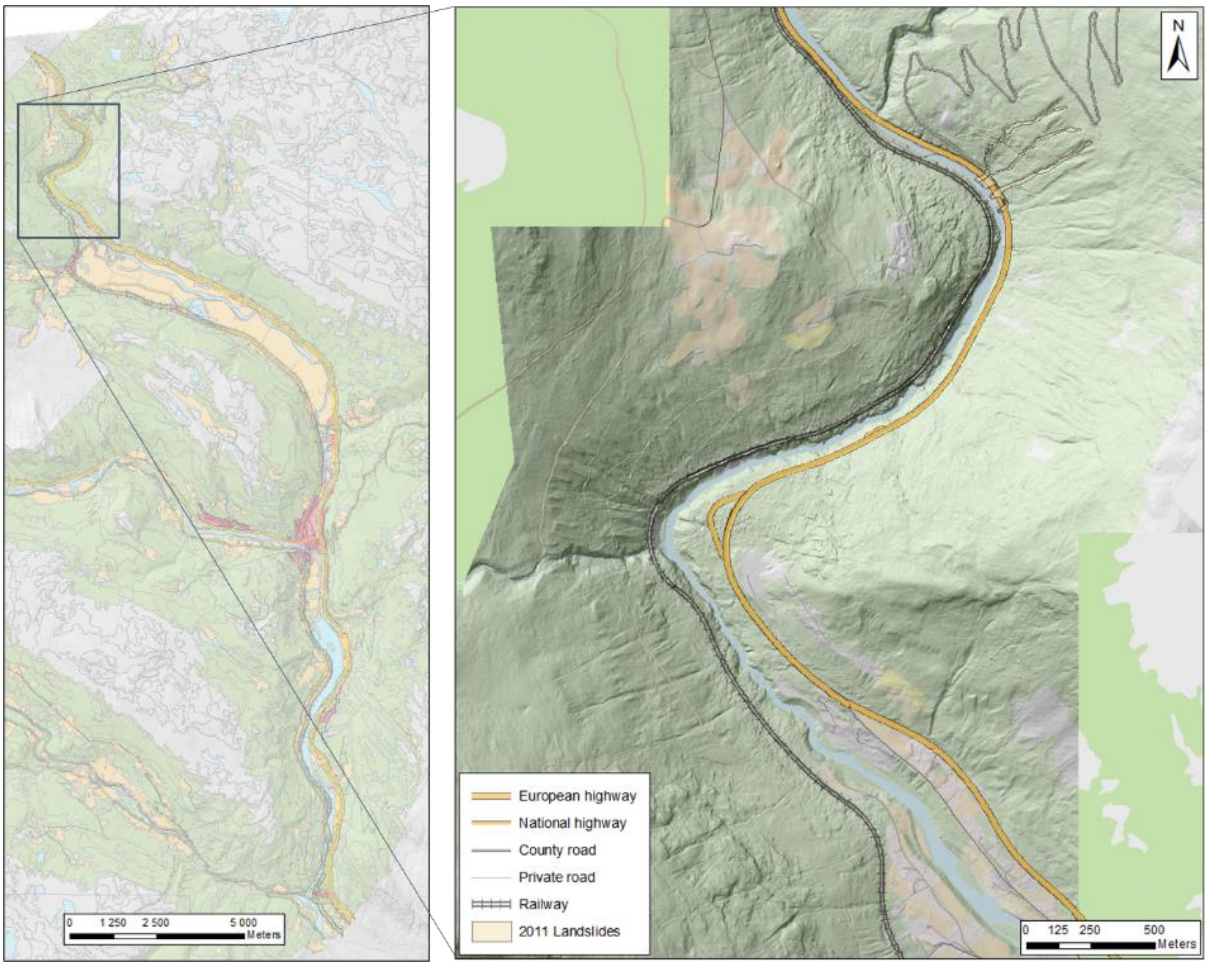

Figure 4.10 - The Rosten area subject to slope stability modelling and landslide runout analysis.

DEM adjustments

Similar to the 2011 calibration inputs, ArcMap is used to generate slope angle and flow direction maps for use as model input. The section of railway where the track runs over Roståa river causes a hydrological inconsistency as the DEM itself does not contain any drainage information. The result of this is a 10m fill of the area which is 'digitally dammed' by the railway, causing flow re-routing and potential debris flow spills over parts of the track where the river in reality has a good drainage solution beneath the railway (Figure 4.11). This issue is resolved by manually modifying the DEM with a channel shaped cut through the railway to avoid the pond-like feature and let the flow direction simulate the realistic drainage of this river.

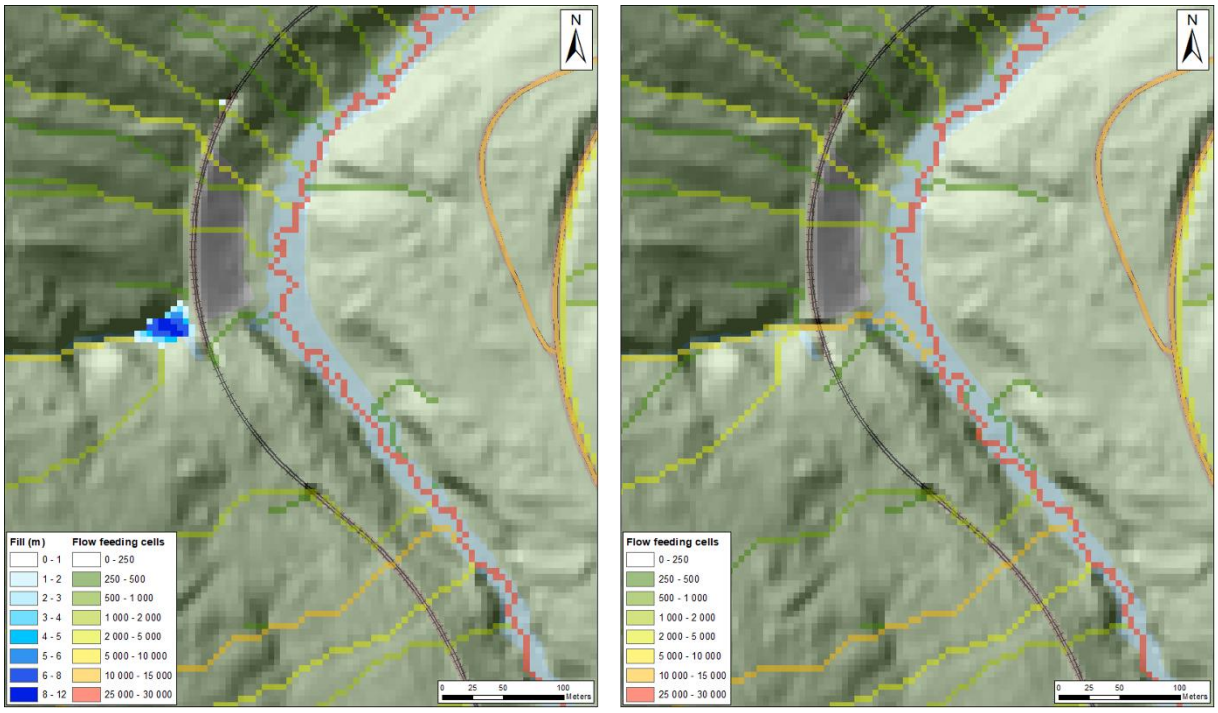

Figure 4.11 - Left: Artificial damming of Roståa river from the DEM of the railway. Right: Manipulated DEM. Cut through the railway lead the river to its natural path and allow for a hydrologically consistent DEM.

Soil thickness

Soil cover thickness estimation is carried out as explained in chapter 4.2.1. Unfortunately, no further soil depth information is available in the expanded part of the study area. Soil thickness is therefore estimated from known depths to bedrock in the 2011 landslide tracks, similar as to the model calibration. The uncertainty of the soil thickness input is consequently increasing with distance away from the calibrated 2011 landslides of Høvringslia. The result in Horgelia is thus expected to be a fair approximation of the model performance if it was put to test in an area without any depth information.

Precipitation scenarios

Four precipitation scenarios are evaluated for current and future climate based on the calibrated model parameters found from the 2011 landslides. With use of gridded intensity vs frequency (IDF) distribution curves for northern Gudbrandsdalen, 24h precipitation values for events of 20-, 50-, 100-, and 200-year recurrence interval are found. The IDF curves used are retrieved from Norsk Klimaservicesenter in January 2022 (Table 4.4, Figure 4.12). As of March 2022, gridded IDF values have become temporarily unavailable due to an update of methodology as described in Dyrrdal et al. (2022). Due to the resulting void in available IDF values for Innlandet

county after March, it is decided to use the gridded values prior to the methodology update. It is therefore likely that IDF values presented and used in this study could see changes in the near future. A 20% climate factor is added to the precipitation scenarios in accordance with Hisdal et al. (2017).

Table 4.4 - Gridded IDF values for Høvringslia, Rosten for present climate and with a 20% climate factor added for future conditions. Data from Norsk Klimaservicesenter (2022)

Rainfall recurrence interval	24h rainfall today (mm)	24h rainfall future (mm + 20%)
20 years	58.5	70.2
50 years	68.9	82.7
100 years	77.4	92.9
200 years	85.7	102.8

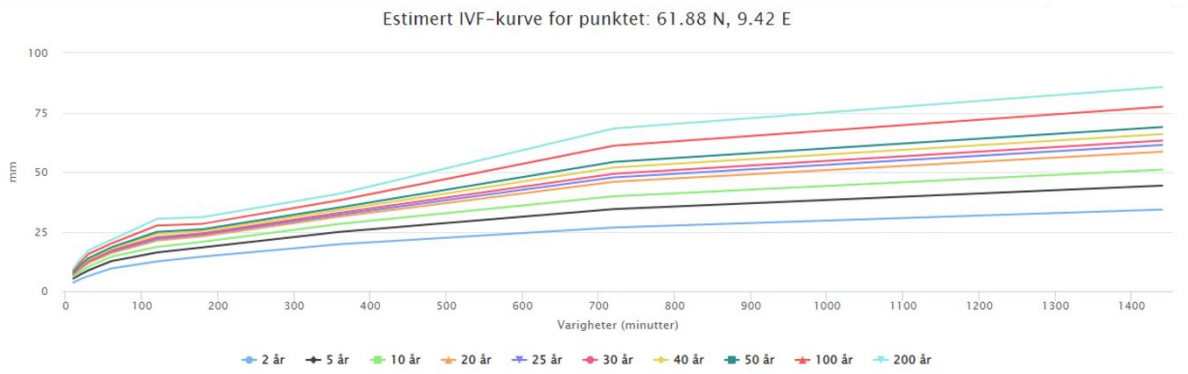

Figure 4.12 - Gridded IDF curves for Høvringslia, Rosten (Norsk Klimaservicesenter, 2022)

Flow accumulation and watershed

A useful way to visualize the runout from these failure cells is the ArcMap tool watershed. It is assumed that a failing cell will cause a flow and only stop when the terrain slope no longer encourages flowing motion. Thus, the mass will always follow the path of least resistance, i.e., the nearby terrain with the steepest slope. The same principle applies in the flow accumulation tool in ArcMap. For each cell, the path of least resistance is calculated from the neighboring cells in the DEM, and then the number of upslope cells flowing through each cell are summed. The result is a realistic picture of surface runoff (Figure 4.13). The point where the flow accumulation tool indicates a "stream" that crosses infrastructure is then used as a pour point input in the ArcMap watershed tool which determines the contributing area to the pour point. Although this is a very simple way of estimating where infrastructure will be affected by a slope failure, it may provide realistic paths for runout during intense precipitation. Even small slope

failures may flow into a stream of surface runoff which may carry the debris all the way downslope to the watershed pour point. It may also increase the erosional force of the stream and evolve into a larger debris flow on its way downslope.

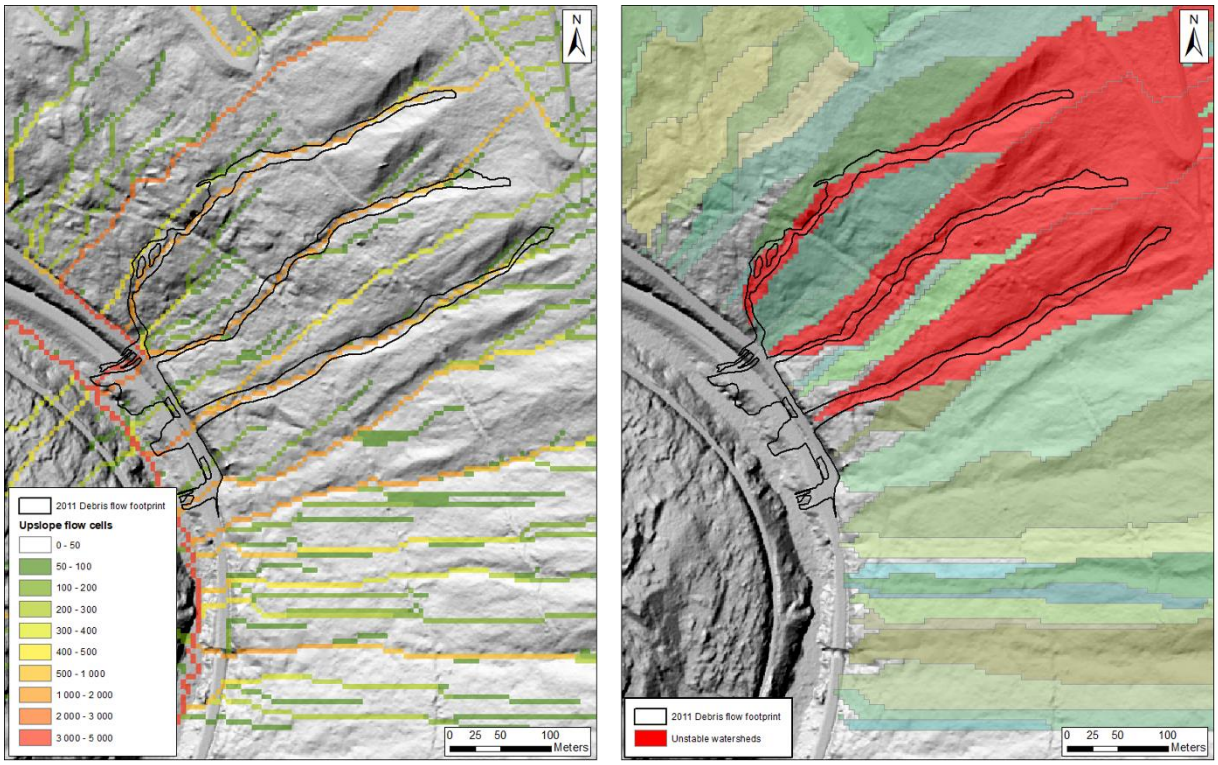

Figure 4.13 - Left: ArcMap flow accumulation tool indicate the degree of surface runoff based on number of upslope feeding cells. Note how the 2011 landslides follow the surface runoff routing. Right: ArcMap watershed tool used to delineate the area of contributing cells upslope from the spill points to the road, thus indicating the vulnerable point of road for any failure occurring within these watersheds.

4.3 RAMMS

4.3.1 Model Calibration

Like the TRIGRS workflow, the first step of runout simulation in RAMMS is to calibrate frictional parameters and erosional properties to the 2011 landslide events of Rosten. The data from this event is limited to the spatial extent of the landslide scars as indicated by aerial photographs, and the volumetric data which can be derived from difference in DEMs before and after the event. The negative difference in the post-event DEM from 2011 compared to the DEM of 2008 show a mean difference of 0.82 meters within the landslide scars. This amounts to a total volume of 7850m^3 from release and erosion, excluding debris which has been re-

deposited within the tracks. There are also parts of the track in which the difference in DEMs suggest a positive change, indicating deposition. This indicates that the total flow volume during the event has likely been significantly larger than what is indicated from the removed volumes. It is not feasible to assess the total volume of deposition as the debris flows reached the Lågen river where the material has been carried away. For the same reason, the total reach of the depositional footprint cannot be assessed. As described in Bartelt et. al 2017, the friction parameters Xi and Mu largely determine the flow velocity and range of the landslide (or more precisely the restriction of velocity and range). Lack of information about the 2011 landslide dynamics therefore makes it difficult to calibrate these values correctly. As the volume estimates are somewhat unreliable, the calibration of frictional parameters and erosion values is therefore aimed at reproducing a good match with respect to the 2011 flow track footprints. The landslide tracks documented by aerial photographs show well defined channels confined by topographic features and likely also by the erosional characteristic of the flow (Figure 4.14). Reproducing a similar morphology is an appropriate approach as the interest in a runout simulation for this study lies in determining the infrastructure at risk, which in the case of the 2011 event equals to the landslide footprint at E6 and Høvringveien.

The calibrations are run with Mu = 0.2 and Xi = 200 as recommended for unknown flows by the RAMMS debris flow user manual (Bartelt et al., 2017). Parameters for erosion rate and critical shear stress for erosion are adjusted for each simulation, while the potential of erosion depth per kPa is kept constantly high to reflect the downward erosion and channeling of runout which is indicated by orthophotos of the event. Maximum erosion, as mentioned, is set to 2 meters for thick till, and 0.5 meters for the organic humus soil cover type, reflecting the soil depth map of Figure 4.5, chapter 4.2.1 (Calibration to 2011 Rosten landslide event: Estimation of soil thickness).

Figure 4.14 - Aerial image of the 2011 landslide tracks one week after the event. Modified from Statens Kartverk et al. (2022a).

The erosion calibration illustrates how much these properties contribute to a good match of the final runout simulation (Figure 4.15). The results show significant change from the different input parameters, both with respect to runout volume and spatial distribution of flow. Only for the southernmost of the landslides are there signs of channeling in the terrain for the runouts with the greatest erosion. For the other two runouts, we see that the maximum flow corresponds well with the 2011 landslide tracks, but that significant spillage gives a generally poor match to the footprints by the simulations with medium and high erosion.

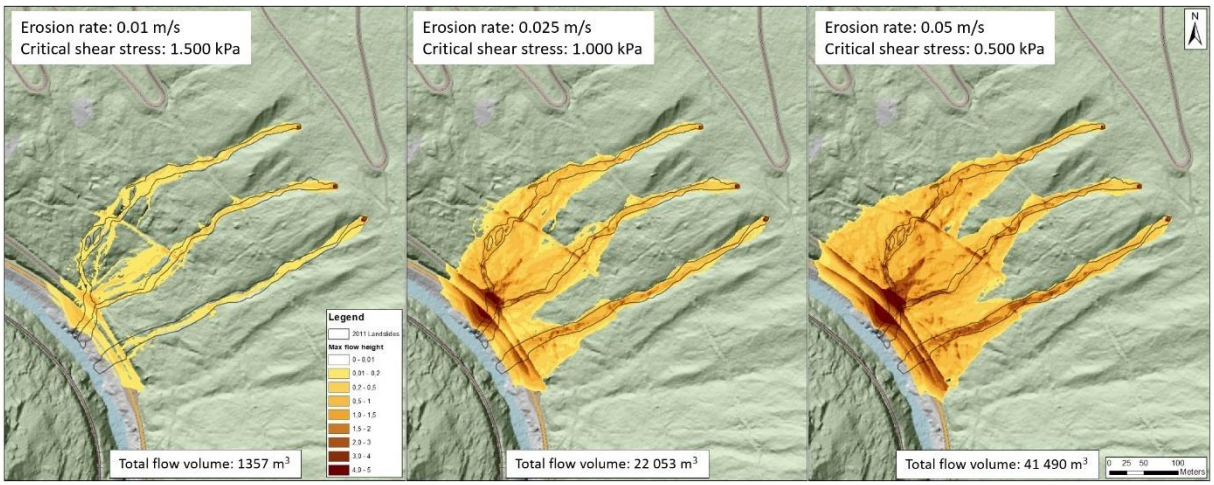

Figure 4.15 – Effect of different soil erosion properties on the runout characteristics modelled by RAMMS

For the runout with low degree of erosion, as simulated with low erosion rate and high critical shear stress, the runout shows a better fit to the observations of 2011 landslide tracks. These landslide tracks are well defined with less spill across the slope. The volume, on the other hand, is much less than what is assumed to be the case from the landslides in 2011. Given the better match of footprints, it is nevertheless this erosion model which is continued for further calibration of friction parameters.

The tested friction parameters are selected from the cluster of most frequently used RAMMS parameters as shown in the literature study by Mikoš and Bezak (2021). The calibration is carried out with 1m DEM resolution in order to capture the subtle changes in runout morphology from the different parameters (Figure 4.16). The results from this calibration show great differences in both volume and morphology. For the turbulent coefficient Xi, the calibration shows less volume when adjusted to higher parameter values. For the friction coefficient Mu, the effect on volume is somewhat less unambiguous. In general, the models show a channeling of flow in the upper part of the slope. Downslope of forest roads, secondary flow and sheet-like shallow can still be seen for several simulations, especially those of greater flow volumes. These flow spills are manually restricted by limiting visualization of the landslides to maximum flow height greater than 0.15m. Lower flow height is shown in the calibration figures as cloudy transparent white color.

The simulations using low turbulent coefficients provide a better match of flow volume with respect to the estimated 7850m^3 of the 2011 event. Although these models show a greater part of the road hit by the landslides than what can be seen from photos of the landslide event, these models accurately show how the landslides flow across the road and further into the river.

This is not the case for simulations with a higher value of Xi where the flow stops as it hits the road. Changes in the friction coefficient Mu shows how the flow is more viscous for lower values. This is particularly evident in the lateral extent of flow along the road from the point where the landslide and the road intersect. For low Mu values the deposition is limited near the point of impact, while for higher values the flow spread out sideways along the road.

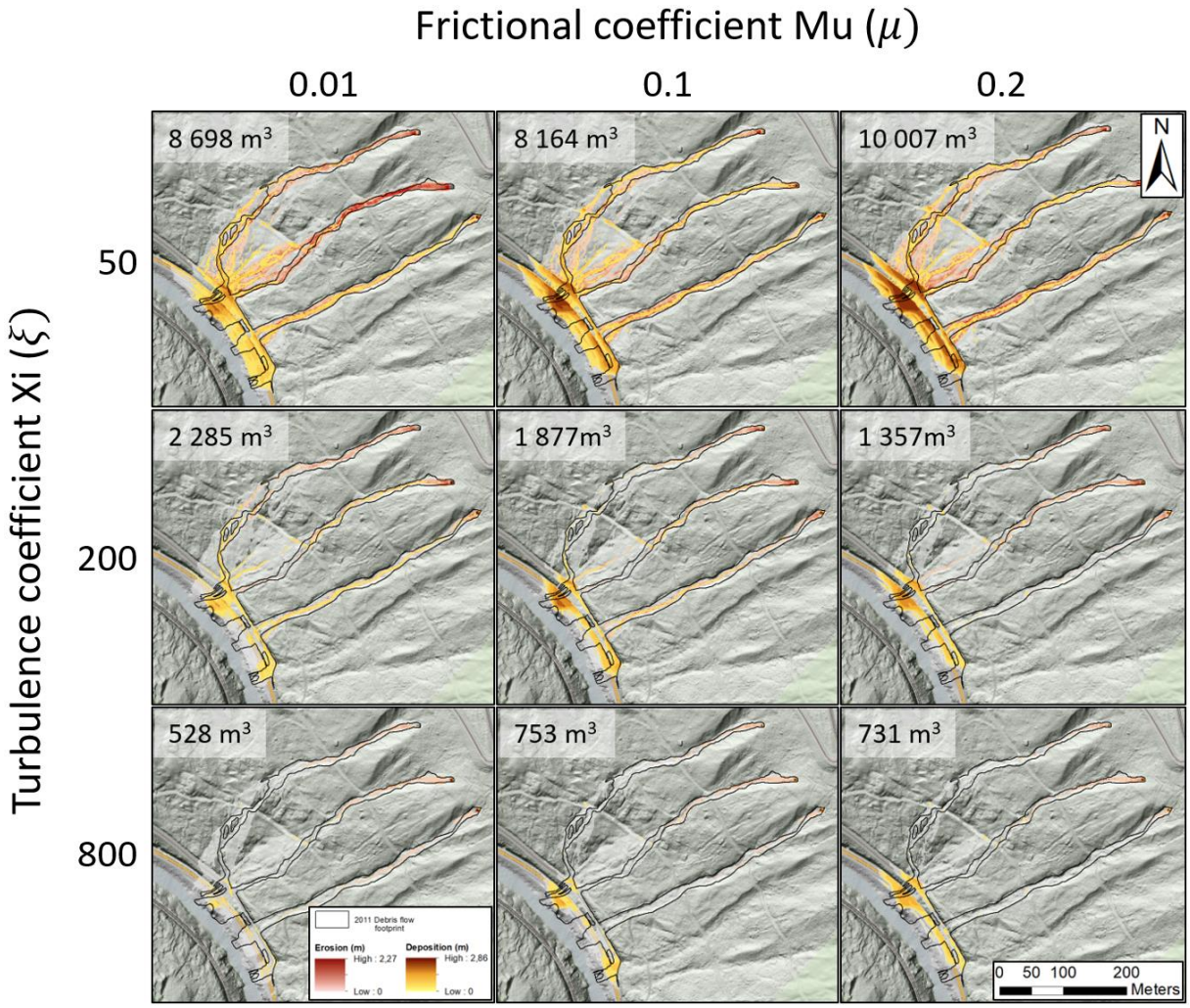

Figure 4.16 – Effect of turbulent coefficient Xi and frictional coefficient Mu on the runout characteristics modelled in RAMMS.

The final selection of parameters is a compromise between the viscous properties of flows with low friction coefficient Mu and the channeling and volume properties of flows with low turbulence coefficient Xi. Simulation with Mu = 0.05 and Xi = 100 shows a good match with the footprint from the 2011 event, with realistic runout volumes and an acceptable degree of channeling in the landslide track (Figure 4.17)

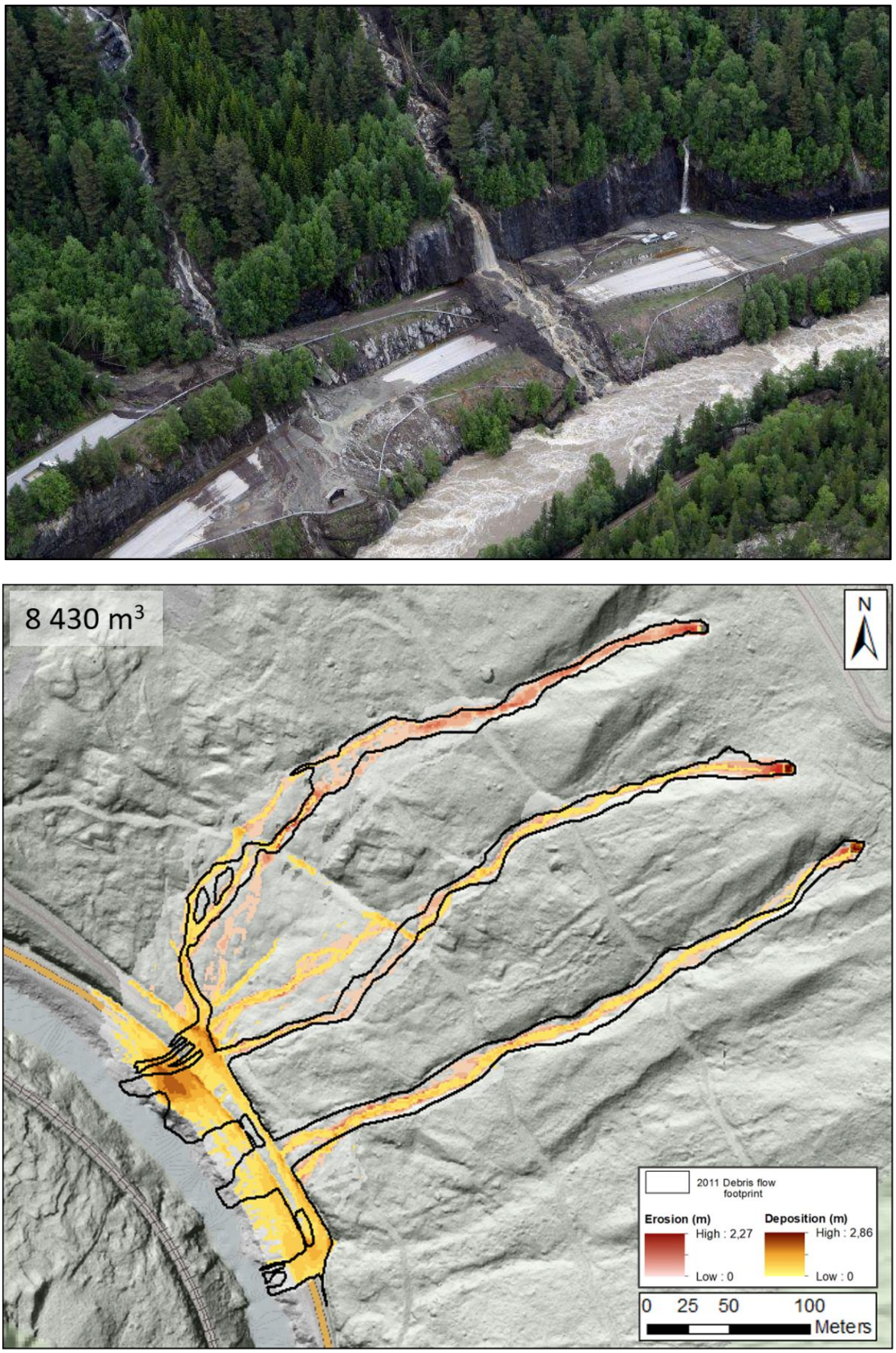

Figure 4.17 – Upper: Runout at Fv437 and E6 from the three debris flows of June, 2011 (SVV, 2012).

Lower: Best fit RAMMS runout simulation from calibration to 2011 event.

Some diversion of flow due to the flat surface of forest roads running perpendicular to the slope can still be seen. It is likely that some diversion and spills occurred in the 2011 flows, and that these are hidden by vegetation canopy in the orthophotos from the event. It is, however, clear from the photos that two of the three main flows developed distinct erosive channels through these roads. As an attempt to limit the flow diversion at forest roads, additional zones of erosion were added reflecting deep and rapid erosion at low shear stress. This proved unsuccessful, resulting in significantly greater flow volumes from the eroded material, but also greater lateral spread in the slope (Figure 4.18). Thus, specific erosional parameters for the forest roads have not been included in further models, even though it is likely that these don't behave similar to the natural terrain slope under impact by debris flows.

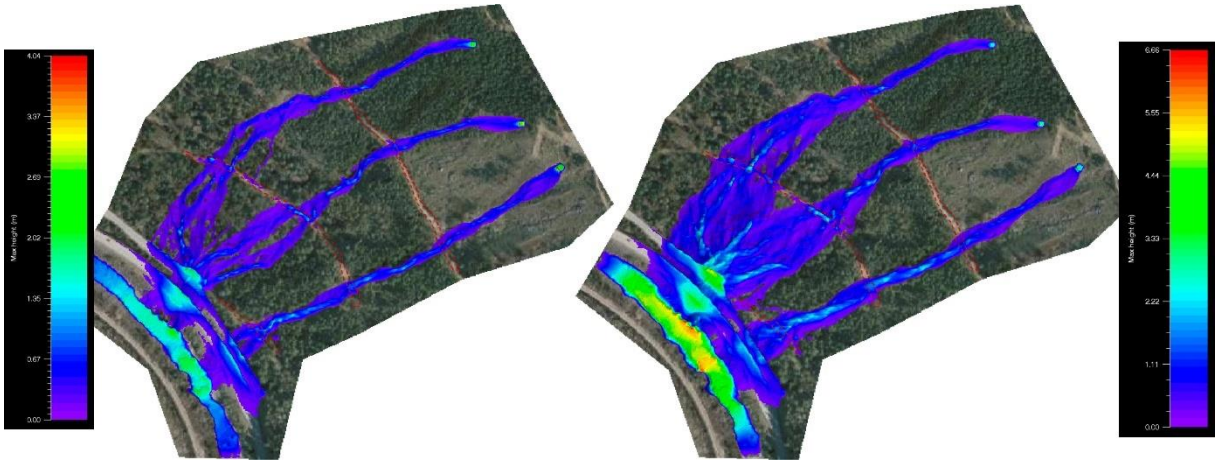

Figure 4.18 – Increased erosion along forest roads was tested as an effort to increase channeling by reducing lateral deflection from these roads. Left: Homogenous erosion parameters. Right: zones of high erosion added to forest roads.

Yield stress input is upward limited to 2 kPa, it is not possible to implement the 7.5 kPa of cohesion used for the release modelling in RAMMS. Yield stress representing cohesion is therefore not included in the runout simulation.

A summary of the input parameters used for the RAMMS runout simulation is presented in Table 4.5.

Table 4.5 – Calibrated parameters for RAMMS runout simulation

General Calculation parameters	
DEM resolution (cell size - m)	5
End time (s)	1500
Dump step (s)	5
Lambda	1
Model parameters	
Density (kg/m3)	2000
Cohesion (Pa)	-
Mu - μ	0.05
Xi - ξ (m/s2)	100
Release	
Area	From TRIGRS result
Block release / hydrograph	Block release
Subtract release from DEM	Yes
Release depth (m)	2
Release delay (s)	0
Erosion	
Erosion density (kg/m3)	2000
Erosion rate (m/s)	0.025
Pot. Erosion depth (per kPa)	0.1
Critical shear stress (kPa)	1
Max erosion thick till (m)	2
Max erosion thin till (m)	0.5
Max erosion humus/organic (m)	0.5

4.3.2 Landslide scenario runout simulation

Debris flow runout is simulated for precipitation scenarios with 20-, 50-, 100- and 200-year return period. The results from TRIGRS are used as release areas for this simulation. These are sorted in ArcMap to exclude areas which fail prior to the rainfall. (Figure 4.19). Most of these cells occur in the southwest part of the study area, furthest away from the hillside of the 2011 landslides subject to the TRIGRS calibration. Some of these failures occur where manmade cuts are made in the soil and bedrock for roads and railway, and some occur on the riverside cliffs beneath the railway. In the western railway bend in Horgelia, the Roståa river runs beneath the rails. TRIGRS indicate significant upslope failure along this river, which is not unlikely

considering how this river is cut into the slope soil cover (Figure 4.20). Despite the clear indication of instability along this river, there are no reports in NLDB or elsewhere of landslide related problems at this section of the railway. This suggests that appropriate considerations have been implemented to ensure that the river has good drainage beneath the railway. As the number of failing cells along this river cause an unrealistically large flow, it may cause spillage to nearby watersheds and mask the runout results of nearby parts of the slope. For a rainfall scenario with 20-year return period, TRIGRS indicate 90 separate release areas within this watershed. Modelling these will result in a high-consequence bias in the results. Failures in this watershed river will therefore not be modelled in RAMMS for the different rainfall scenarios.

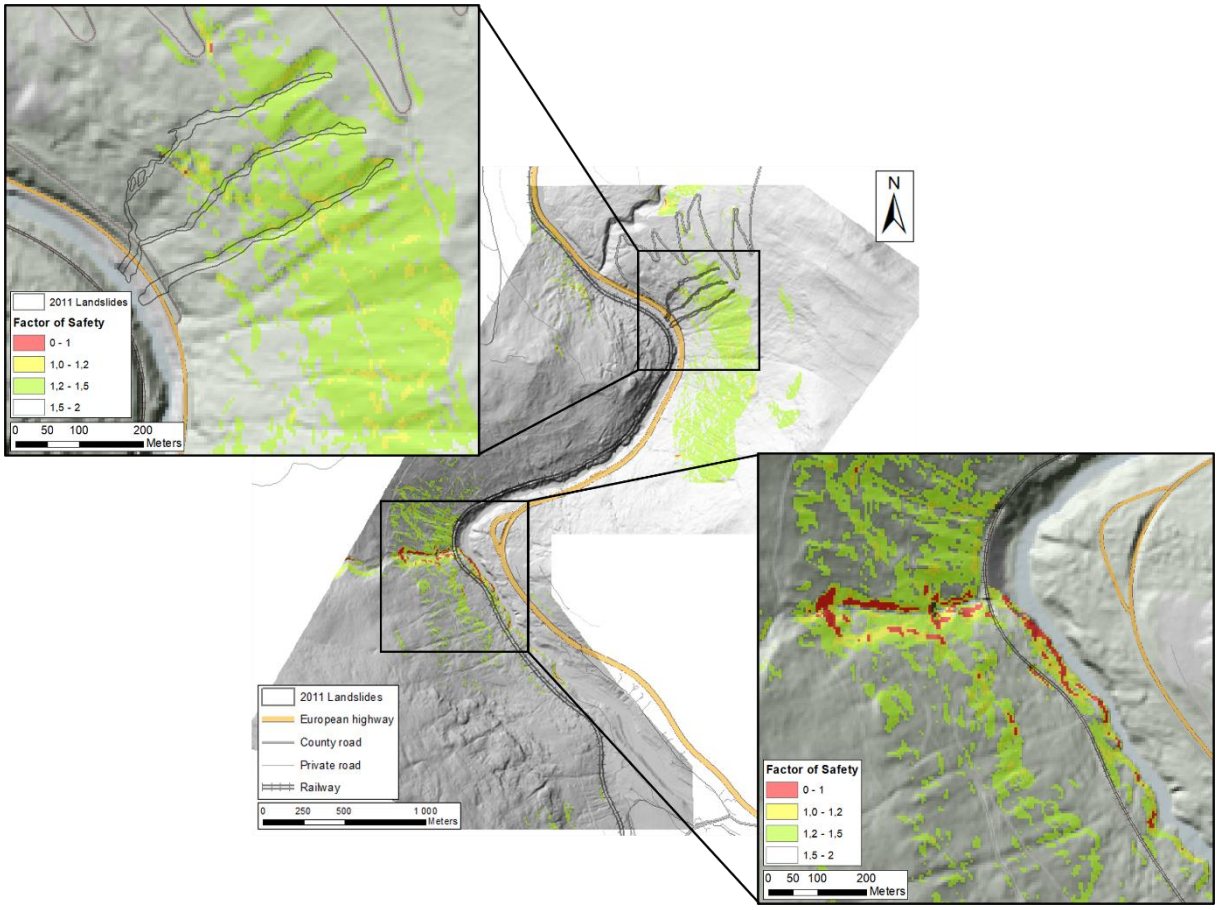

Figure 4.19 – Slope stability map of Rosten at t0 show areas of failure prior to rainfall. Most failures occur in Horgelia.

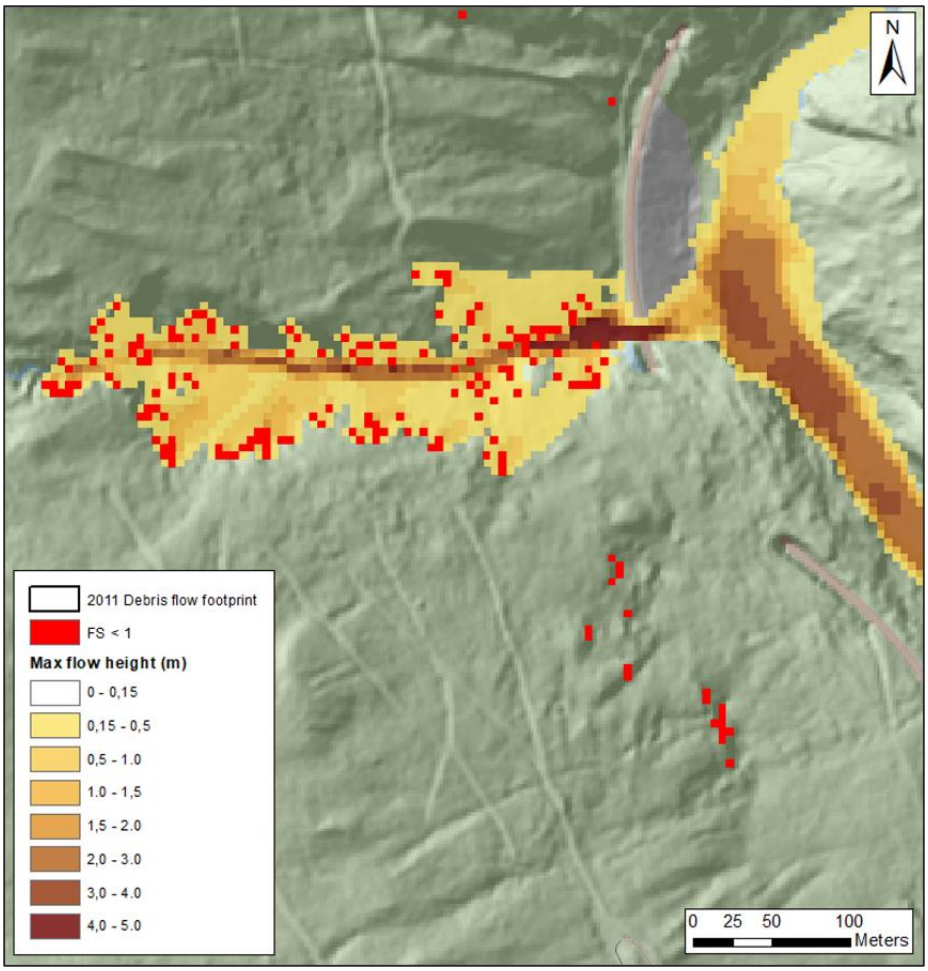

Figure 4.20 – Runout simulation of TRIGRS-release cells from a 20-year precipitation event (today) in Horgelia. The area around Roståa river illustrate significant failure.

TRIGRS failure cells are imported as polygons and set as individual release areas. Release depth is set at 2 meters for all, reflecting the soil depth of ± 2 m estimated for the thick till in the area. Output maps of maximum flow height, erosion and deposition, as well as a summary of volumes and moving mass, are then exported to ArcMap for further analysis of the model results.

5 Results

5.1 TRIGRS

Table 5.1 - Numerical results from landslide initiation modelling using TRIGRS. Results indicate number of failing cells and cells near failure as a response to different rainfall scenarios. Right part of the table shows the impact on the results when a climate factor of +20% precipitation is introduced to each scenario.

	Today (number of cells)		Future (number of cells)		Climate induced change (%)	
Rain event return period (y)	**FS < 1**	**FS 1 - 1.2**	**FS < 1**	**FS 1 - 1.2**	**FS < 1**	**FS 1 - 1.2**
20	91	2778	119	3261	30.8	17.4
50	116	3219	172	3802	48.3	18.1
100	144	3564	221	4266	53.5	19.7
200	189	3948	267	4687	41.3	18.7

These results present the number of cells with FS < 1 after removing failing cells prior to rainfall (t0). There are 482 removed cells, almost exclusively located in and around Lågen and Roståa rivers (Figure 4.19). Cells with FS of 1.0 – 1.2 at f0 are not subtracted from the final results. As mentioned in chapter 4.3.2, TRIGRS indicate an unrealistically widespread failure within the watershed of Roståa river. For all precipitation scenarios, this watershed produces more than 50% of the cells at failure for the study area. To avoid a corruption of the trends for the rest of the study area, cells in this specific watershed is excluded in the results. As seen in Table 5.1, the change in stability as response to the 20% increase in precipitation is most pronounced for FS < 1. In several cases failure occur in clusters of up to 20 cells, and as response to increased precipitation, these clusters may grow larger. Thus, an increase in the number of failing cells is not directly corresponding to the number of release areas. As described in chapter 4.2.2 – Flow accumulation and watershed, the use of delineated watersheds is a helpful tool for graphical representation of the failing cells at greater scale, as these to a certain degree also illustrate changes in landslide scenario with respect to linear infrastructure in the valley. The results are therefore shown graphically below as active or inactive watersheds in response to cells indicating failure within them (Figure 5.1 and Figure 5.2). Map view of TRIGRS cell-by-cell raw results can be seen in appendix E.

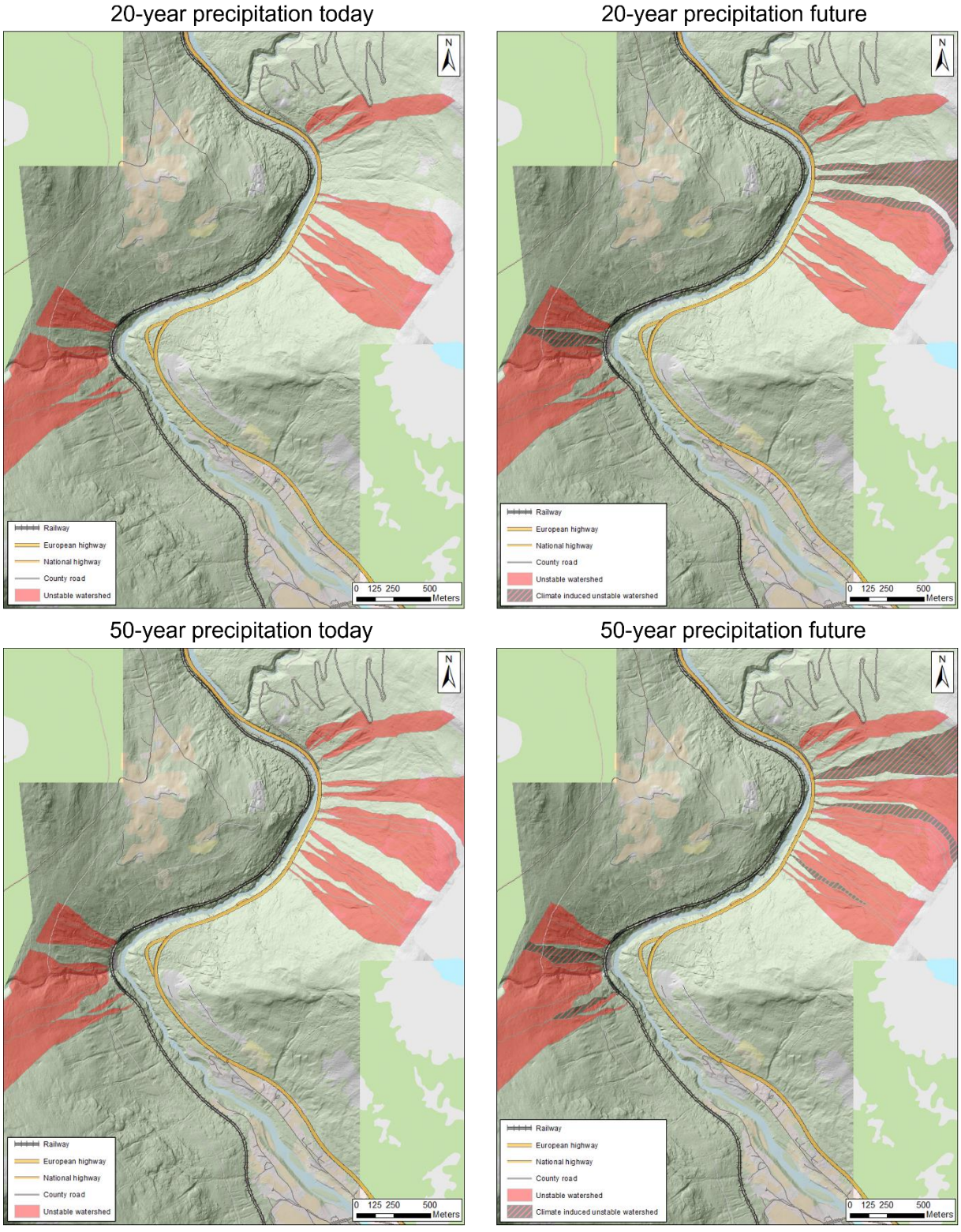

Figure 5.1 - Map view of watersheds with active slip failure during precipitation events of 20- and 50-year return period (Upper and lower figure, respectively) as indicated by TRIGRS modelling. Black/red striped watersheds indicate additional activation of watersheds for the given scenario as response to a 20% increase in precipitation.

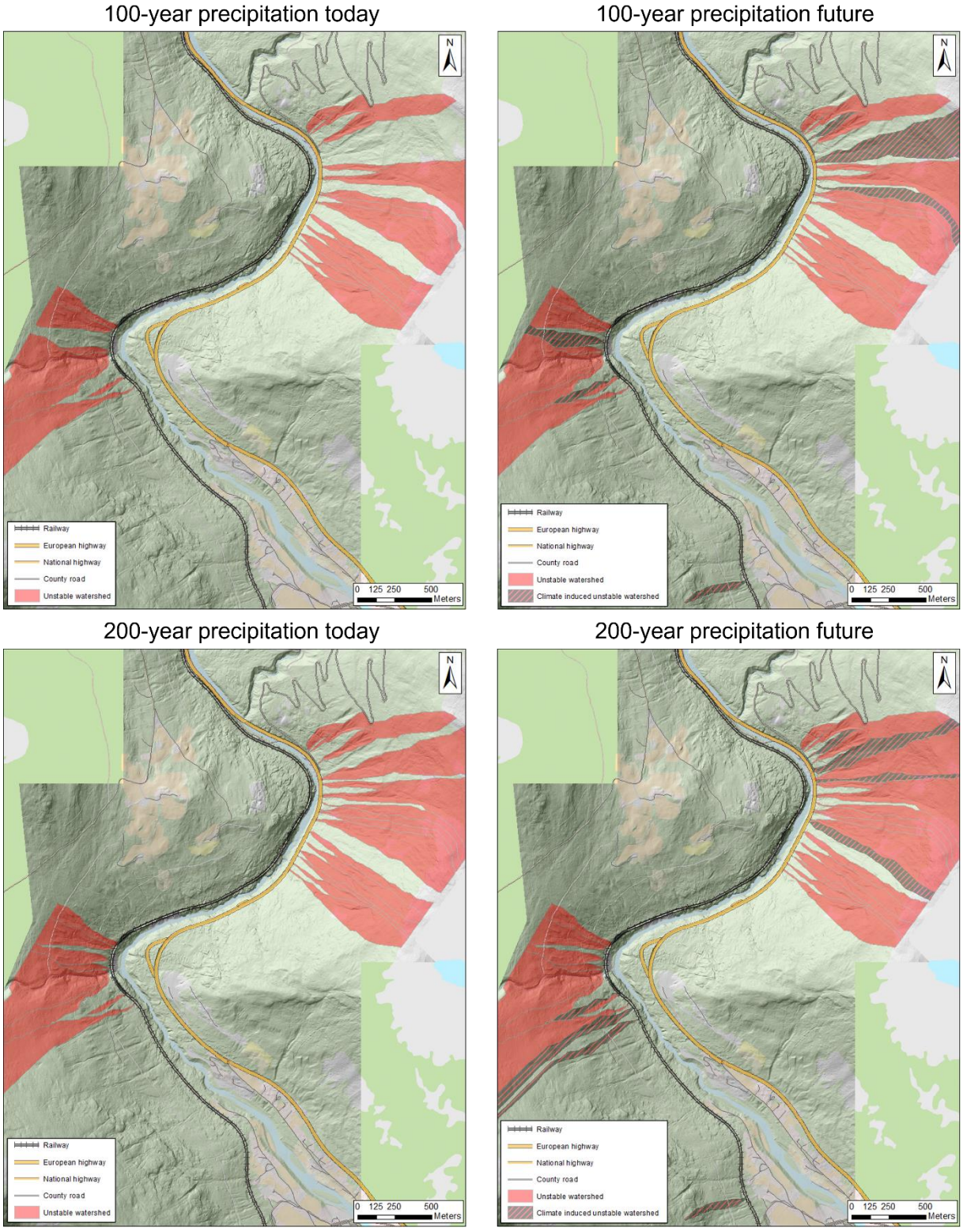

Figure 5.2 - Map view of watersheds with active slip failure during precipitation events of 100- and 200-year return period (Upper and lower figure, respectively) as indicated by TRIGRS modelling. Black/red striped watersheds indicate additional activation of watersheds for the given scenario as response to a 20% increase in precipitation.

In contrast to the numerical results presented in table ??, the 200-year precipitation event show the most dramatic change in response to climate with eight activated watersheds in addition to the ones active in present climate. Although the climate related difference in number of failing cells is 31% and 48% for 20- and 50-year precipitation events, these represent four and five new activations of watersheds, respectively. This clearly illustrate the clustering effect of the failure cells, and how an increase in precipitation often causes new failures in already active watersheds. Clustering of failure cells does, however, influence runout volume and therefore also the runout dynamics. For the relative degree of landslide activity within each watershed and the relative changes in landslide scenario, we must look to the RAMMS runout simulation.

An interesting observation throughout the different rainfall scenarios is the early outline of endpoint watersheds along the infrastructure, illustrating the most hazardous stretches of road and railway. Except for a southward extension of hazardous watersheds along the railway, the newly activated watersheds all occur within the stretch of previously active watersheds. For the southernmost part of the focus area, note how a new watershed is activated in a different part of the valley for future events of 100- and 200-year return period rainfalls.

5.2 RAMMS

Following are the results of runout simulation from the precipitation induced failure results from TRIGRS (Figure 5.3 and Figure 5.4). Keep in mind that the return period representing each runout simulation does not reflect the return period of the landslide scenario, but rather the simulated stability response from a 24h rainfall event with the given statistical recurrence interval. The return period of the landslides are likely shorter as other trigger conditions such as intense snowmelt or a combination of moderate snowmelt and rainfall could initiate failure as well.

The maximum flow height output from RAMMS is used to illustrate the different runout scenarios from the release areas modelled with TRIGRS. As illustrated in Figure 4.16 and Figure 4.17 in chapter 4.3.1, the calibration results with best match to the 2011 Rosten landslides in terms of volume estimations and track footprint, includes limiting the display of the landslide to flow height> 0.15m. This limitation is introduced to decrease the amount of spillage resulting from lack of channel confinement in the model.

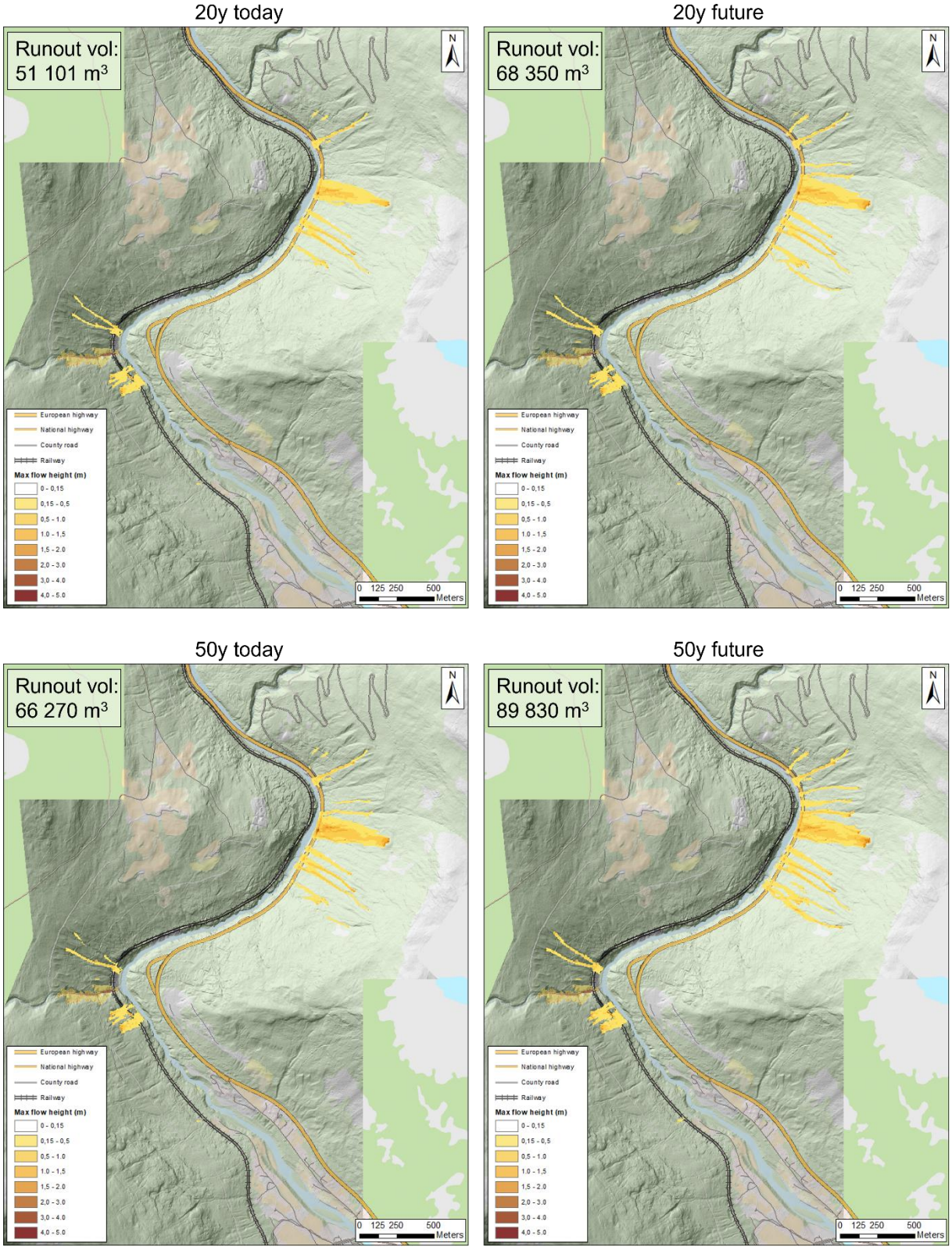

Figure 5.3 - RAMMS runout simulation of landslides initiated by precipitation events of 20- and 50-year return period (Upper and lower figure, respectively). Release areas correspond to grid cells of FS < 1 from TRIGRS modelling of the respective events.

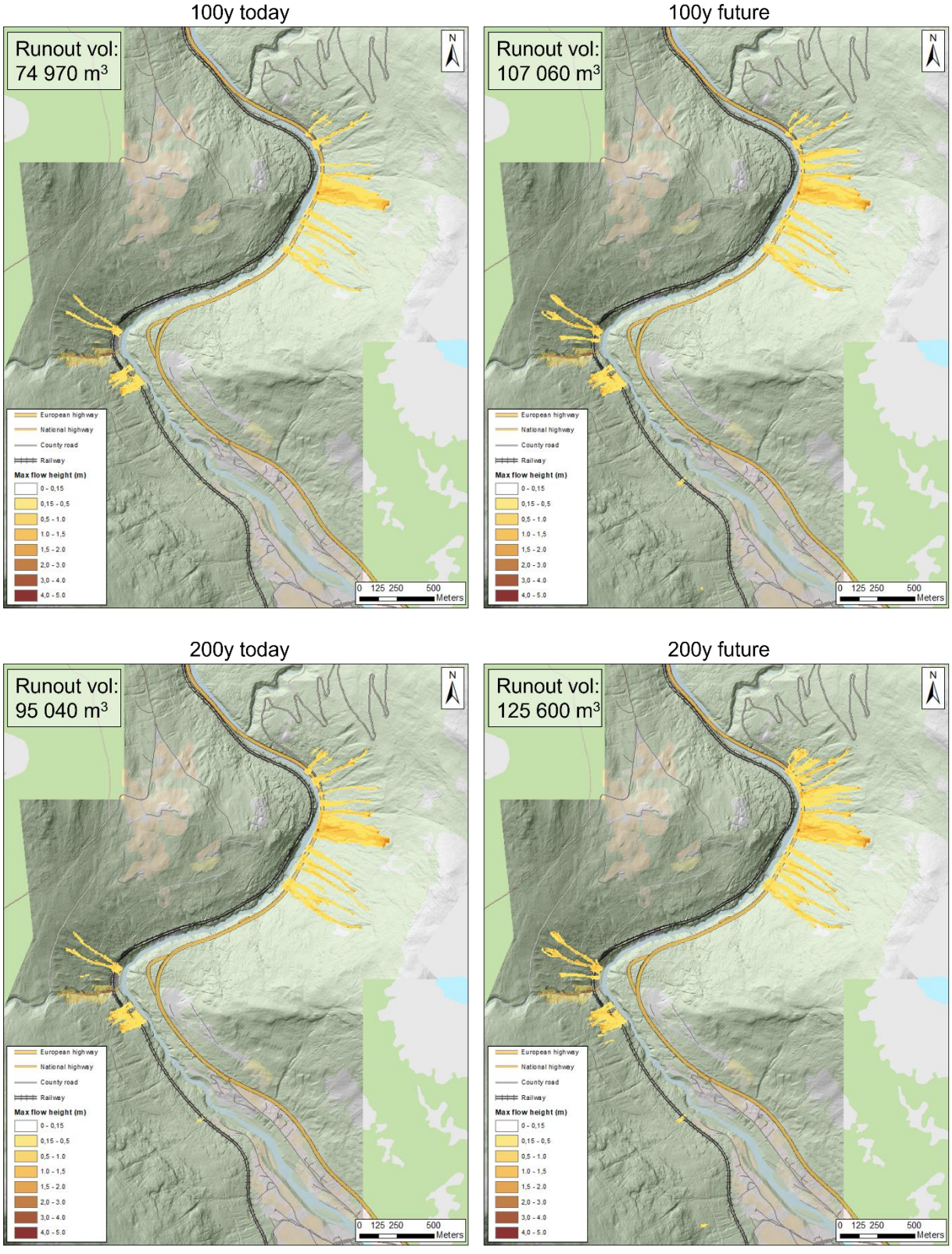

Figure 5.4 - RAMMS runout simulation of landslides initiated by precipitation events of 100- and 200-year return period (Upper and lower figure, respectively). Release areas correspond to grid cells of FS < 1 from TRIGRS modelling of the respective events.

As shown in the TRIGRS results, extensive failure is indicated for the area along the Roståa river by the western railway bend. When modelling these in RAMMS, it is likely that the combined flow from all the release areas spill into other parts of the slope, and thus challenging the integrity of the results. Cells indicating failure in this area have therefore only been modelled with a rainfall event of 20-year return period of the current climate. The runout from this simulation is shown with a 50% transparency in the presentation of the results to indicate the uncertainty related to the area. The results are also cut where the landslide tracks run out into the Lågen river as this is regarded as a relatively flat surface in RAMMS, causing an unrealistic runout pattern with both up- and downriver flow.

The runout volume calculations in RAMMS are made up of two parts - release volume and added volume from runout erosion. Release volume largely follows the number of new failure cells calculated from TRIGRS as presented in Table 5.1. Exceptions are new cells of failure in the mentioned watershed around Roståa river, as well as failure cells indicated in steep areas of exposed bedrock in railway- or roadcuts. The size of release areas also vary in response to slope angle as the 2D grid of failure cells is draped onto the 3D terrain surface in RAMMS. Eroded volume depends on the shear stress exceeded by the flow onto the slope surface and is thus largely controlled by the release volume, as well as the flow velocity generated by the terrain gradient in which a landslide is initiated.

Table 5.2 shows significantly less change for the runout volume in response to the different climate scenarios compared to the TRIGRS results. One explanation for this could be that a number of the new failing cells indicated by TRIGRS occur downslope of existing release areas, thus not introducing new volume as they are already included from erosion in previously modelled events.

Table 5.2 - Volume estimations from RAMMS runout simulations of precipitation events with different statistical return period.

Rain event return period (y)	Present climate runout volume (m3)	Present climate runout volume (m3)	Climate induced change (%)
20	56 101	68 350	21.8
50	66 270	89 830	35.5
100	74 970	107 060	42.8
200	95 040	125 600	32.2

5.3 Infrastructure exposure

Results from RAMMS runout simulations has been used to assess infrastructure vulnerability for the different rainfall scenarios. In contrast to the display of active watersheds and their pour points to roads and railway, RAMMS analysis provides a more realistic impact scenario for the infrastructure as the relative amount of failure in an area as well as runout dimensions have been implemented. Similar to the presented runout simulation results RAMMS, max flow height > 0.15 m is the basis for the results that is used to indicate the flow intersection with road and rail.

Table 5.3 - Vulnerability analysis of linear infrastructure in Rosten by landslides from precipitation events of different statistical return period.

Rainfall return period (y)	Elements at risk, present climate (m)			Elements at risk, future climate (m)			Climate induced change (%)		
	E6	Fv437	Railway	E6	Fv437	Railway	E6	Fv437	Railway
20	452	53	204	607	72	204	34.3	35.8	0.0
50	517	56	206	737	78	230	42.6	39.3	11.7
100	651	83	209	771	91	270	18.4	9.6	29.2
200	770	84	230	869	134*	277	12.9	59.5	20.4

The results presented in Table 5.3 clearly indicate a more severe increase in amount of vulnerable road compared to railway for the two events of 20- and 50-year return period. In fact, there is no change in the railway vulnerability in a 20-year rain event today and in the future. There is a more significant increase in vulnerable portions of railway for the two events of 100- and 200-year return period. For the same two periods, the expansion of vulnerable road is decreasing. The large variations in climate induced change for Fv437 is largely due to a very short area of exposure to the modelled landslides. One small runout in this section of road therefore equals to a great change in vulnerability percentage. In addition, a significant contribution to the increase of vulnerable road at Fv437 for the 100- and 200-year events, is from runout along the short, flow-parallel section of the road at the intersection with E6.

The following figures show the spatial development of vulnerable infrastructure in response to the different rainfall scenarios (Figure 5.5 and Figure 5.6).

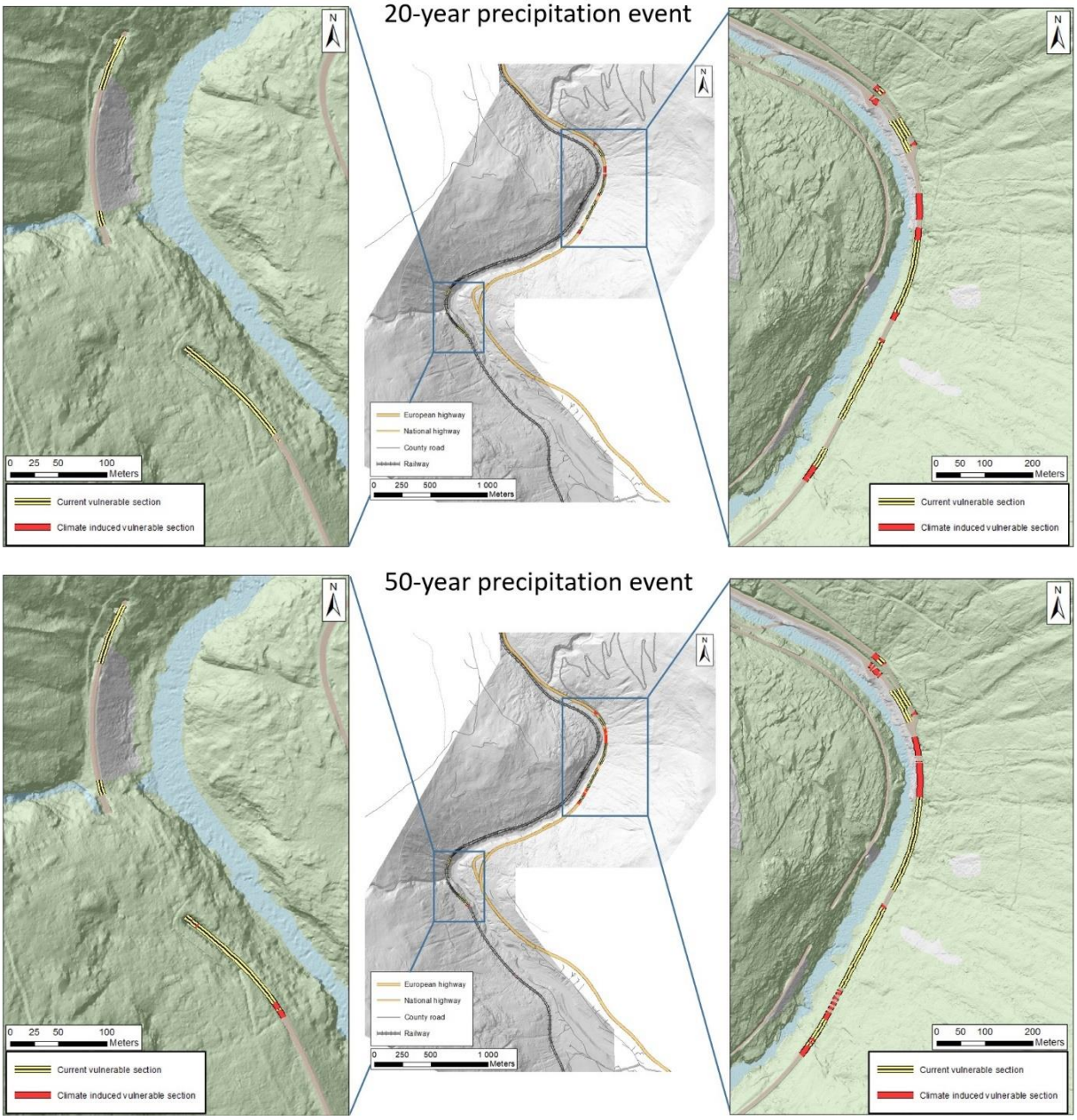

Figure 5.5 - Map view of the spatial development of vulnerable infrastructure as a response to precipitation events of 20- and 50-year return period (Upper and lower figure, respectively). Areas along the road and railway indicate the sections of infrastructure intersected by the RAMMS-simulated landslide runouts of the respective events.

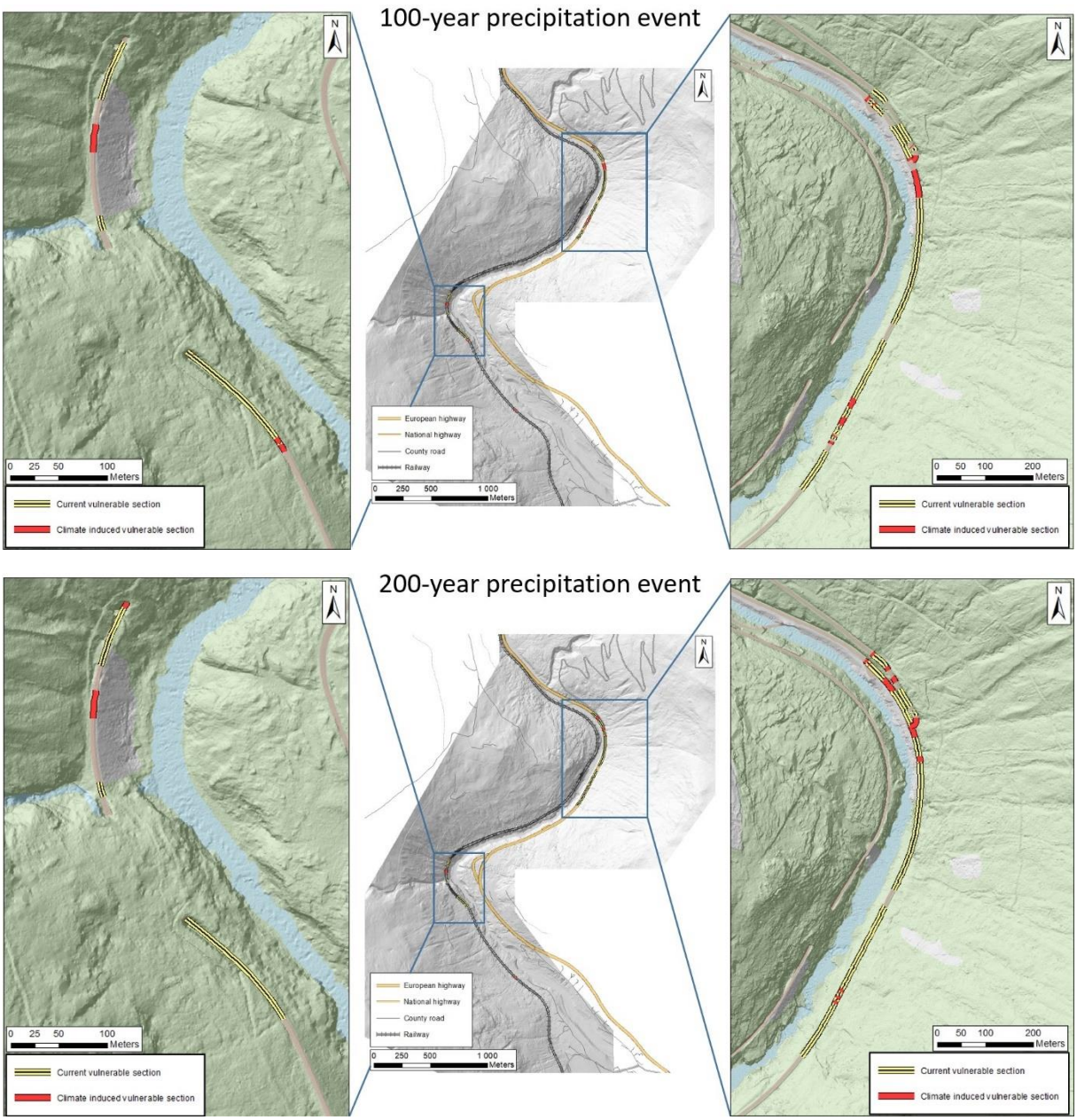

Figure 5.6 - Map view of the spatial development of vulnerable infrastructure as a response to precipitation events of 100- and 200-year return period (Upper and lower figure, respectively). Areas along the road and railway indicate the sections of infrastructure intersected by the RAMMS-simulated landslide runouts of the respective events.

The results show a greater change between the different climate scenarios compared to the change between precipitation scenarios of different recurrence intervals. Because of this, the climate-induced vulnerable sections of infrastructure overlap between the different return intervals. Similar to the results for active watersheds, the vulnerable sections of roads and railway shows how the exposed areas are limited to a particular part of the valley. This section is already well-defined during precipitation events of 20 years return period. A further increase in precipitation is then seen in form of an increasing amount of road and track that is hit because of new initiation of landslides and greater spill effect from existing runouts in the already active landslide area.

The results suggest a relatively even distribution of new affected sections along E6 within the already hazardous area. For the 200-year event, most climate induced increase in vulnerable sections are found in the northern part of the focus area, coincidently the same part of the road section which saw the greatest impact from the 2011 landslide event which the models are calibrated to. As the 2011 event had the 24h rainfall of approximately 20 years statistical return interval, this illustrates some of the spatial uncertainties related to this analysis.

For the railway, the analysis shows a climate induced increase in vulnerable track towards the south for events of 50- and 100- years return interval. For events of 200-year return interval, the increase is seen in the northern part of the railway focus area. It is evident that the tunnel in the middle of the railway focus area protects parts of the track from potential runout for all precipitation scenarios. The upper tunnel, however, serves protecting purpose for future events of 200-year recurrence interval or greater.

The southernmost watershed which is indicated as unstable for future events with return period greater than 100 years (Figure 5.2), does not affect the railway according to the RAMMS runout simulation. This shows how a modelled slip failure not necessarily always produces a landslide with significant downslope consequences but is also dependent on flow-inducing terrain and/or nearby cells to produce significant runout.

6 DISCUSSION

6.1 Results and model performance

As the climate factor of 20% is greater than the difference between the individual precipitation events, the increase in precipitation also shows a greater impact on the slope stability for a given recurrence interval than what can be seen when comparing slope stability from one design event to the next.

For the four different precipitation scenarios tested, the results show a climate induced change of 31, 48, 53 and 41 percent in number of failing cells in response to a 20 % increase in precipitation. These numbers suggest that for Rosten, as well as for other landslide prone areas with similar conditions, landslide release probability have a stronger response to climate change than the recurrence interval of the precipitation. The same effect can be seen in runout volume estimations for all events, and for several events in the road and railway vulnerability analysis. For the latter, the increasing effect is largely due to new runout filling out the gap in-between already vulnerable sections, thus leading to a drop in climate induced vulnerability increase as more and more of the landslide prone section of infrastructure is active for the corresponding precipitation event of present-day climate.

The most appropriate comparison of results to other studies in the area, is seen when comparing the climate induced increase in TRIGRS release areas with the results from Jaedicke et al. (2008). This study was concentrated in an area of similar size concentrated around Otta as a part of the GeoExtreme project. For a precipitation event corresponding to a 100-year return interval, they saw areas of up to 25% increase in probability of failure when applying a 20% increase in 24-hour rainfall. This supports the result of an amplification of the climate induced increase in slope failures compared to the increase in extreme precipitation. It also indicates that the 53.5% increase in failure cells for a 100-year design event in this study represents an over-estimation of climate induced hazard. The other study of climate induced increase in hazard in the area is the one of Melchiorre and Frattini (2012). Considering a wide range of climate scenarios, their results indicate a systematic decrease in slope stability for worst case climate scenario. Potentially masked by the uncertainty related to the climate models, they did however declare the trends as statistically insignificant. The increasing trend was found most

pronounced for events without antecedent precipitation, whereas scenarios with significant wetting of the soil prior to the extreme event show little change from present climate to any of the future climate scenarios. This conflicts with the results of the present study as saturated soil are considered as initial conditions for all modelled scenarios. Other studies on a broader regional or national level, however, conclude on an increase in future precipitation induced landslide hazard without estimation of probability of failure or increase in number of landslides(Dyrrdal et al., 2012; Frauenfelder et al., 2017; Hanssen-Bauer et al., 2017). Gariano and Guzzetti (2016) did a literature review on landslide-climate studies and found that about 80% of the studies conclude on causal relationships between increase in climate change and increase in number of landslides. They did, however, point out that there is a bias towards regions of high landslide activity (e.g., Southern Europe, North America, Scandinavia).

In general, these other studies support the predictions of an increase in rainfall induced landslides for the future. Registered events of landslides in Rosten do however, suggest that the presented results for both present and future climate conditions, show an over-estimation of hazard towards the infrastructure. To understand the integrity of the coupled results, it is necessary to investigate the performance of each individual model.

6.1.1 TRIGRS performance

When assessing the hazard towards infrastructure it is practical to investigate the large-scale stability of watersheds, as these often correspond to the topographic confinement determining flow runout routing. On watershed level, the calibrated stability model performs well in outlining unstable watersheds with good correspondence to the runout of the 2011 landslides.

On a smaller scale however, the limited cell-by-cell performance of TRIGRS causes a great number of false failure predictions for each correctly predicted failure. This forces the model operator to choose an appropriate balance between accurate predictions and number of failures. As this study aims to produce a realistic runout scenario towards infrastructure, a high rate of false positive rates is acceptable.

The main limitation of TRIGRS, and reason for the poor cell-by-cell accuracy, is the detail of physical characteristics of surface and sub-surface required to successfully capture the natural

variations of a slope. The quality of the results from TRIGRS modelling is therefore strongly related to the aggregated quality and uncertainty of the input parameters. In addition, the modelling methods itself is based on a few assumptions which adds to the total uncertainty. One such assumption is a homogeneous soil with nearly uniform material properties both laterally and vertically. As described in chapter 3.1.3 (Controlling factors: Material properties of soil), these properties may however, have significant variations within one type of soil.

Changing geotechnical parameters and rainfall intensities only changes the factor of safety in a scaled relation for all cells. In other words, from a series of model simulations with different geotechnical parameters and rainfall intensities, the cells at failure will be the same every time, occurring in the same order. The input determining the relationship of FS between the different cells, and thus the cell-by-cell accuracy of results, are the spatially dependent model inputs. The three following parameters are thus likely to have the greatest influence on the model performance:

- Soil depth
- Slope inclination
- Flow direction

Soil depth is found to be one of the input factors with the greatest impact on slope stability (Schilirò et al., 2021). With no available thickness data in Rosten, accuracy of this input is reduced to a best-fit estimation derived from DEM comparison, adjusted to slope angle and idealized soil type thickness.

The slope inclination is derived from high detail DEMs and is thus generally of good quality. Its accuracy is however naturally reduced for a 5 x 5m resampled model compared to the original DEM, thus also affecting the model with respect to terrain detail.

An accurate flow direction grid, as well as subsequent flow direction grid, is largely dependent on a hydrologically correct DEM. The calibrated results from Høvringslia shows the most accurate stability results for the southernmost landslide of 2011. Of the three landslides, this has the only release area which is not significantly affected by the upslope road with respect to surface runoff routing. The same effect can be seen in the landslide susceptibility maps of Rosten, which also fail to include the release areas of the two 2011 landslides downslope of the road (Figure 6.1). These release areas suggest a drainage pattern at the road which is not accurately represented by the DEM, either from culverts, damming and spillage or both.

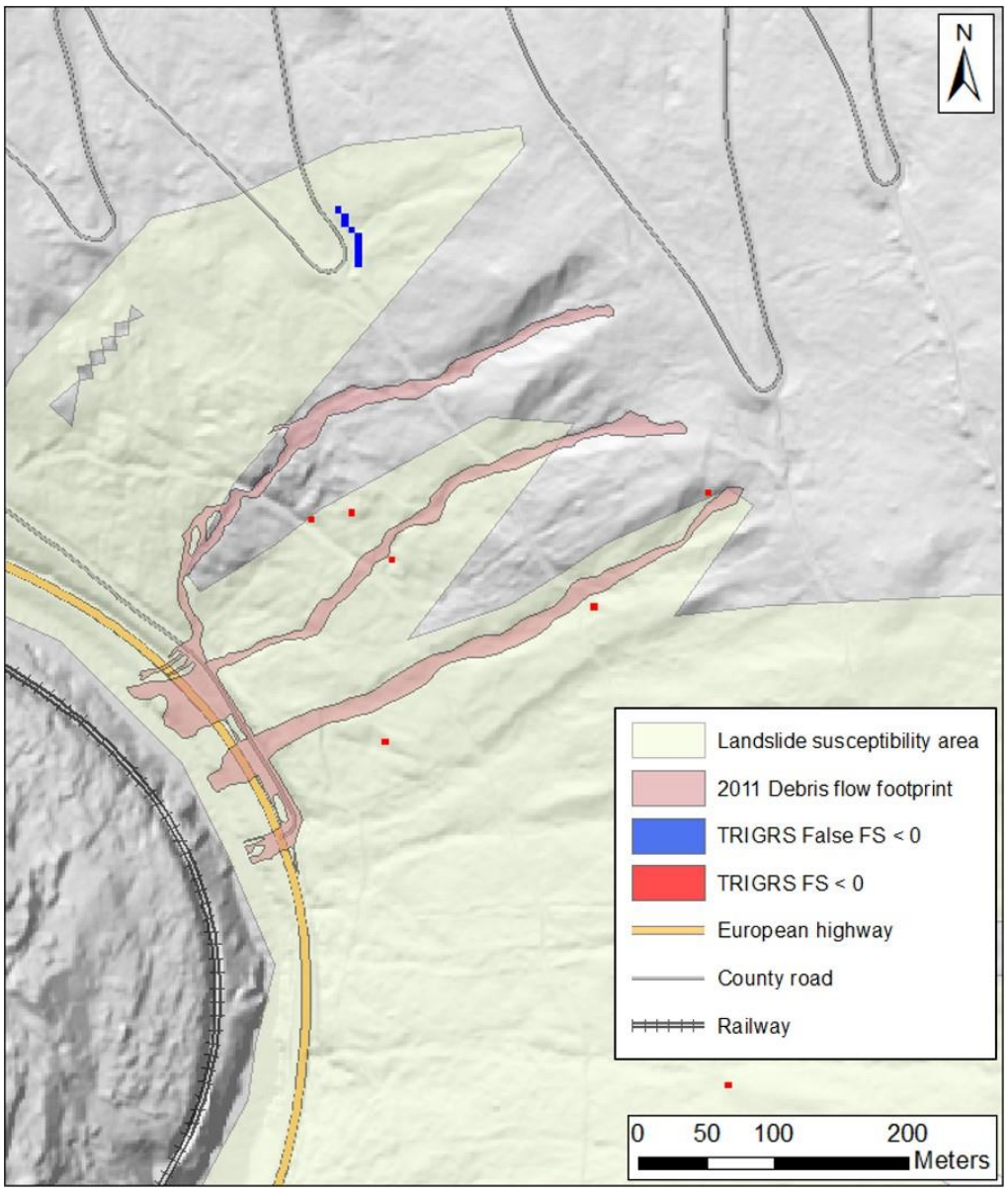

Figure 6.1 – Relative position of slope failure indicated by TRIGRS, interpreted tracks of the 2011 landslide events in Høvringslia, and the landslide susceptibility map of the area. Similar to TRIGRS, the landslide susceptibility map fail to capture the release areas from two of the three landslides of 2011.

Running TRIGRS in an area with existing soil depth data and DEM adjusted to culverts would therefore allow a calibration of higher quality, thus also raising the integrity of the final model results. The inaccuracy of the calibration likely produces an overestimation of release areas in the larger Rosten area as the uncertainty grows larger away from the calibrated landslides of Høvringslia.

Uncertainty of reference data

Some apparent over-estimation in number of release areas is probably also seen, related to the registered data which the presented results are compared to. For example, the NLDB registration for the debris flow event in Høvringslia of May 23. 2013 indicate how several failures are registered as one event:

> *"There have been many minor slips in the slope. At the exit to Høvringen, surging streams have washed large rocks into the road from great heights" (NVE, 2022).*

In addition, registered landslides are biased towards high-consequence runout scenarios as events with no consequence are likely not registered either due to lack of observation or because of little or no prior knowledge to landslides, classification, or registration by the observer. As trained personnel in road- and railway authorities register their observations, a majority of the registrations in NLDB are events along the transportation network. Most events in the database are registered as they have caused some degree of devastation or disruption to these infrastructure types (Krøgli et al., 2018). However, events such as the one in Høvringslia in 2011, illustrate how significant landslide events can be left out of the database.

6.1.2 RAMMS performance

Parameters for friction and erosion are very variable and depend on slope material and its distribution, hydro-meteorological conditions, and the terrain in which the landslide moves. A summary of friction parameters used in a number of published landslide modeling studies using RAMMS is presented in Mikoš and Bezak (2021). They conclude that it is not possible to observe any clear pattern in the frequency at which these parameters occur in published work where RAMMS is used, and that appropriate parameters are highly dependent on local conditions. Parameters used in this study however, do match well with the observed data from the Illgraben debris flow test site from which the guiding values in the RAMMS user manual are estimated (Bartelt et al., 2017).

The results of the model are limited to the resolution of the input map layers. As seen in field, this resolution may not be sufficient to capture all terrain details and soil characteristics playing a role in release and flow mechanisms. Consequently, the flow runout may be routed in other directions in the model than would be the case in the terrain.

Most of the hazard overestimation from the coupled model is probably related to the import of unstable slope results from TRIGRS as release areas in RAMMS. A following assumption of a uniform soil cover in the Rosten area, a consistent depth of release and thus relatively similar release volume from each failure cell, fail to capture the degree of failure. As discussed above, failure may in several cases lead to smaller runouts in well drained riverbeds, and not necessarily landslides of great damage potential. Additional inaccuracies in the runout may have been produced by a simultaneous release of all failed cells. Instances where two or more modelled landslides interact may produce a greater runout with consequently more erosional potential, thus enabling further growth. Such a scenario is possible, but it is more likely that the failing cells occur over a range of time, leading to a number of individual landslides.

The potential of model calibration to the depositional fans of previous landslides is poor due to the runout into Lågen river. With insufficient information related to volume, velocity, or the flow characteristics of the 2011 landslides, this event is not optimal for calibration of the RAMMS model. The resulting runouts are therefore similarly uncertain.

6.1.3 Performance of TRIGRS-RAMMS coupled method

All uncertainties considered, the model performance is an important result as it illustrates the level of accuracy of a remotely based hazard and consequence analysis based on open access data. This data coverage is representable for a great part of the Norwegian areas affected by geohazards. The use of highlighted watersheds, and maps showing landslide runout and intersection with infrastructure illustrate how the individual methods complement each other in highlighting different aspects of the landslide scenario. It is also worth pointing out how the results outline the historically most active parts of Rosten, with six out of seven documented landslides in the area occurring within the mapped hazard intervals of the road and railway (Figure 6.2). Only one debris flow of the 2011 event occurred outside of the indicated vulnerable infrastructure for a future 200-year scenario. The major landslide of the 1789 Storofsen event is also registered outside of the hazard area. However, as stated in the event description, this landslide was in the “Rosten area” and the map position of the event is thus uncertain (NVE, 2022).

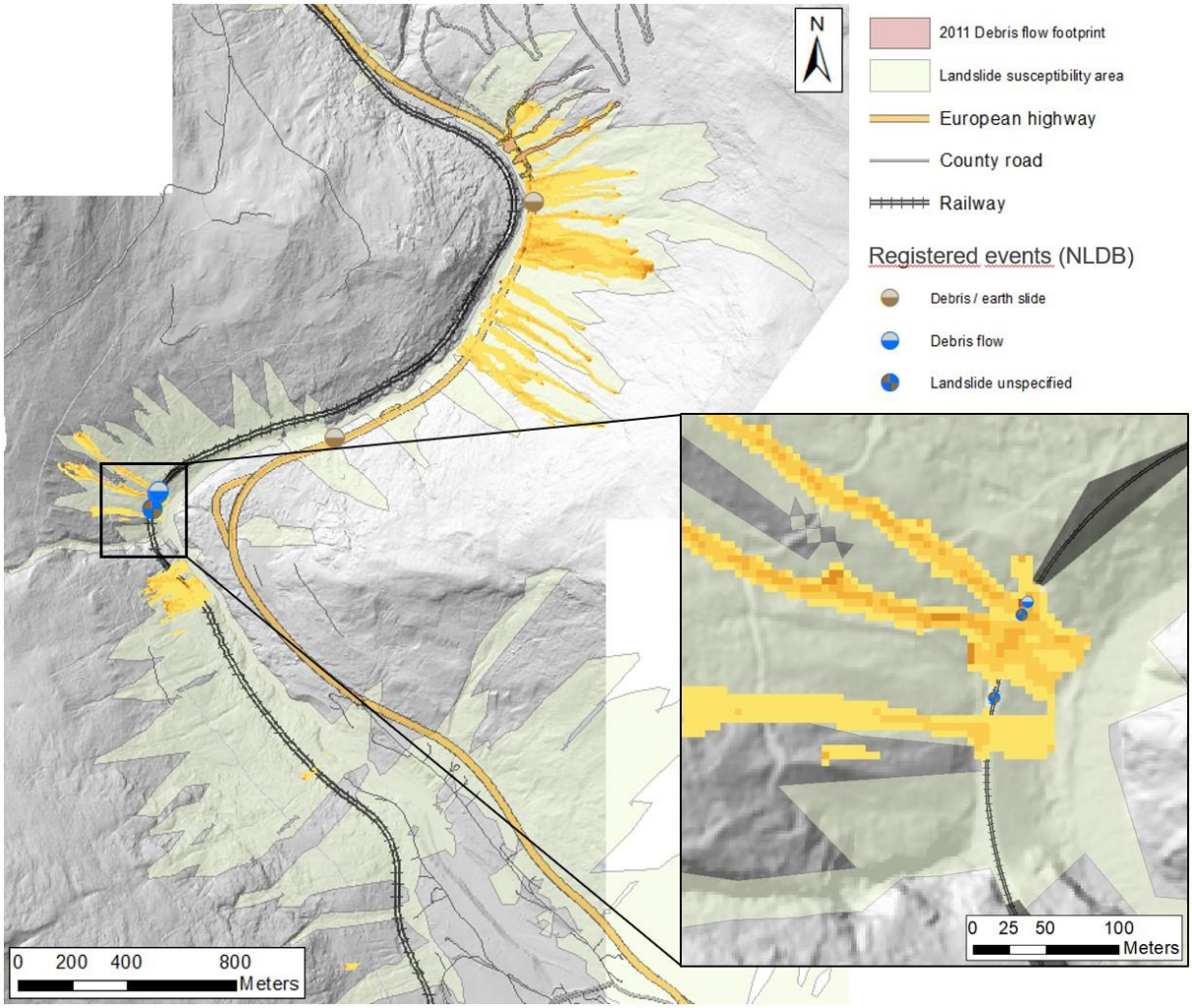

Figure 6.2 – A majority of the modelled landslides from a future climate 200-year precipitation event falls within the mapped landslide susceptibility area. The results also show a good correspondence with historically documented landslides, with 6 of 7 events falling within the modelled landslide runout zones.

Zhou et al. (2022) estimated an accuracy of 76.77% for the coupled model when backmodelling the Dazhuang landslides and following debris flows of July 2013. The calculation for this accuracy is based solely on the observed match of depositional fan from aerial imagery observation of the accumulated down-valley debris flow to the runout produced by the coupled TRIGRS-RAMMS simulation (Figure 6.3 B). It is therefore not directly comparable to the performance of individual landslide modelling from this study. Zhou et al. (2022) also presents the performance of the TRIGRS release area modelling (Figure 6.3 A).

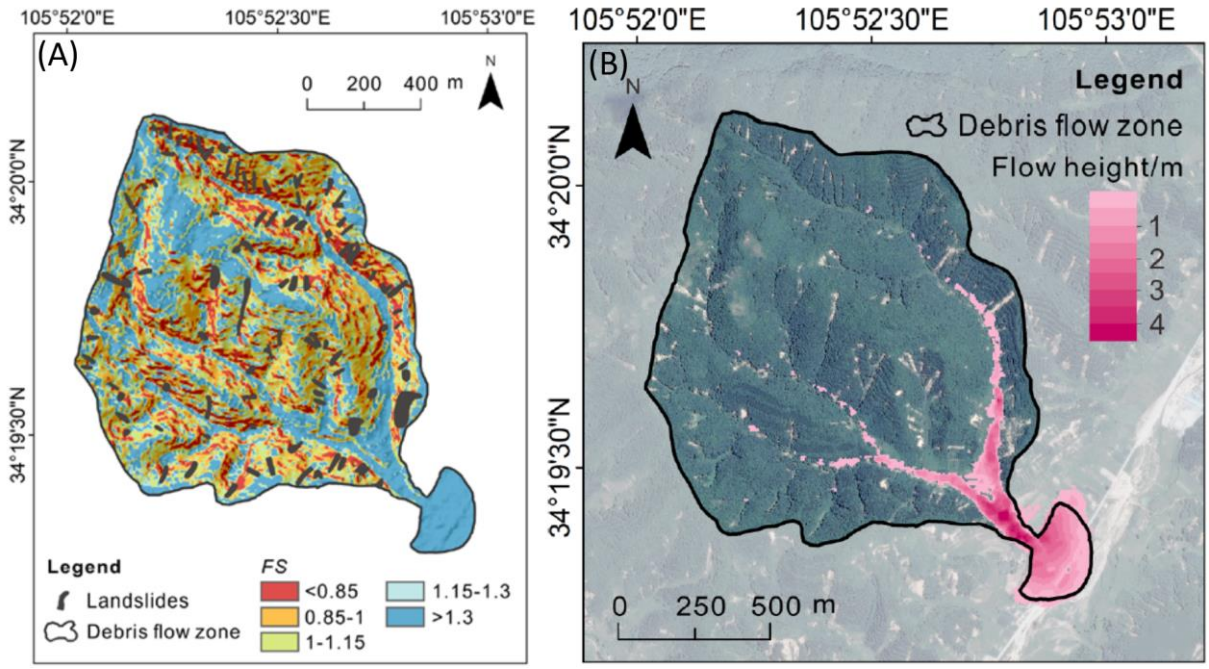

Figure 6.3 – Model results from Zhou et al. (2022). A) Map showing factor of safety as calculated by TRIGRS. B) RAMMS runout simulation based on TRIGRS-simulated landslides.

By superimposing observed landslide scars from aerial imagery to their TRIGRS result, they show how areas of FS < 1 contain more than 75% of the number of landslides. The success rate of TRIGRS landslide mapping is calculated to almost 82%. In this calculation, they do not compare the modelled release areas to the observed release areas in terms of size, number, and position. In fact, about 35% of the studied area have a modelled FS < 1, suggesting a third of the total study area should fail during the precipitation event. It is unclear from the study which of the TRIGRS results were used as release areas in the RAMMS simulation, but use of all areas with FS < 1 seems unrealistic. Due to the differences in method application and result interpretation, the model performance of the present study is not directly comparable to the study of Zhou et al. (2022).

Hill shade of the DEM show other areas with visible landslide tracks in Rosten which this method fails to include (Figure 6.4). These areas have more gentle slope inclination, but still have deep tracks. This may suggest surface and river erosion as the main trigger for debris flow initiation in these areas. A lack of modelled slope failure in these areas indicate how TRIGRS only model one aspect of the two-part story that is landslide initiation in Rosten.

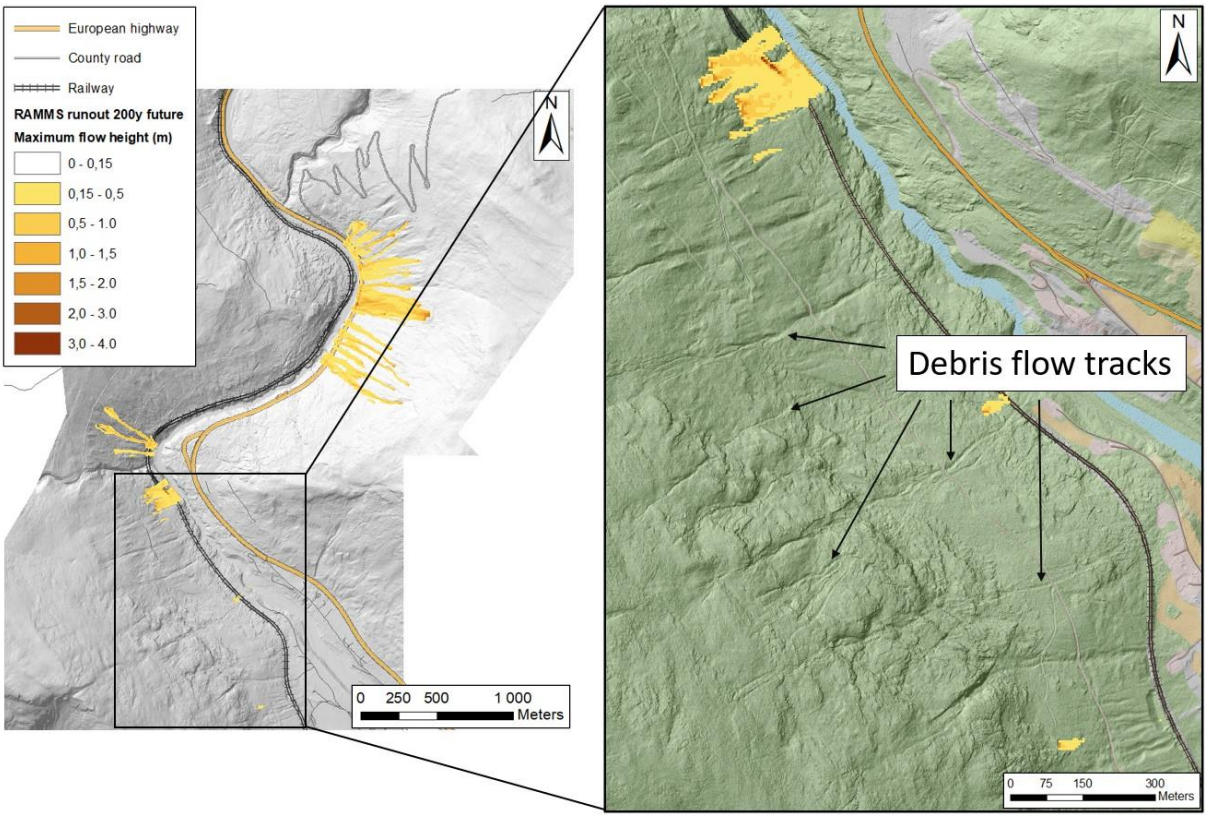

Figure 6.4 – ArcMap hillshade tool applied on a high-resolution DEM reveal several tracks from previous debris flows occurring outside of the modelled hazard areas. These are likely the result of enhanced river erosion rather than slip failure and are therefore not captured by TRIGRS.

It must therefore be emphasized that the TRIGRS-RAMMS coupled model is only applicable for identifying landslides initiated from slip failure in shallow soil as response to heavy precipitation. It is not expected to successfully identify landslides triggered by surface erosion, earthquakes, human activity etc. It is also not suitable for identification of other types of landslides such as quick clay slides or landslides from solid bedrock such as rock fall or rock avalanches.

In this study, the estimation of hazard suffers from the uncertainties related to the individual models but performs well both in illustrating the difference in hazard scenarios of present and future conditions, and in illustrating the related climate induced increase in vulnerability of the infrastructure. Applied in areas with appropriate data coverage, this coupled method could therefore be a useful supplement to the established methods for landslide hazard identification in large parts of Norway.

6.2 Uncertainty in physically based modelling

Several of the uncertainties in this study are not method specific, but rather uncertainties for landslide modelling and vulnerability analysis in general. Most of these uncertainties occur when complex factors controlling slope stability are simplified and generalized when fitted into computational models, thus not capturing natural variations at the small scale in which they occur. When such complex factors are used as input, its related uncertainty is also incorporated into the result.

For example, precipitation values from IDF-curves and the 20% climate factor used as inputs are best estimates from statistical frequency analysis and climate modelling. For the IDF-curves, there is an uncertainty related to the extrapolation of extreme values from the reference dataset of 1971-2000, whereas the climate factor is estimated from climate projections with uncertainties related to future emissions, natural climate variations and the climate modelling itself (Hanssen-Bauer et al., 2017; Stocker et al., 2013). As demonstrated by Melchiorre and Frattini (2012), the selection of climate scenario and downscaled precipitation model is more relevant for the hazard modelling than the model parametrization.

6.2.1 Spatial and temporal uncertainty

Of the uncertainties related to the natural landslide processes, there are factors of both temporal and spatial variability which needs to be considered. As a simplification, we can consider the spatial and temporal conditions as determinants of which parts of the slope is prone to failure, and when the unstable areas do in fact fail.

Examples of spatial variables include soil cover type and depth, slope angle, hydrological contributing area, proximity to streams, vegetation type and manmade slope alterations. Within soils of similar characteristics with respect to the above-mentioned variables, there may be additional significant differences operating at a smaller scale. Complex sedimentation patterns and un-even post-sedimentation compaction cause natural variations in hydrological conditions as well as strength and deformation characteristics. Local variation of factors such as grain distribution, soil composition, degree of cementation, soil permeability, and groundwater infiltration, are just some of the factors contributing to the complexity of slope stability (Cuomo

et al., 2021; NGI, 2014). Thus, a completely accurate model representation of the slope conditions is not feasible on a small scale.

This spatial variability is very well visualized in the individual release areas from the three 2011 Rosten landslides (Figure 6.5). With similar topographic conditions and within the same mapped soil type, their release volumes are quite different across a span of some tens of meters, indicating small scale variabilities controlling the degree of failure.

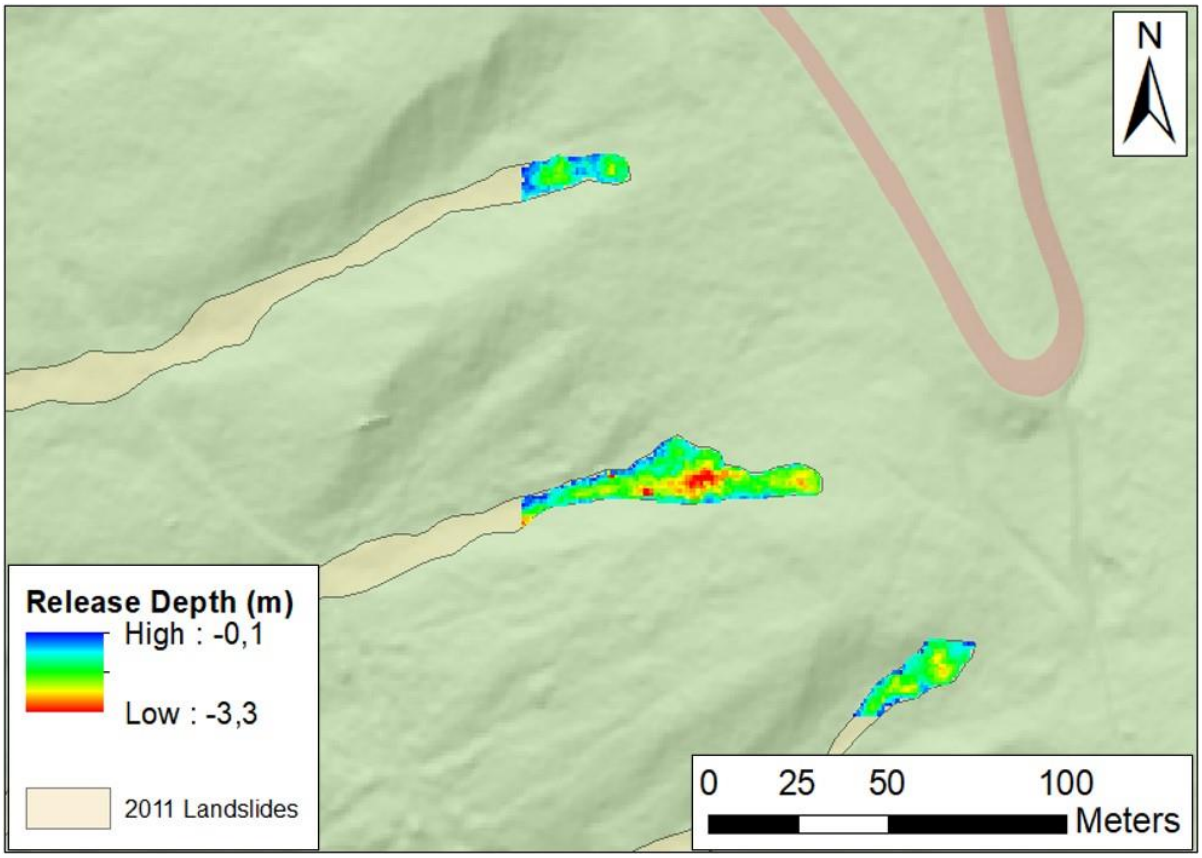

Figure 6.5 – Depth of release for the 2011 landslides in Høvringslia illustrate the natural spatial variability of landslide controlling factors.

In addition to the spatial variations, there are several factors of temporal variability controlling the timing of slope failure. To demonstrate the effect of these, it is worth investigating the 2011 extreme precipitation event to other extreme precipitation events registered in Rosten, and why other events failed to produce similar landslide scenarios in the same slope.

Extreme precipitation events in Rosten

Since 1975, gridded data from the SeNorge series show 8 events in Rosten with precipitation exceeding 45mm in 24 hours. Of these, two occur in November and December, and the precipitation is reported as snow. One additional event occurring in March of 2011 saw the precipitation as rain, but on a snow-covered surface. In such an event, a lot of the rain is absorbed within the snow profile. Slope processes during such an event is therefore more likely dominated by slush avalanches than shallow landslides from the soil layer (NGI, 2014). Thus, over the last 50 years, five events with 24h rainfall greater than 45mm can be found in the SeNorge data series (Table 6.1). Of these, registered debris flows in NLDB are only seen for the events of June 2011 which has been subject to model calibration in this study, and for the event of May 2013.

Table 6.1 - The five greatest 24h rainfall events in Rosten. Data from MET. (2022b)

dd.mm. yyyy	24 h Rainfall (mm)
25.06.2010	50.7
10.06.2011	50.6
16.07.1994	49.3
23.05.2013	47
11.08.2018	46.9

Unfortunately, the temporal resolution to most rainfall events is limited to 24h, as hourly data registrations was first installed in September 2013 for nearby gauges. An approximation of the intensity-duration trends for these events may, however, be assessed through hourly data from gauges at Skåbu and Leirflaten, 38 and 20 kilometers south and southeast of Rosten, respectively (Figure 6.6). For both events, daily data suggest relatively saturated soil conditions from precipitation in the two weeks preceding the events (Figure 6.7 and Figure 6.8). The hourly data from Skåbu shows how most of the rain in the 2011 event occurred in a 12-hour period from 00.00 to 12.00 on the 10th of June. Intensities >5mm/ hour is registered for several hours, and a peak intensity of 11.3mm between 10.00 and 11.00. For the 2013 event, hourly data from both Skåbu and Leirflaten show a wider distribution of rainfall throughout a 24h period, with a peak intensity of 4.6mm/hour in Leirflaten. These data could suggest that the two landslide-producing events had different triggering conditions for the debris flows, with a 12h rainfall controlling the triggering in 2011 and a 24h rainfall of lower intensity controlling triggering in 2013. No hourly data is available for the region around northern Gudbrandsdalen prior to 2011,

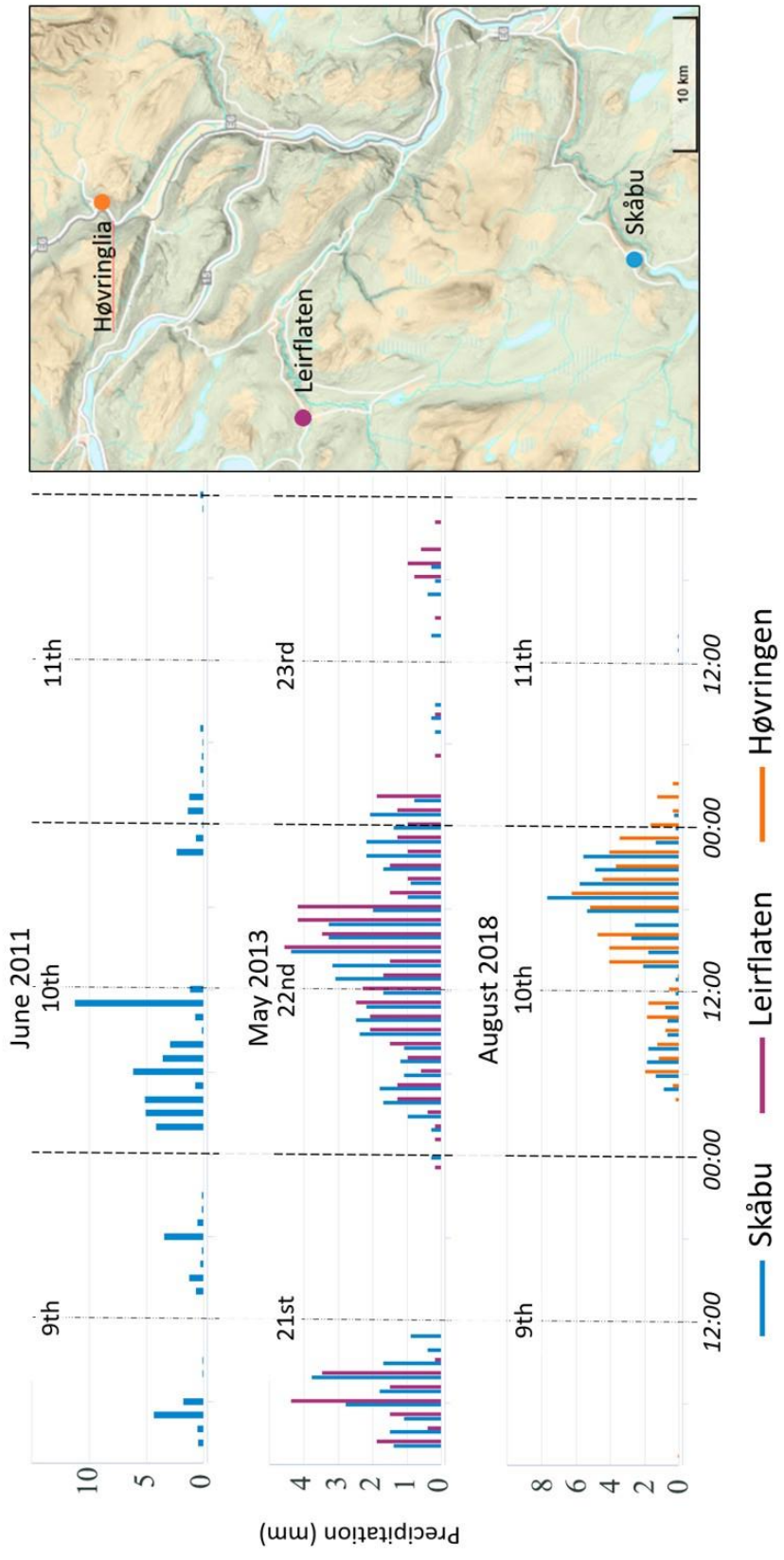

Figure 6.6 - Hourly precipitation data for Skåbu (2011, 2013, 2018), Leirflaten (2013) and Høvringen (2018). Data from MET. (2022a). Map indicates position of the three weather stations. Modified from Kartverket (2022).

and the rainfall intensities during the events of June 2010 and July 1994 can therefore not be further assessed. Both of these events do, however, show relatively small amounts of precipitation in the two weeks prior to the extreme event, suggesting unsaturated initial conditions (Figure 6.8). For the 2018 event, hourly precipitation from Høvringen weather station show a 24-hour distribution of rain during the extreme event, with peak intensity of 6.3mm/h. This event also saw relatively wet initial conditions from significant amounts of precipitation in the days leading up to the extreme event. This event is therefore quite similar to the conditions of the 2013 event with respect to precipitation. However, important differences in initial conditions for these events is the degree of additional snowmelt contribution to the saturation of the soil and to surface runoff, as well as the potential of local patches of frozen soil. This was likely a contributing factor in May 2013, but not in august 2018. Remnant of winter frost in the ground may cause a major decrease in the water infiltration capacity of the soil and act as a shallow slip surface, which may have been a key component to the 2013 slip failures.

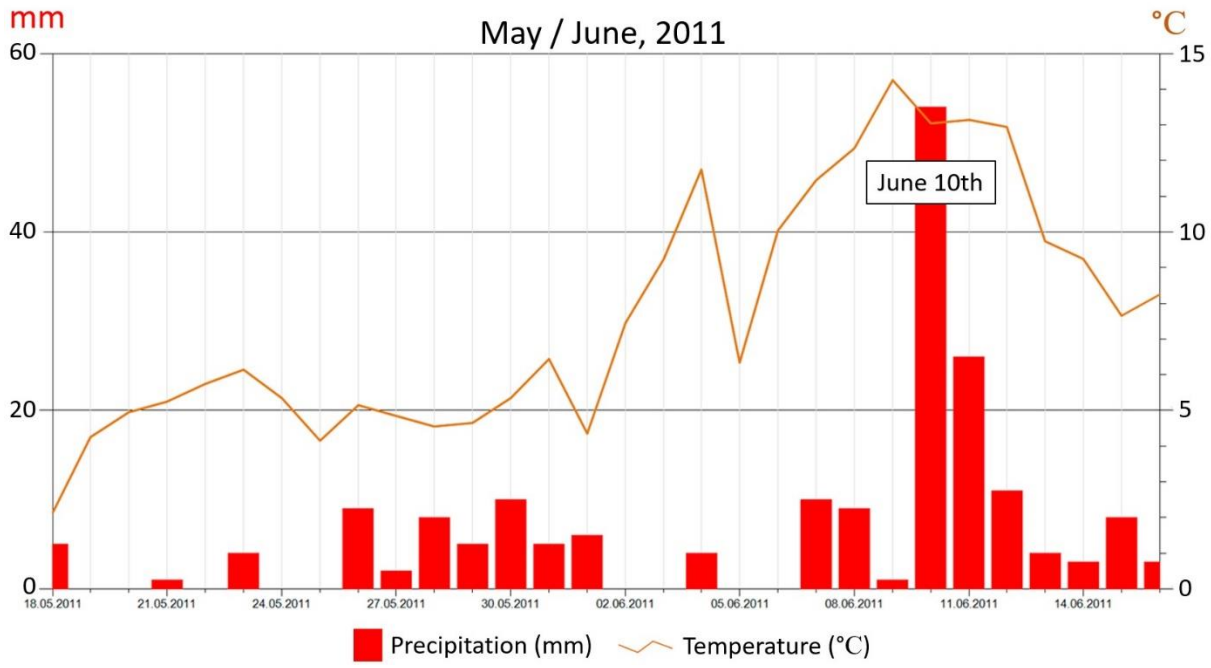

Figure 6.7 - Daily precipitation and temperature for Rosten in May – June 2011. Several landslides occurred June 10th in the Otta area, including the three landslides in Rosten subject to calibration in this study. Modified from MET. (2022b).

Another controlling factor to the initial soil wetness is the rate and degree of evapotranspiration. This largely depends on seasonal variations in solar radiation, weather conditions, distribution and type of vegetation, air and ground temperature, wind, slope aspect, and human activities in the drainage area (Cuomo et al., 2021). With respect to temperature, May of 2013 saw significantly colder weather prior to the extreme precipitation than what is seen for august of 2018, which suggest a higher degree of evapotranspiration for the latter. The initial soil conditions in 2018 may therefore have been dryer, enabling greater infiltration in the soil, resulting in more rainfall required to reach critical pore pressure and trigger landslides.

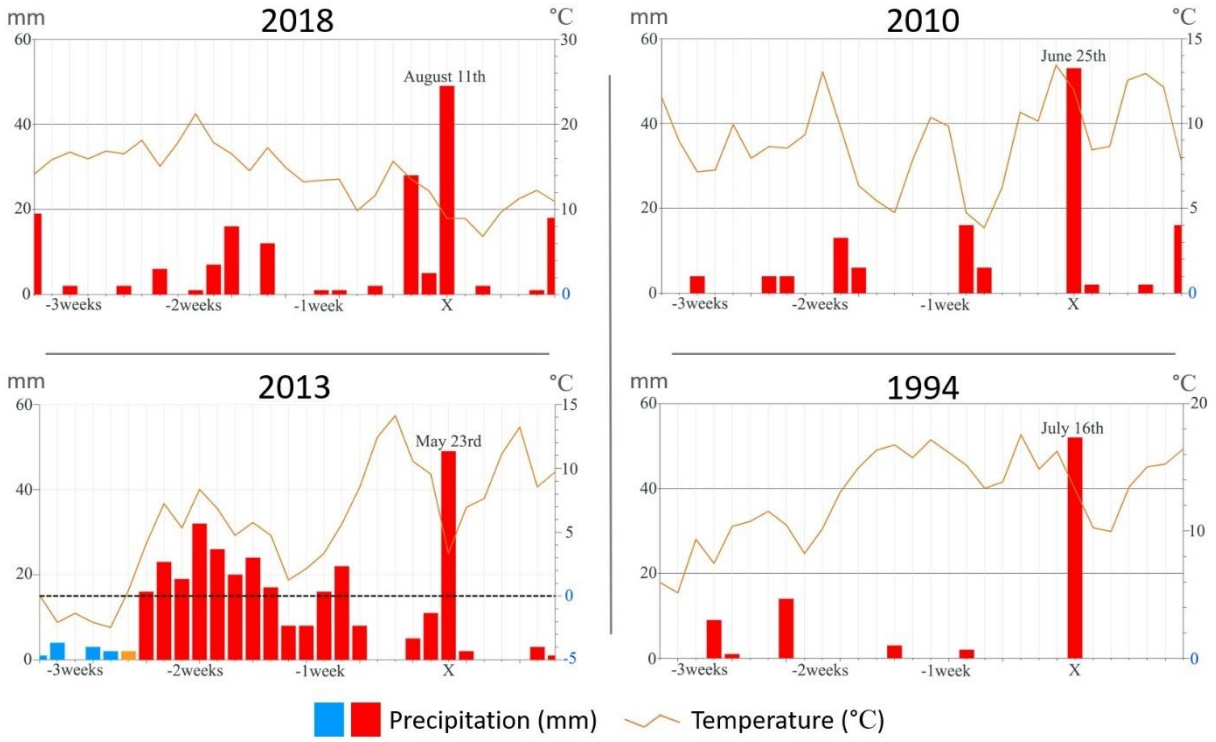

Figure 6.8 - Daily precipitation and temperature for Rosten for other extreme precipitation events. Modified from (MET., 2022b).

It is therefore likely that relatively saturated initial soil followed by the 12-hour intensity-duration of precipitation was a crucial factor in producing the widespread slope failure seen for the 2011 event, while for other extreme events showing less intense precipitation, the slope stability and following landslide scenario has been determined by a combination of other factors of temporal variation. If the total precipitation of the 2011 event did in fact fall during a span of 12 hours, this duration-intensity correspond to an event of 20–30-year return period, and not the 24-hour event of 10-year recurrence which has been assumed due to lack of hourly rainfall data in nearby gauges.

6.2.2 Role of vegetation

Estimations of apparent cohesion from rooting range from 1-2 kPa (landslide back-analysis by Greenwood et al. (2004)) to 10-20 kPa for industrial forests (root network analysis and strength tests by Schmidt et al. (2001)). The absolute effect of roots depends largely on soil type, tree size, species, and subsurface character of the root networks, as is often controlled by land-use practice, fires, climate change etc. (Roering et al., 2003). This cannot be accurately determined for this study, in part because it is impossible to distinguish vegetation effect from uncertainty ranges related to other inputs in the data set. Values for cohesion in glacial deposits by Melchiorre and Frattini (2012) is estimated at 4 ± 1.5 kPa. The minimum 7.5 kPa cohesion required to simulate stable initial slope conditions for Rosten could therefore suggest a contribution from vegetation somewhere in between the above-mentioned ranges. However, the effect of vegetation is of great spatial variability, and can also have significant temporal variation.

The slope stability analysis in this study is calibrated to past landslides in a forested area. As this calibration serves the basis for stability assessments of current and future climate, stabilizing effects from vegetation is incorporated in all the presented results. This means that the integrity of the presented results depends on a permanent forest cover in the valley sides also in the future. This is, however, not the case in Rosten. Both Høvringslia and Horgelia has seen de-forestation from logging after the landslide events of 2011. From arial photos, it can be determined that most of the de-forestation in Høvringslia took place in the summer of 2011. The logging in Horgelia, as well as an upslope expansion of the field in Høvringslia, occurred at some point between 2011 and 2015 (Figure 6.9).

Figure 6.9 - Aerial photo acquisitions of Rosten reveal the activity from logging in Høvringslia. Modified from Statens Kartverk et al. (2022b, 2022c, 2022d).

The temporal change in vegetation may present a significant uncertainty in slope stability calculations in general. Not only due to the inconsistency from logging, but also from the natural growth and decay cycle of trees. The warming climate and an increase in summer precipitation cause an increase in growth season, stimulating greater and more dense forest growth. The general trend in southern Norway is thus greater and denser forests, increasingly expanding to higher elevations (Aarrestad et al., 2015). There are, however, climate related effects on forests that could also prove significant changes on local and regional scale and have a de-stabilizing effect on slopes. Stress on the vegetation from drought, insect outbreaks, infestations from parasites and fungi may cause severe damage on trees, and are all expected to increase with warmer climate (Aarrestad et al., 2015). Warmer temperature and more extreme weather types also see a greater number of forest fires. Days with risk of forest fire in south and east of Norway is expected to increase with 50% by 2050 (Aall et al., 2018). In short, the state of vegetation and its effect on soil stability is expected to vary over time and should therefore be consistently assessed for practical use of a slope stability analysis in forested areas.

It is interesting to note that parts of Høvringslia in 2017 was given status as a national reserve due to its natural forest which includes several red-listed types of flora. Not only does this newfound status protect vulnerable species, but it also restricts forestry and other activities which could disturb the natural slope stability in this area.

6.3 Contribution to the NordicLink project

The results of this study contribute mainly to the NordicLink work package 2 and 5 with an assessment of the landslide hazard in Rosten for current and future climate. The results also provide a basis for work package 4 and evaluation of mitigation strategies. For instance, the calibrated soil parameters offer a starting point for estimating the soil stabilizing effect from vegetation and further potential of forestation as a NBS solution. Although the results from this study are both site specific and specific of slope scale, it successfully demonstrates the potential of a TRIGRS-RAMMS coupled model and the data coverage prerequisite for optimal model performance, thus enabling expansion of the hazard analysis to other areas.

6.4 Perspectives

6.4.1 Risk analysis

Hazard assessments like the one presented in this study are of great societal value. To improve safety and reliability along the transportation network it is important to design this infrastructure and implement appropriate measures to meet the hazard scenario of the future.

Hazard maps are fundamental inputs in a risk analysis. Such analyses take both hazard and consequences into consideration and are more applicable for practical use than hazard maps alone. Typically, risk is defined as:

$$Risk = Hazard * Consequence \quad (10)$$

where hazard can be further broken down to factors of spatial and temporal probability of hazard occurrence, and consequence often is broken into degree of damage, elements at risk and utility cost of these elements.

With respect to slip failure landslides triggered by extreme rainfall, this study assesses the spatial and temporal probability of hazard as well as the elements at risk for each scenario. The results can thus be put to practical use for risk analysis by infrastructure stakeholders. When areas exceeding thresholds for acceptable risk are identified, appropriate mitigative measures can be assessed.

6.4.2 Landslide mitigation measures

Damage reducing measures

Several measures can be installed to reduce landslide risk, either by changing the hazard pattern or lowering the vulnerability of infrastructure. Such measures vary in cost and magnitude, and span from installation of great catch dams to ensuring that waterways are cleared of obstacles.

The runout and infrastructure vulnerability assessment outline the road section of high hazard, suggesting the area in which waterways should be regularly maintained and cleared for

obstacles in case of extreme precipitation events. Additionally, the outlined unstable watersheds suggest position of streams and drainage networks which could be reinforced and upgraded. Mitigative measures within these drainage networks may include installation of soil drainage pipes, or plastering of stream beds to ensure erosion control. Particularly active streams could also see ring nets as an appropriate measure to catch debris and reduce the damage potential of landslides (Figure 6.10).

Figure 6.10 - Debris ring net installed in a historically active drainage channel near the town of Otta (Photo: Øystein Grasdal)

Climate induced increase in hazard also suggest a significant increase in maintenance and reparational cost of infrastructure in the future. It has been pointed out in the zoning plan for Sel municipality that closure of E6 in Rosten will lead to a severe lack of accessibility for certain areas, thus limiting emergency response (Sel Kommune, 2017). A small forest road in Høvringslia has been considered improved as an emergency road, but this was not feasible due to the river crossing of Roståa river. Considering the future hazard scenario and the socio-economic importance of E6, a comprehensive but effective measure for Rosten would be to build a new tunneled section of E6 in this area and maintain the current road as an alternative route. The climate induced increase in hazard presented in this project would provide useful input to a cost-benefit analysis for such an evaluation.

Early warning system

In addition to physical installations, a cost-effective measure to reduce risk with low economic and environmental impact is a well-functioning early warning system. The current national early warning system for rainfall- and snowmelt-induced landslides has been operative since 2013, and was developed as a joint initiative between NVE, the Norwegian Meteorological Institute, the Norwegian Public Road Administration, and the Norwegian Rail Administration. This system uses a combination of meteorological forecasts, hydrological models, and initiation thresholds derived from historic events in the NLDB to provide a 3-day forecast on a regional level based on observations from a network of meteorological and hydrological stations (Krøgli et al., 2018). The relative landslide hazard for each region is then evaluated by landslide experts, and communicated to the public via varsom.no, and by SMS for users subscribing to natural hazard notifications. The method is validated through a statistical analysis of historic awareness levels compared to the situational hazard scenario of the corresponding days. For the four-year period of 2013 to 2017, the analysis showed a total of 96% correct assignment of awareness level when analyzing all days, while for "challenging days" the number was reduced to 88%. From an investigation of these results, new work on improvement of landslide initiation thresholds have been carried out, specifically aimed to reduce the number of false high-awareness situations (Boje, 2017).

Accurate early warning allows local authorities and infrastructure operators to plan for a potential hazard event by inspecting drainage channels and culverts for obstructions, plan and communicate alternative routes and implementing potential preventive measures. Such measures may potentially reduce costly damage to the infrastructure, and socio-economic costs related to traffic disruption and prolonging delays.

Figure 6.11 shows the conceptual map of processes involved in the current early warning for landslides in Norway. The upper right part of the figure shows how susceptibility maps and regional threshold values are used to evaluate the development of hazard as a response to weather observations. With potential for hour-by-hour stability evaluation in TRIGRS and following runout simulation in RAMMS, the coupled model of the present study could ideally provide a supplement to the early warning system for selected areas. With proper calibration, the model may provide early warning operation on slope scale, adding to the information from susceptibility maps and threshold values, thus giving additional hazard estimation for the further expert evaluation.

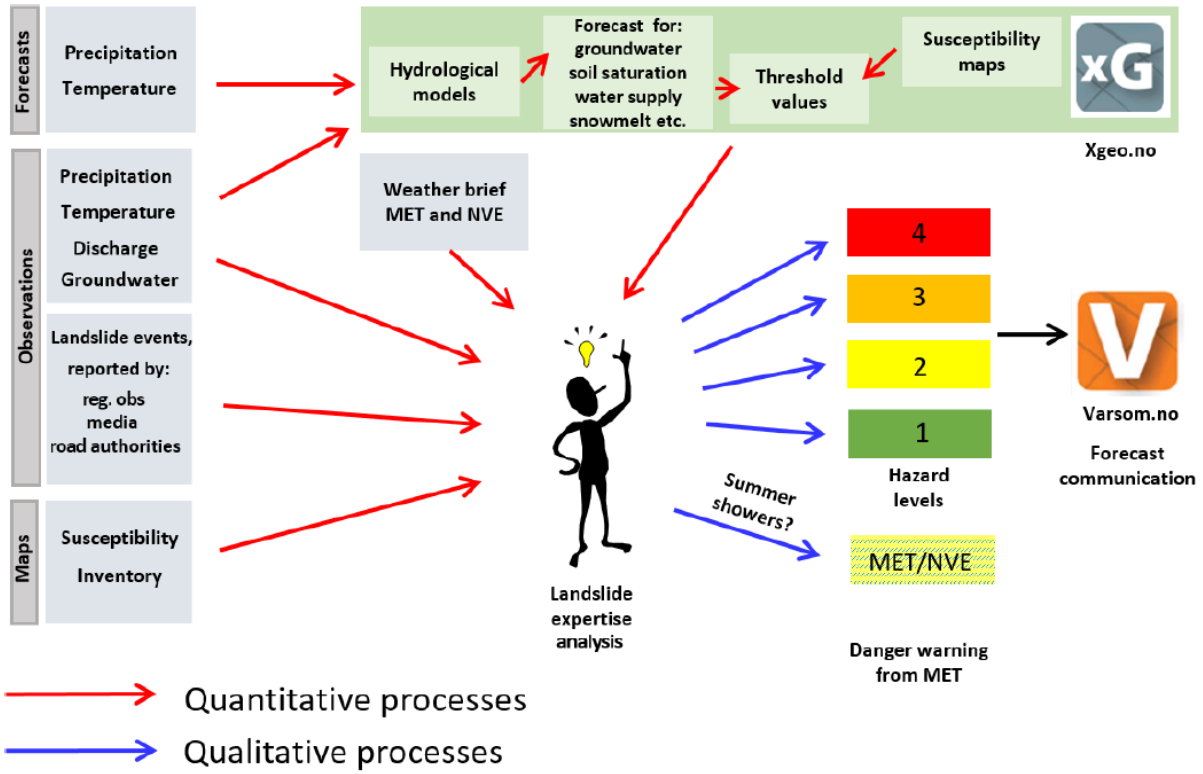

Figure 6.11 – Conceptual illustration of how the daily landslide hazard assessment is performed. From Krøgli et al., (2018).

On a local scale, sensors monitoring stress-change, tilt and creep of the soil could also predict failure and stop traffic, thus potentially limiting vulnerability of transportation network users.

6.5 Further work

The purpose of the workflow in this thesis has been remotely assessment of stability and hazard scenarios based on open access data. However, the present analysis has shown that the model performance could easily be improved with a bit of field work. Mapping of sediment thickness, either by probing or through geophysical acquisition with following interpolation of data to the study area, would significantly reduce the uncertainty related to this factor which is one of great influence to the TRIGRS model result.

Obtaining rainfall data at hourly resolution is key to a better understanding of landslide initiation thresholds, and thus also to optimize early warning and early re-direction of traffic.

As for now, model simulations must be inaccurately based on 24h data, thus not capturing the critical conditions at which landslide initiation occur.

The coupled model is therefore proposed tested for a set of slip-initiated historical landslides with full-extent runout in an area with existing soil thickness measurements and hourly rainfall data in order to evaluate its performance under optimal conditions.

As the hazard is only evaluated for 24h rainfall scenarios, it would be of practical importance also to assess the climate induced hazard also for events of shorter duration.

Mapping of culverts gives the possibility to redirect surface flow accumulation in areas where roads affect drainage. As discussed, this is a problem which is likely to affect slope stability models and can be seen as a cause of inaccuracy also in the landslide susceptibility map. With position of culverts, it is possible to manually solve this issue in ArcMap, thus raising the confidence in hazard mapping.

Liu et al. (2021) demonstrated improved hazard prediction using machine learning algorithms compared to TRIGRS in Kvam. For the Rosten case site, it would be interesting to test the performance of this method in backmodelling of the 2011 landslides, as this is less dependent on soil mechanical properties.

7 Conclusion

A comprehensive hazard chain assessment from precipitation scenario to slope stability and subsequent landslide runout was conducted using a TRIGRS-RAMMS coupled model in the Rosten area north of Otta. Each model has been calibrated to past landslides in Rosten to incorporate local conditions in the assessment. By implementing a climate factor to the precipitation scenarios, the climate adaption is carried through the hazard chain and enables projection of future climatic effects on slope stability and landslide runout. From difference in runout scenarios, it is demonstrated how the relative exposure of transportation networks to landslide hazard in Rosten is likely to change from present to future climatic conditions.

With this approach, there are two perspectives to the findings of this study. One is related to the future hazard and exposure scenario of infrastructure in Rosten, while the other relates to the performance of the coupled hazard prediction model.

With respect to the hazard scenario in Rosten, the main findings of this study are:

- A significant increase of unstable areas with response to climate induced increase in precipitation intensity is observed for extreme rainfall events of 20-, 50-, 100- and 200-year return period.

- An increase in number of unstable active watersheds, and thus an increase of active debris flow spill points towards road and railway, is expected in the future as response to increase in precipitation.

- A more severe hazard scenario towards the transportation networks in Rosten for the future in terms of number of landslide runouts, runout volumes and portion of exposed road and railway.

- Climate adjusted hazard maps suggest suitable sections for installation of risk-reducing measures and regular maintenance of waterways by outlining the sections of road and railway with the greatest exposure to landslides.

- Calibrated soil parameters for Rosten, providing a basis for further studies in the area.

With respect to performance of the TRIGRS-RAMMS coupled hazard model, the main findings from this study are:

- By introducing a climate factor to the precipitation intensity, the model successfully carries the climatic effects through the hazard chain and enables assessment of climate induced change in infrastructure exposure to landslides.

- Limited cell-by-cell accuracy of TRIGRS stability modelling due to low-resolution input. Locally poor representation of runoff routing occurs where insufficient detail in DEM fail to capture established drainage pathways, thus also affecting the accuracy of the stability modelling.

- RAMMS show a poor flow channeling compared to observations from the calibration event, resulting in downslope spillage and lateral flow, and thus an over-estimation of exposed infrastructure where the runout intersects road and railway.

- Observation of landslide tracks and registration of an event outside of the mapped hazard areas, indicate how potential release mechanisms other than slip failure contribute to the landslide hazard in Rosten, and is not accounted for by TRIGRS.

- Model performance is highly dependent on detailed spatial and temporal input and precise calibration. For the Rosten site, the performance is particularly limited by the lack of hourly precipitation data and depositional footprint from landslides of the calibration event, as well as the lack of data for soil cover thickness. These results emphasize the importance of carefully selected application sites for full performance of the coupled model.

References

Bane Nor. (2015). InterCity. *Prosjekter*. Retrieved from https://www.banenor.no/Prosjekter/Inter-City-/InterCity/

Bane Nor. (2016). Dovrebanen. *Baner (A - Å)*. Retrieved from https://www.banenor.no/reisende/Banene/Dovrebanen/

BaneNor. (2013). Rørosbanen. *Baner (A - Å)*. Retrieved from https://www.banenor.no/reisende/Banene/Rorosbanen/

Bartelt, P., Bieler, C., Bühler, Y., Christen, M., Deubelbeiss, Y., Graf, C., . . . Schneider, M. (2017). *RAMMS::DEBRISFLOW User Manual*.

Baum, R. L., Savage, W. Z., & Godt, J. W. (2008). *TRIGRS: a Fortran program for transient rainfall infiltration and grid-based regional slope-stability analysis, version 2.0*: US Geological Survey Reston, VA, USA.

Beyer-Olsen, A., & Johansen, L. (2013, 07.06.2013). Ordfører om E6-ras: - Tidsspørsmål før det skjer ighen. *VG*. Retrieved from https://www.vg.no/nyheter/innenriks/i/a66v5/ordfoerer-om-e6-ras-tidsspoersmaal-foer-det-skjer-igjen

Blikra, L. H., & Nemec, W. (1998). Postglacial colluvium in western Norway: depositional processes, facies and palaeoclimatic record. *Sedimentology, 45*(5), 909-960.

Boje, S. (2017). Hydrometeorologiske terskler for jordskredfare på Sørlandet og Østlandet. *NVE rapport, nr 64-2017*.

Breien, H., Høydal, Ø. A., & Jensen, O. A. (2015). Oppsummeringsrapport for skog og skredprosjektet. Samanstilling av rapportar frå prosjektet. *NVE rapport, 92/2015*.

Bryhni, I., & Askheim, S. (2021). Ottaskifer. Retrieved from https://snl.no/ottaskifer

Cuomo, S., Masi, E. B., Tofani, V., Moscariello, M., Rossi, G., & Matano, F. (2021). Multiseasonal probabilistic slope stability analysis of a large area of unsaturated pyroclastic soils. *Landslides, 18*(4), 1259-1274.

Depina, I., Oguz, E. A., & Thakur, V. (2020). Novel Bayesian framework for calibration of spatially distributed physical-based landslide prediction models. *Computers and Geotechnics, 125*, 103660.

Devoli, G., Eikenæs, O., Taurisano, A., Hermanns, R., Fischer, L., Oppikofer, T., & Bunkholt, H. (2011). Plan for skredfarekartlegging–Delrapport steinsprang, steinskred og fjellskred. *NVE rapport, 15*, 2011.

Dyrrdal, A. V., Isaksen, K., & Hygen, H. O. (2011). Past changes in frequency, intensity, and spatial occurrence of meteorological triggering variables relevant for natural hazards in Norway. *Met.no report, no. 03/2011*.

Dyrrdal, A. V., Isaksen, K., Hygen, H. O., & Meyer, N. K. (2012). Changes in meteorological variables that can trigger natural hazards in Norway. *Climate Research, 55*(2), 153-165.

Dyrrdal, A. V., Lutz, J., & Grinde, L. (2022). IVF-verdier for norske nedbørstasjoner. *MET report, 02-2022*.

Edvardsen, D. H. (2013). *Utløsningsårsaker og utløsningsmekansimer til flomskred i moreneavsetninger.: Feltstudie av terrengtyper og inngrep i naturen som potensielt kan føre til skred inn mot fremtidige vegprosjekter. Eksempel fra Kvam, Norge.* (Master thesis), NTNU,

Fergus, T., Hoseth, K., & Sæterbø, E. (2010). Vassdragshåndboka: håndbok i vassdragsteknikk. *Ny rev. utg. Trondheim: Tapir akademisk forl*.

Fergus, T., Høydal, Ø., Johnsrud, T., Sandersen, F., & Schanche, S. (2011). *Skogsveger og skredfare*. Veileder. NVE, NGI, SKI.

Fischer, L., Rubensdotter, L., & Stalsberg, K. (2014). *Aktsomhetskart jord-og flomskred: Metodeutvikling og landsdekkende modellering* (0800-3416). Retrieved from

Follestad, B. A., & Bergstrøm, B. (Cartographer). (2004). Otta. Kvartærgeologisk kart; Otta; 17184; 1: 50 000; trykt i farger

Frauenfelder, R., Solheim, A., Isaksen, K., Romstad, B., Dyrrdal, A. V., Ekseth, K. H., . . . Hygen, H. O. (2017). Impacts of extreme weather events on transport infrastructure in Norway (InfraRisk). *Natural Hazards and Earth System Sciences Discussions*, 1-24.

Frekhaug, M. H. (2020). Veileder for risiko-og sårbarhetsanalyser i vegplanlegging. *Statens Vegvesens Rapporter, Nr. 632*.

Furseth, A. (2006). *Skredulykker i norge*: Tun media.

Gariano, S. L., & Guzzetti, F. (2016). Landslides in a changing climate. *Earth-Science Reviews, 162*, 227-252.

Greenwood, J. R., Norris, J., & Wint, J. (2004). Assessing the contribution of vegetation to slope stability. *Proceedings of the Institution of Civil Engineers-Geotechnical Engineering, 157*(4), 199-207.

Hanssen-Bauer, I., Førland, E., Haddeland, I., Hisdal, H., Lawrence, D., Mayer, S., . . . Sandø, A. (2017). Climate in Norway 2100–a knowledge base for climate adaptation. *NCCS report, 1*, 2017.

Heyerdahl, H., & Høydal, Ø. A. (2017). *Geomorphology and susceptibility to rainfall triggered landslides in Gudbrandsdalen valley, Norway.* Paper presented at the Workshop on World Landslide Forum.

Highland, L., & Bobrowsky, P. T. (2008). *The landslide handbook: a guide to understanding landslides*: US Geological Survey Reston.

Hisdal, H., Vikhamar-Schuler, D., Førland, E. J., & Nilsen, I. B. (2017). Klimaprofiler for fylker. *Et kunnskapsgrunnlag for klimatilpasning*.

Holt, O. F. (2022). *Flom i Otta; En analyse av direkte og indirekte konsekvenser for vei og jernbane.* (Master thesis), Universitetet i Oslo, Department of Geosciences.

Høydal, Ø. (2002). Flomsonekart, Delprosjekt Selsmyrene. *Flomsonekart, nr 11/2002*.

Iverson, R. M. (2000). Landslide triggering by rain infiltration. *Water resources research, 36*(7), 1897-1910.

Jaedicke, C., Solheim, A., Blikra, L. H., Stalsberg, K., Sorteberg, A., Aaheim, A., . . . Mestl, H. (2008). Spatial and temporal variations of Norwegian geohazards in a changing climate, the GeoExtreme Project. *Nat. Hazards Earth Syst. Sci., 8*(4), 893-904. doi:10.5194/nhess-8-893-2008

Jørgensen, P., Sørensen, R., & Prestvik, O. (2013). Norske jordarter. In: Bioforsk.

Kartverket. (2022). Norgeskart, Bakgrunnskart: Enkel. Retrieved from https://norgeskart.no/

Kleivane, I. (2011). Flaumen i Sør-Noreg, juni 2011. *NVE dokument, nr. 11/2011*.

Kristensen, L. L., Jensen, O. A., Devoli, G., Rustad, B. K., Verhage, A., Viklund, M., & Larsen, J. O. (2015). Terminologi for naturfare.

Krøgli, I. K., Devoli, G., Colleuille, H., Boje, S., Sund, M., & Engen, I. K. (2018). The Norwegian forecasting and warning service for rainfall- and snowmelt-induced landslides. *Nat. Hazards Earth Syst. Sci., 18*(5), 1427-1450. doi:10.5194/nhess-18-1427-2018

Larsen, H. B. (2021). *Physically Based Modelling of Shallow Landslides with" TRIGRS": A Review of Applications and an Implementation in the Case Study of Jølster 2019, Western Norway.* (Master thesis), NTNU,

Liu, Z., Gilbert, G., Cepeda, J. M., Lysdahl, A. O. K., Piciullo, L., Hefre, H., & Lacasse, S. (2021). Modelling of shallow landslides with machine learning algorithms. *Geoscience Frontiers, 12*(1), 385-393.

Lussana, C. (2020). SeNorge observational gridded datasets. *MET report, 07/2020*.

Melchiorre, C., & Frattini, P. (2012). Modelling probability of rainfall-induced shallow landslides in a changing climate, Otta, Central Norway. *Climatic change, 113*(2), 413-436.

MET. (2022a). Seklima: Observasjoner og værstatistikk. Retrieved from https://seklima.met.no/observations/

MET. (2022b). SeNorge: Observational gridded datasets for temperature and precipitation. Retrieved from https://www.xgeo.no/

Mikoš, M., & Bezak, N. (2021). Debris Flow Modelling Using RAMMS Model in the Alpine Environment With Focus on the Model Parameters and Main Characteristics. *Frontiers in Earth Science*, 732.

Mitchell, J. K., & Soga, K. (2005). *Fundamentals of soil behavior* (Vol. 3): John Wiley & Sons New York.

NGI. (2014). *Skred: skredfare og sikringstiltak : praktiske erfaringer og teoretiske prinsipper*: Universitetsforlaget.

NGU. (2022). Berggrunn - Nasjonal bergrunnsdatabase. Retrieved from https://geo.ngu.no/kart/berggrunn_mobil/

Nordby, B.-M., Grøttum, E.-T. L., & Beyer-Olsen, A. (2013, 07.06.2013). Bil tatt av steinras på E6 - Mann (54) omkom. *VG*. Retrieved from https://www.vg.no/nyheter/innenriks/i/Ov4rA/bil-tatt-av-steinras-paa-e6-mann-54-omkom

Norem, H., & Sandersen, F. (2012). *Flom-og sørpeskred: Høringsutgave av veileder* (1893-1162). Retrieved from Oslo:

Norsk Klimaservicesenter. (2022). Nedbørsintensitet (IVF-verdier). Retrieved from https://klimaservicesenter.no/ivf?locale=nb

Norsk Skogmuseum. (n.d.). Gudbrandsdalslågen, Selsmyrene. Retrieved from http://www.flommer.no/gudbrandsdalslagen/side.cfm?ID_art=77

NVE. (2013). Jordskred og flomskred. *NVE faktaark, 2013*.

NVE. (2022). Temakart: Skredhendelser Retrieved from atlas.nve.no

Nye Veier. (2021). E6 Øyer - Otta, Planprogram for E6 Sjoa -Solhjem og kryss E6 x rv.15.

Riksrevisjonen. (2022). Riksrevisjonens undersøkelse av myndighetenes arbeid med å tilpasse infrastruktur og bebyggelse til et klima i endring. *Dokument nr. 3:6*.

Roald, L. A. (2013). *Flom i Norge*: Tom & Tom.

Roald, L. A. (2015). *Flommen på Østlandet i mai 2013*. Retrieved from

Roering, J. J., Schmidt, K. M., Stock, J. D., Dietrich, W. E., & Montgomery, D. R. (2003). Shallow landsliding, root reinforcement, and the spatial distribution of trees in the Oregon Coast Range. *Canadian Geotechnical Journal, 40*(2), 237-253.

Sandersen, F., Bakkehøi, S., Hestnes, E., & Lied, K. (1997). The influence of meteorological factors on the initiation of debris flows, rockfalls, rockslides and rockmass stability. *Publikasjon-Norges Geotekniske Institutt, 201*, 97-114.

Saulnier, G.-M., Beven, K., & Obled, C. (1997). Including spatially variable effective soil depths in TOPMODEL. *Journal of hydrology, 202*(1-4), 158-172.

Schilirò, L., Cepeda, J., Devoli, G., & Piciullo, L. (2021). Regional Analyses of Rainfall-Induced Landslide Initiation in Upper Gudbrandsdalen (South-Eastern Norway) Using TRIGRS Model. *Geosciences, 11*(1), 35.

Schmidt, K., Roering, J., Stock, J., Dietrich, W., Montgomery, D., & Schaub, T. (2001). The variability of root cohesion as an influence on shallow landslide susceptibility in the Oregon Coast Range. *Canadian Geotechnical Journal, 38*(5), 995-1024.

Sel Kommune. (2017). *Kommuneplanens arealdel 2016-2025: Konsekvensutredning og risiko- og sårbarhetsanalyse*.

Siedler, C. E. (2015). Samfunnsøkonomiske kostnader av Gudbrandsdalsflommen 2013. *NVE rapport, 93-2015*.

Skaugen, T., Astrup, M., Roald, L., & Skaugen, T. E. (2002). Scenarios of extreme precipitation of duration 1 and 5 days for Norway caused by climate change. *NVE-report A, 7*(02).

Sletten, K., & Blikra, L. H. (2007). Holocene colluvial (debris-flow and water-flow) processes in eastern Norway: stratigraphy, chronology and palaeoenvironmental implications. *Journal of Quaternary Science: Published for the Quaternary Research Association, 22*(6), 619-635.

Statens Kartverk, Geovekst, & Kommunene. (2022a). Gudbrandsdal Flom 2011. Retrieved from https://norgeibilder.no/

Statens Kartverk, Geovekst, & Kommunene. (2022b). Hedmark Nord 2009. Retrieved from https://norgeibilder.no/

Statens Kartverk, Geovekst, & Kommunene. (2022c). Nord-Gudbrandsdal 2011. Retrieved from https://norgeibilder.no/

Statens Kartverk, Geovekst, & Kommunene. (2022d). Nord.Gudbrandsdal 2020. Retrieved from https://norgeibilder.no/

Stocker, T. F., Qin, D., Plattner, G.-K., Tignor, M., Allen, S. K., Boschung, J., . . . Midgley, B. (2013). IPCC, 2013: climate change 2013: the physical science basis. Contribution of working group I to the fifth assessment report of the intergovernmental panel on climate change. In: Cambridge University Press.

SVV. (2012). *Rapport om skadeflom i pinsehelga 2011*. Retrieved from Lillehammer, R.vegkt:

Taylor, D. W. (1948). *Fundamentals of soil mechanics* (Vol. 66): LWW.

Terzaghi, K. v. (1936). *The shearing resistance of saturated soils and the angle between the planes of shear.* Paper presented at the First international conference on soil Mechanics, 1936.

Varnes, D. J. (1978). Slope movement types and processes. *Special report, 176*, 11-33.

Walberg, N. A. K., & Devoli, G. (2014). Regional varsling av jordskredfare. *NVE Rapport 44/2014*.

Yao, K. (2012). *Human activity as a cause for landslides in Norway: Case study of two man-made debris flows in Otta, Central Southern Norway.* (Master thesis), University of Oslo, Department of Geosciences.

Zhou, W., Qiu, H., Wang, L., Pei, Y., Tang, B., Ma, S., . . . Cao, M. (2022). Combining rainfall-induced shallow landslides and subsequent debris flows for hazard chain prediction. *CATENA, 213*, 106199.

Østgren, L. M. E. M. (2017). *Mitigation of Uncertainties in Rainfall-Induced Landslide Prediction Models in a Changing Climate-Kvam Case Study.* (Master thesis), NTNU,

Aall, C., Aamaas, B., Aaheim, H. A., Alnes, K., Oort, B. v., Dannevig, H., & Hønsi, T. (2018). Oppdatering av kunnskap om konsekvenser av klimaendringer i Norge. *CICERO Report*.

Aarrestad, P. A., Bjerke, J. W., Follestad, A., Jepsen, J. U., Nybø, S., Rusch, G., & Schartau, A. K. (2015). Naturtyper i klimatilpasningsarbeid. Effekter av klimaendringer og klimatilpasningsarbeid på naturmangfold og økosystemtjenester.

Appendix

A) Photo locations in the Gudbrandsdalen Area

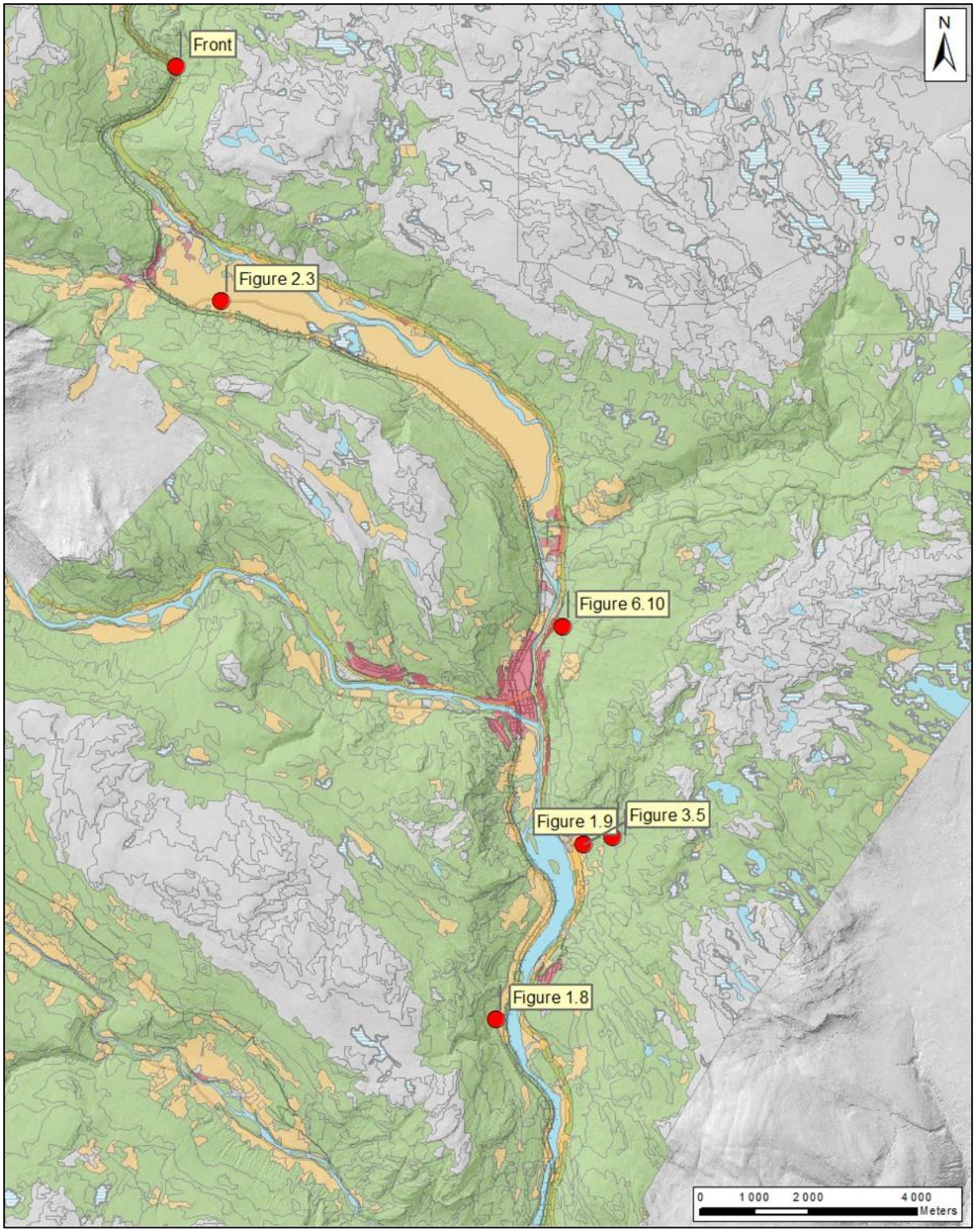

B) Quaternary deposits in the Rosten case study site.

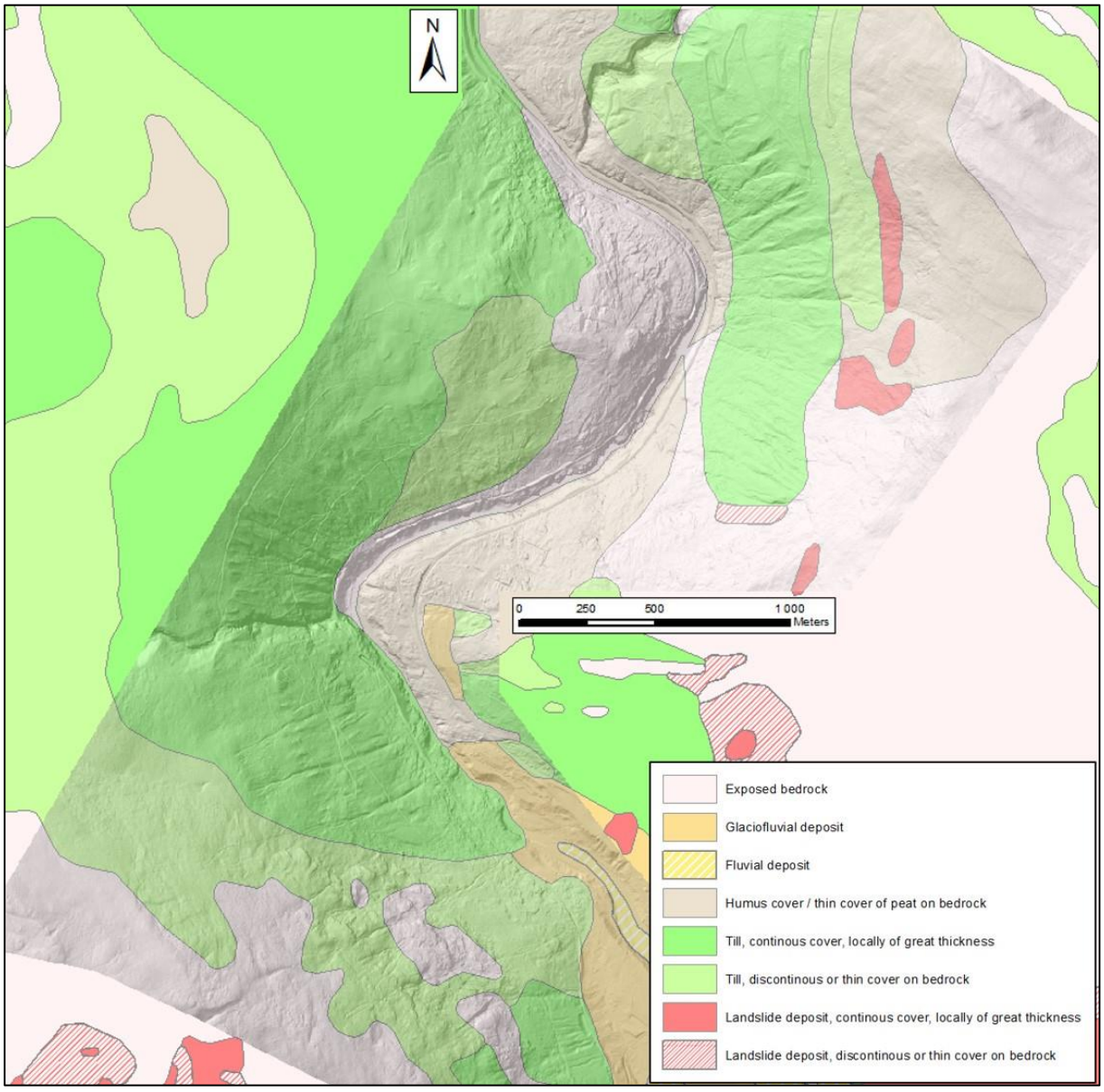

C) Rosten area model input

C1 – Rosten DEM (visualized with hill shade)

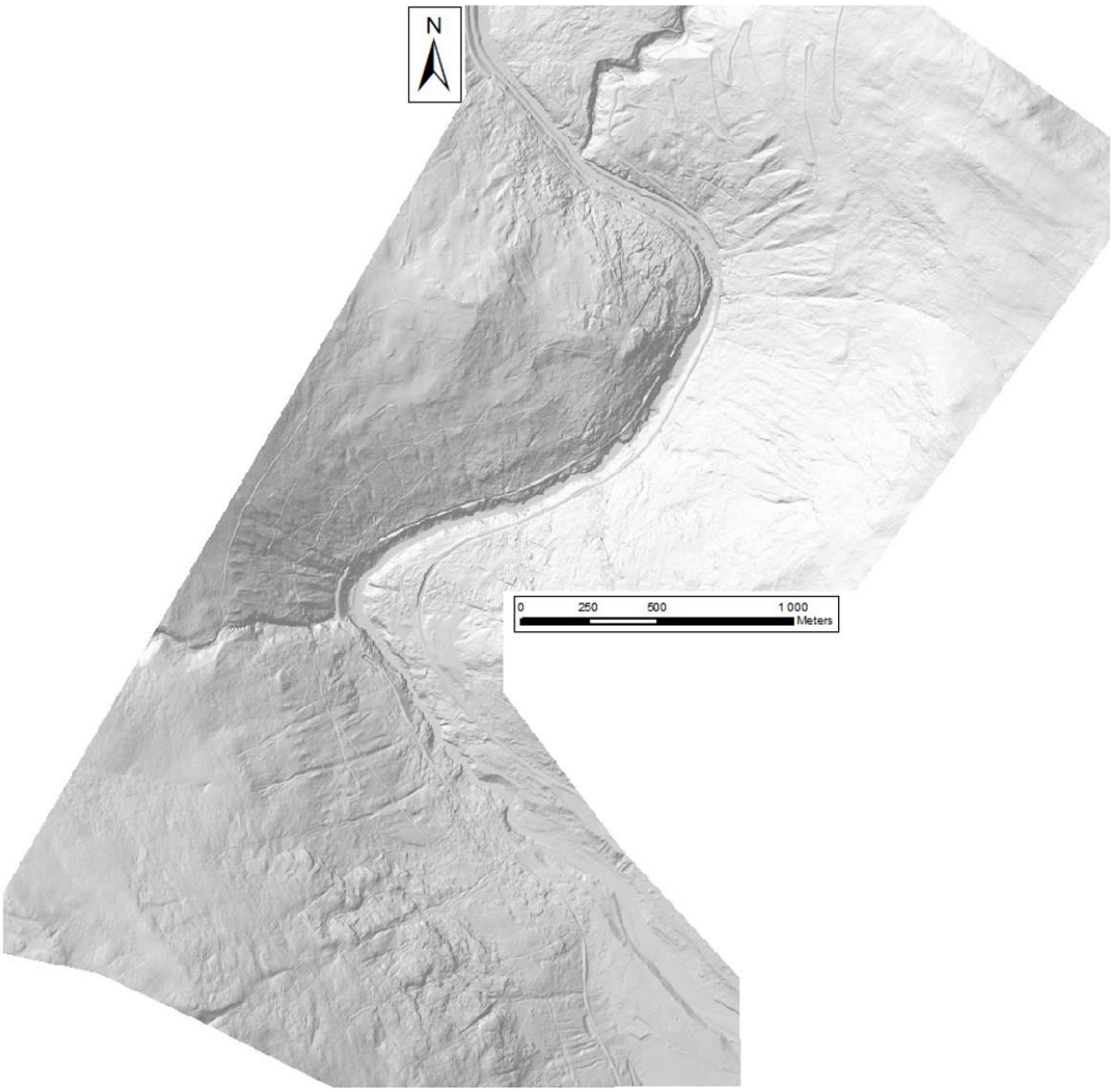

C2 – Rosten slope inclination map

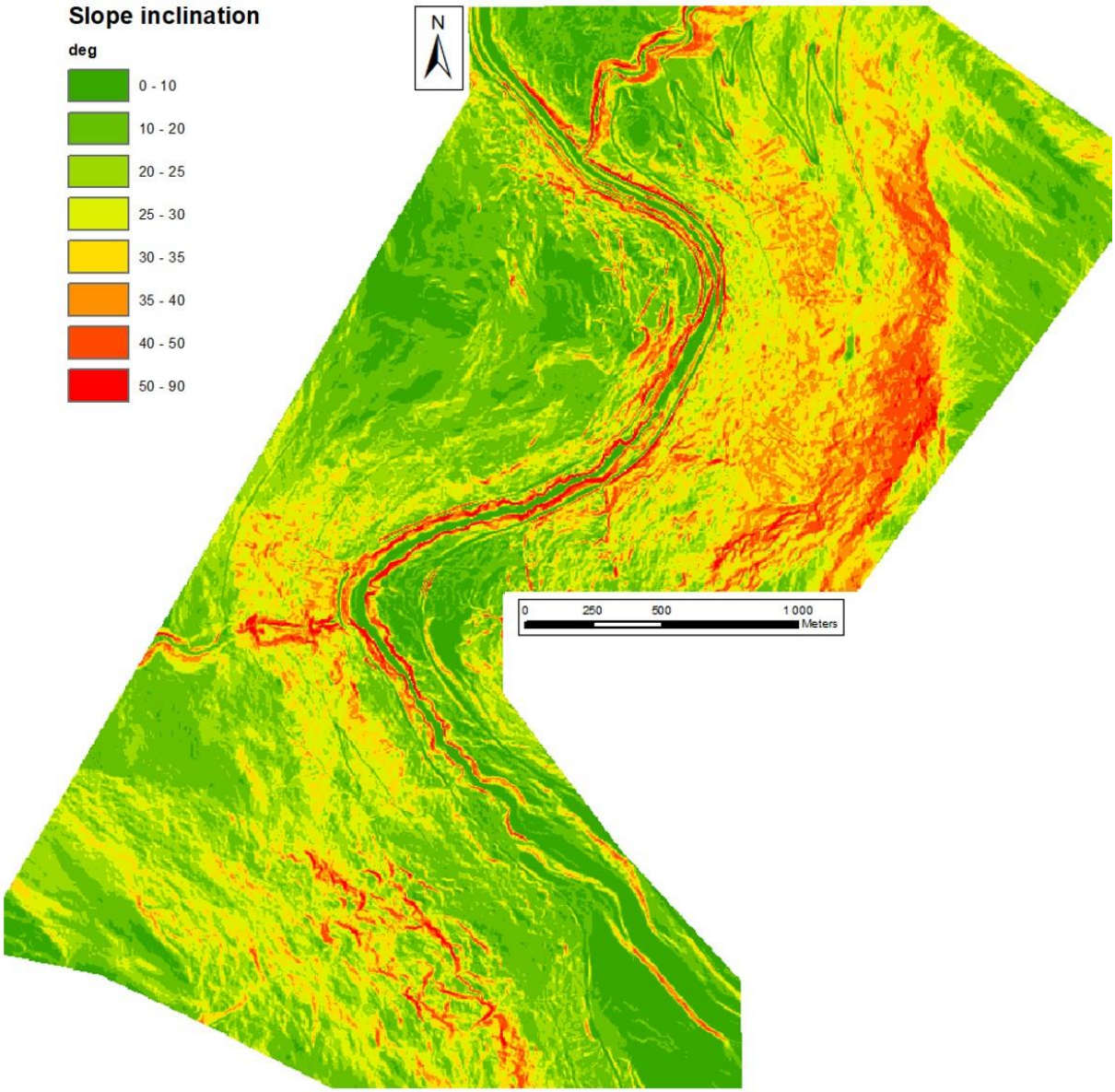

C3 – Rosten flow direction map

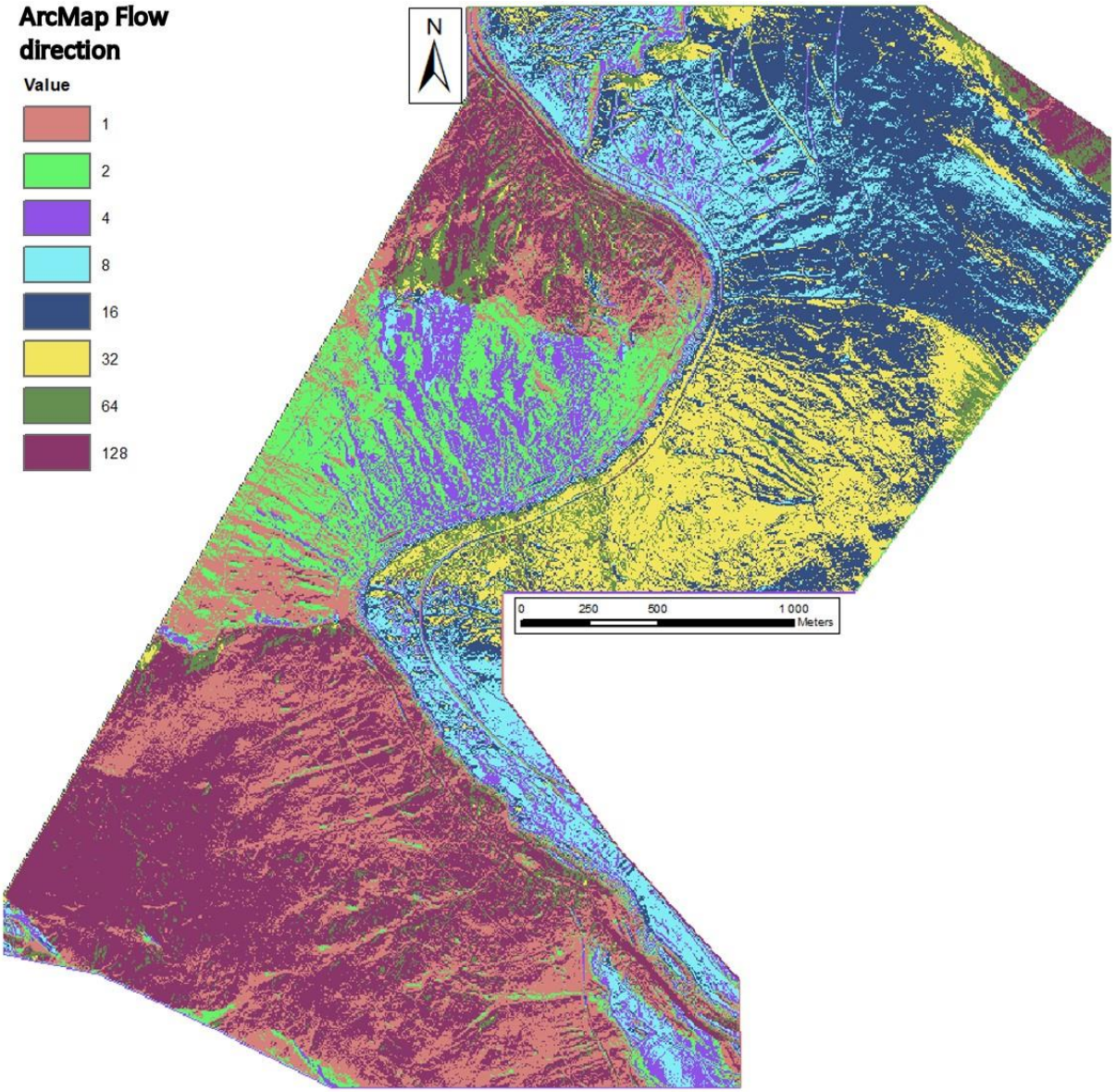

C4 – Rosten soil thickness map

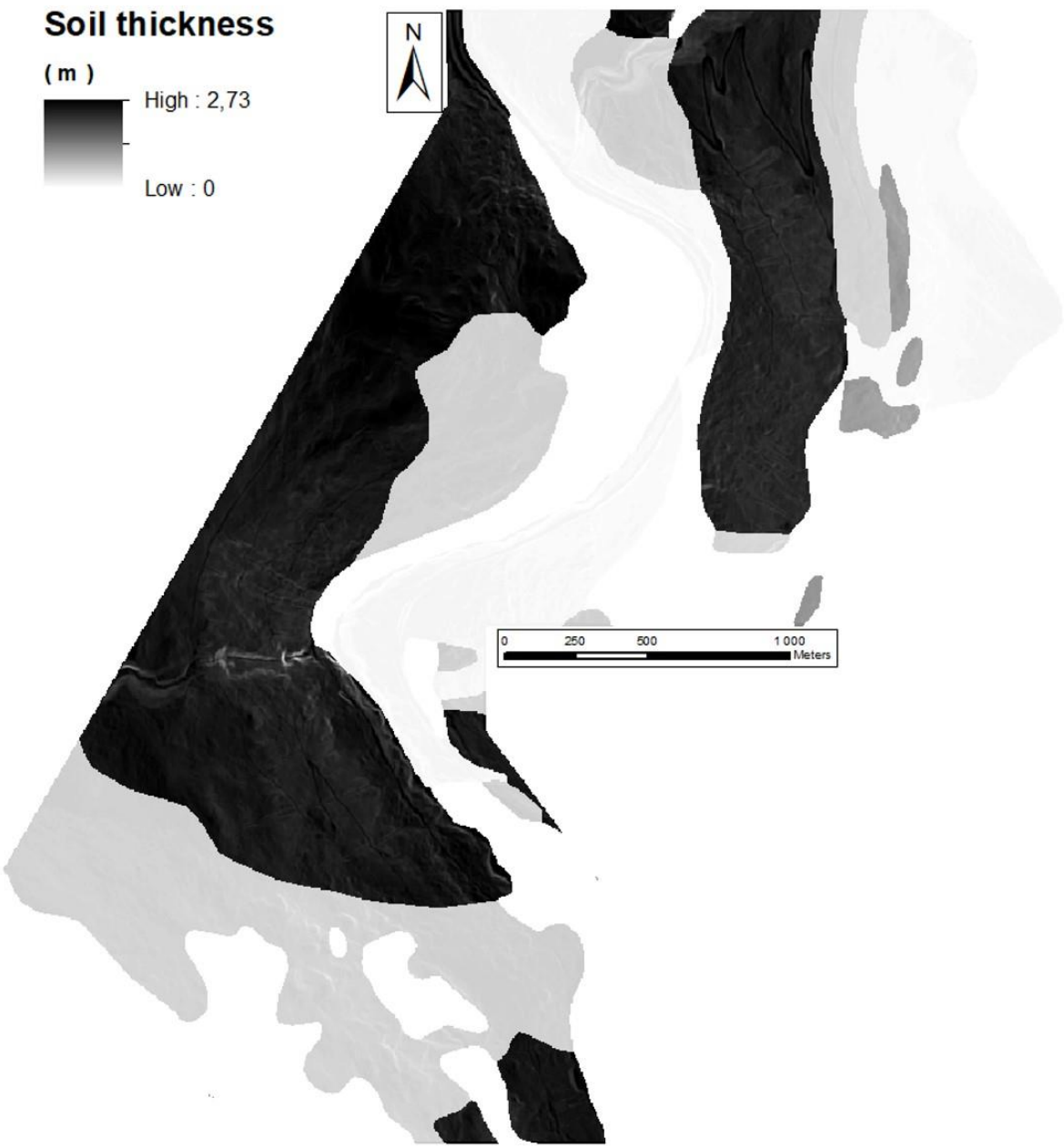

D) Python script

Script for estimation of soil thickness.

```
Created on Tue Jan  4 10:53:39 2022

@author: Øystein

import numpy as np

#Load files excluding header
input = np.loadtxt('slope_inclination.txt', skiprows=6)
Slopefactor = np.loadtxt('Soiltypefactor.txt', skiprows=6)

#Minimum and maximum observed thickness
Hmin = 0.5
Hmax = 2.87

#Minimum and maximum observed slope inclination
SlopeMin = 0.5
SlopeMax = np.max(input)


#Equation ?? (Schilirò et al. (2022))
Thickness_inclination = (Hmax* ( 1 - (((np.tan(input * np.pi / 180) -
(np.tan(SlopeMin * np.pi / 180)))/((np.tan(SlopeMax * np.pi / 180)) -
(np.tan(SlopeMin * np.pi / 180)))) * (1 - (Hmin/Hmax)))))

#Adjustment to soil type definitions
Thickness_soiltype = Thickness_inclination * Slopefactor

#Adjust nodata values back to -9999
Soil_thickness = np.where(Thickness_soiltype<-0.01, -9999, Thickness_soiltype)

#Save thickness map
np.savetxt("Soil_thickness_map.txt",Soil_thickness,delimiter=" ", fmt='%1.2f')
```

E) TRIGRS Slope stability maps

E1 – 24h precipitation event of 20-year recurrence interval, current climate

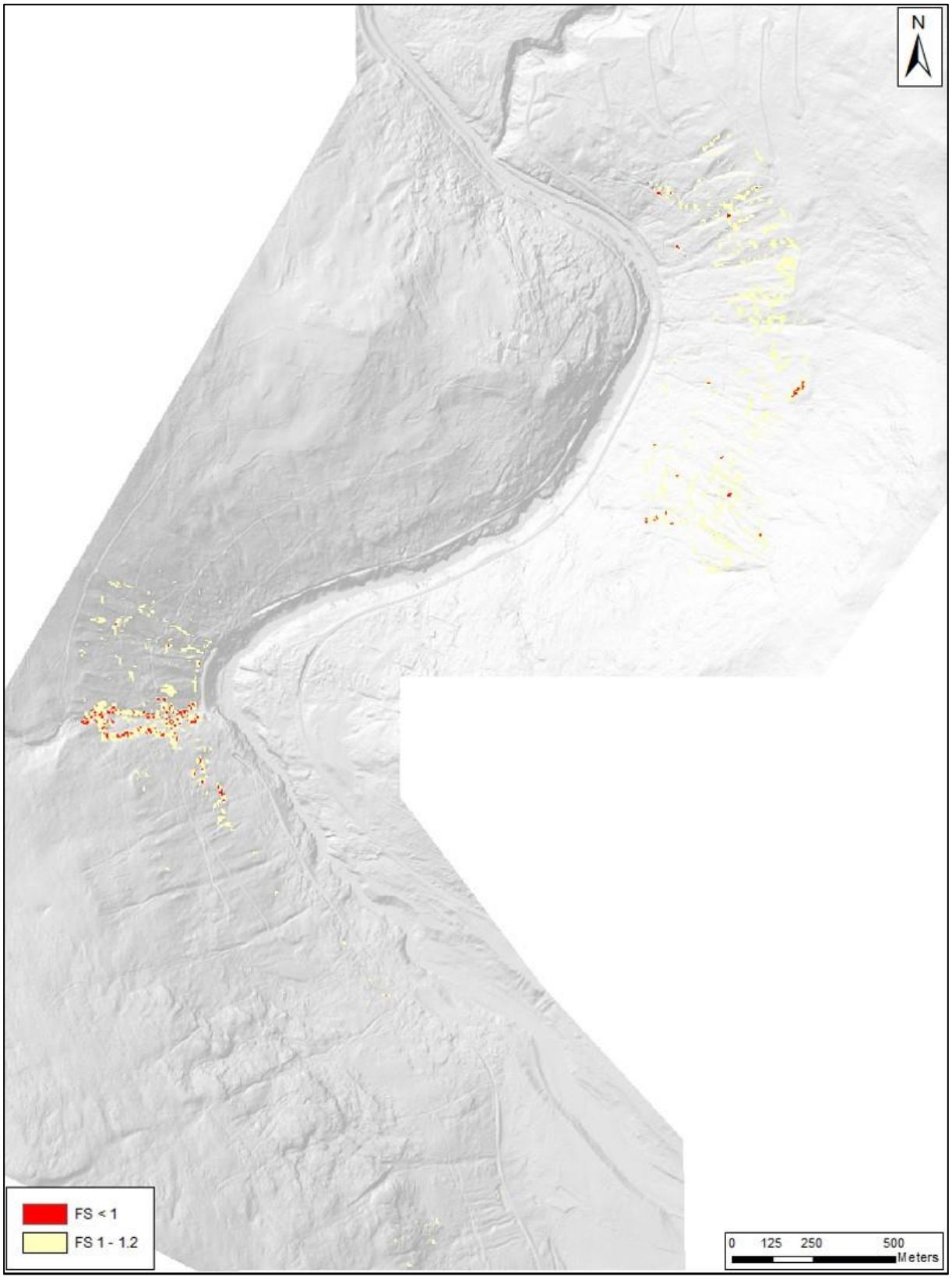

E2 – 24h precipitation event of 20-year recurrence interval, future climate

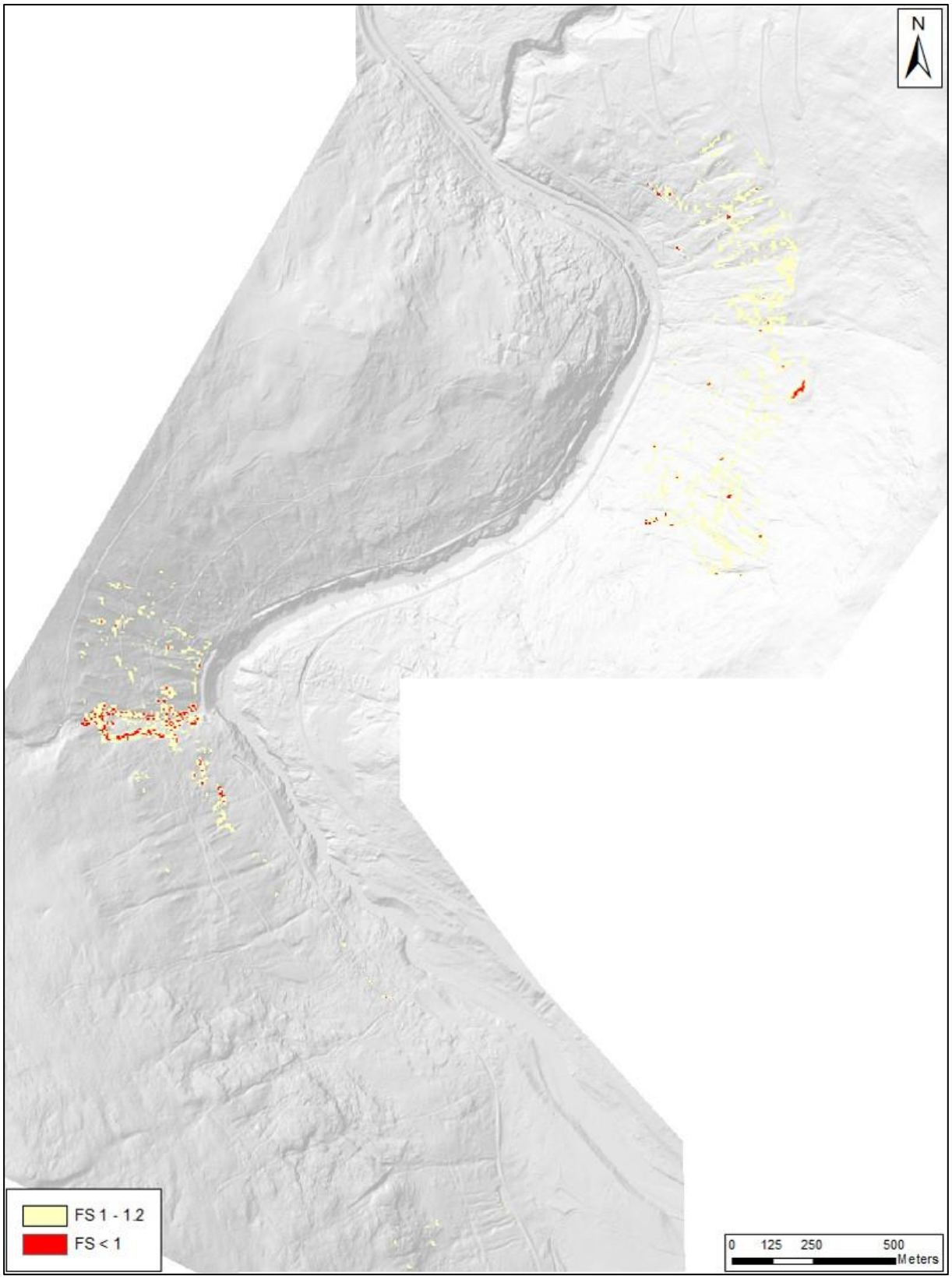

E3 – 24h precipitation event of 50-year recurrence interval, current climate

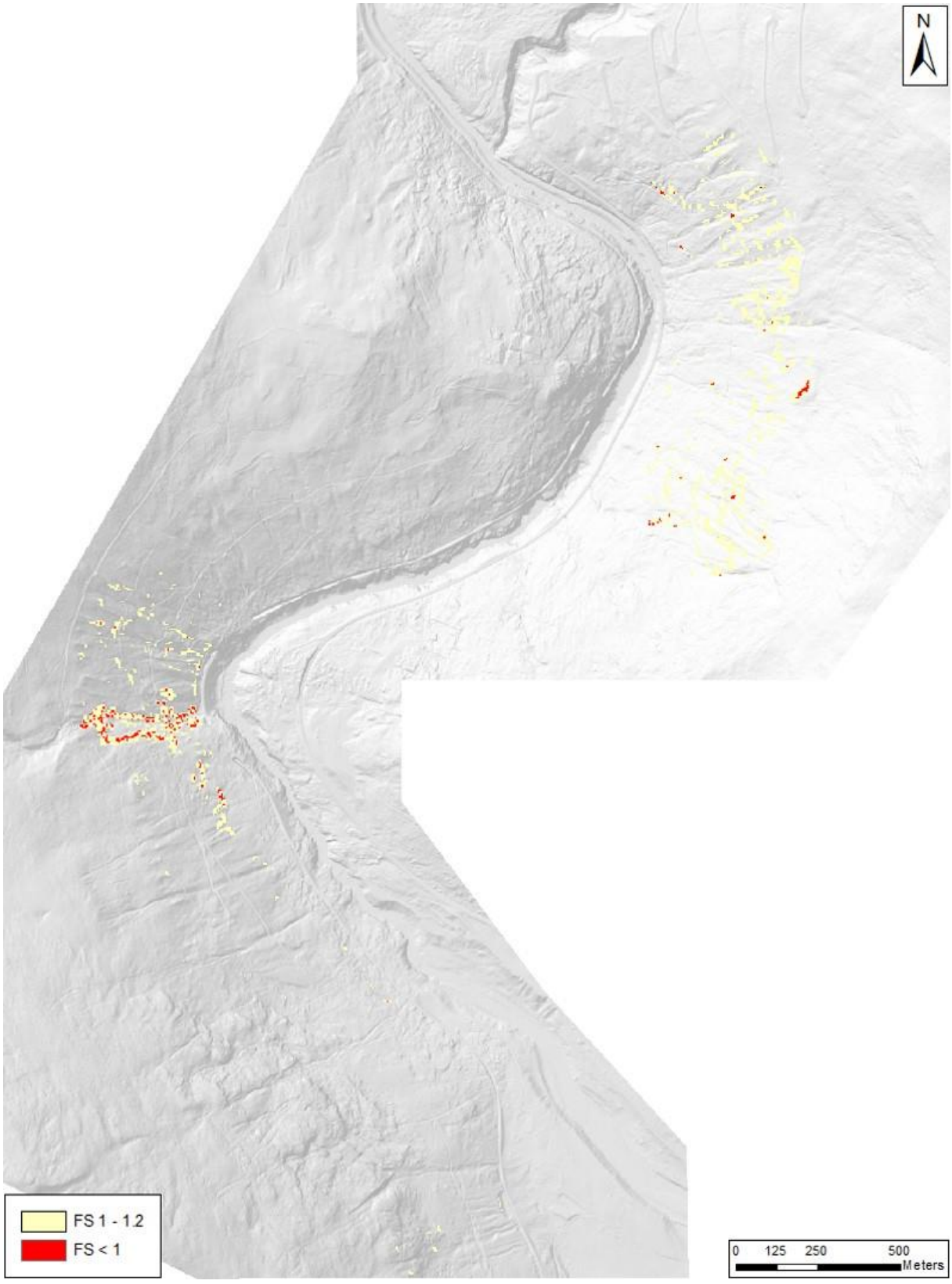

E4 – 24h precipitation event of 50-year recurrence interval, future climate

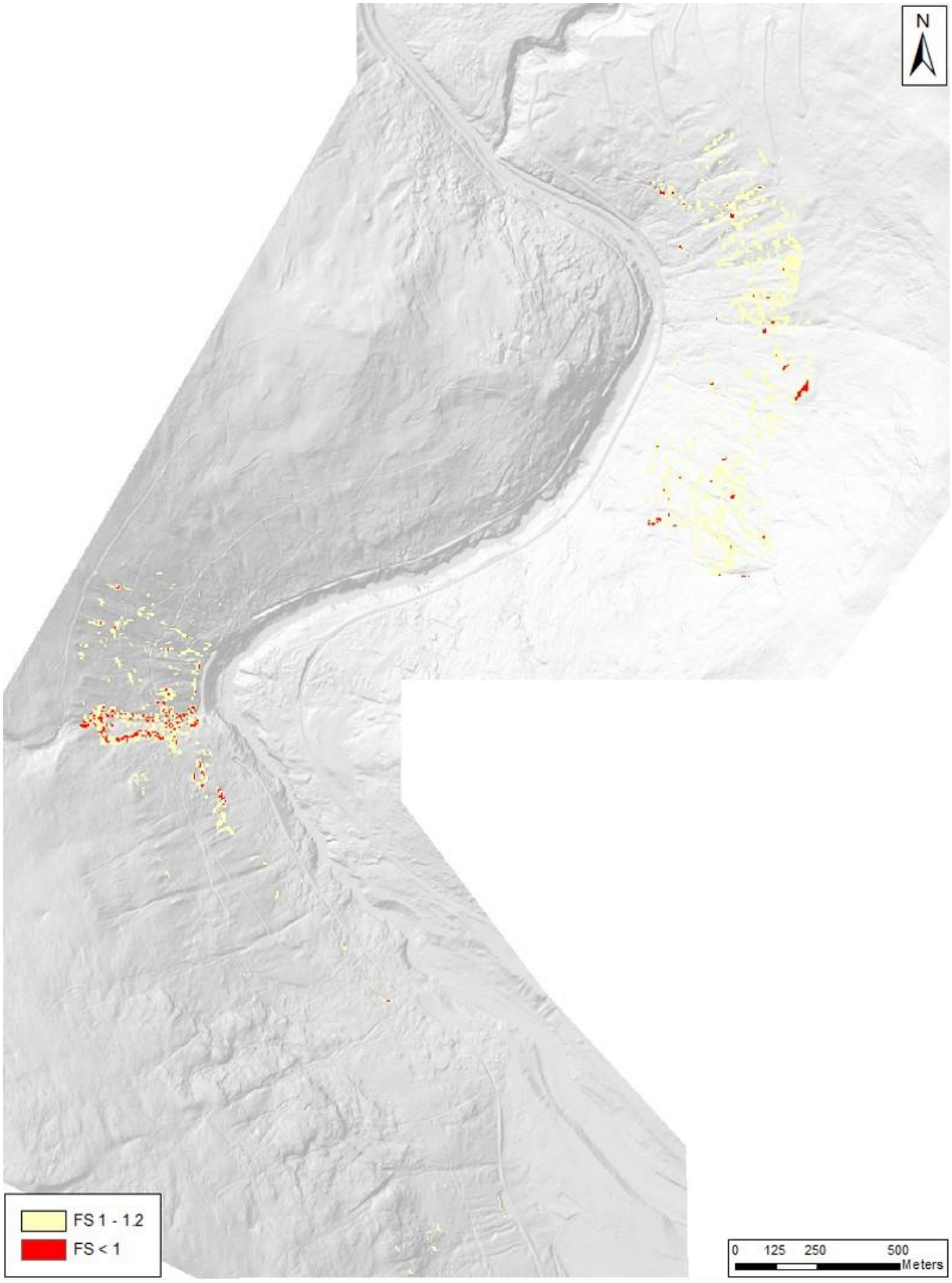

E5 – 24h precipitation event of 100-year recurrence interval, current climate

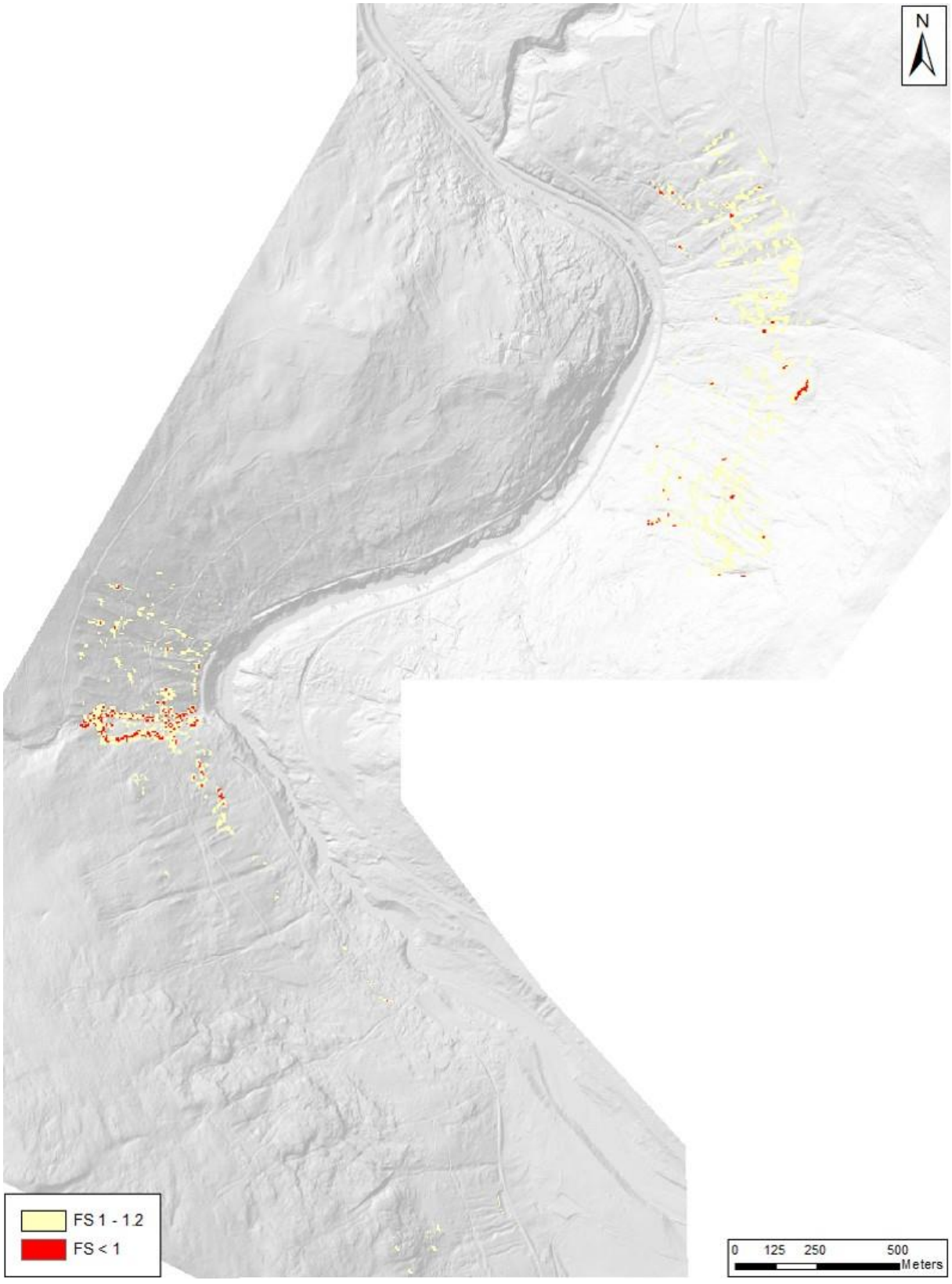

E6 – 24h precipitation event of 100-year recurrence interval, future climate

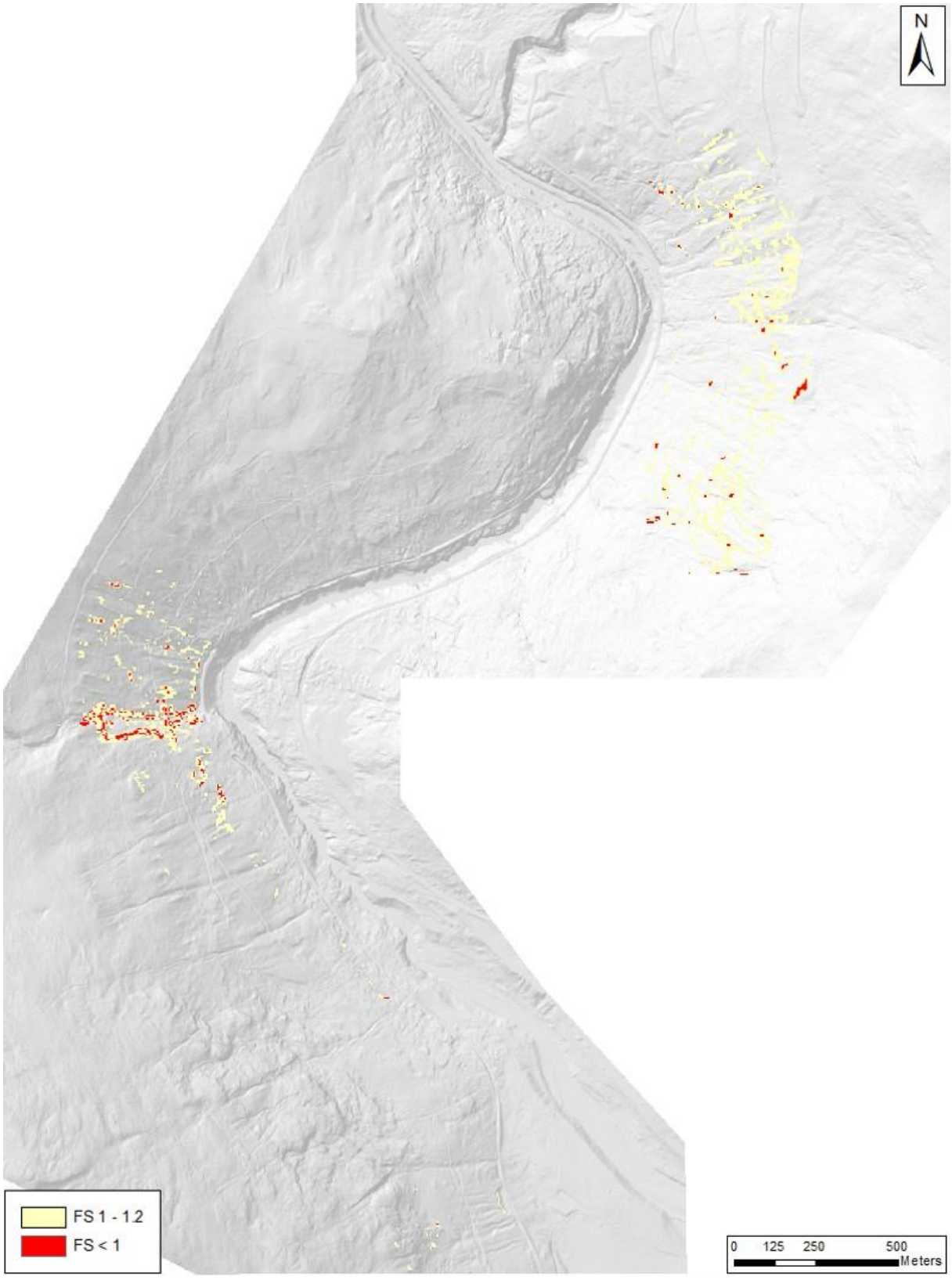

E7 – 24h precipitation event of 200-year recurrence interval, current climate

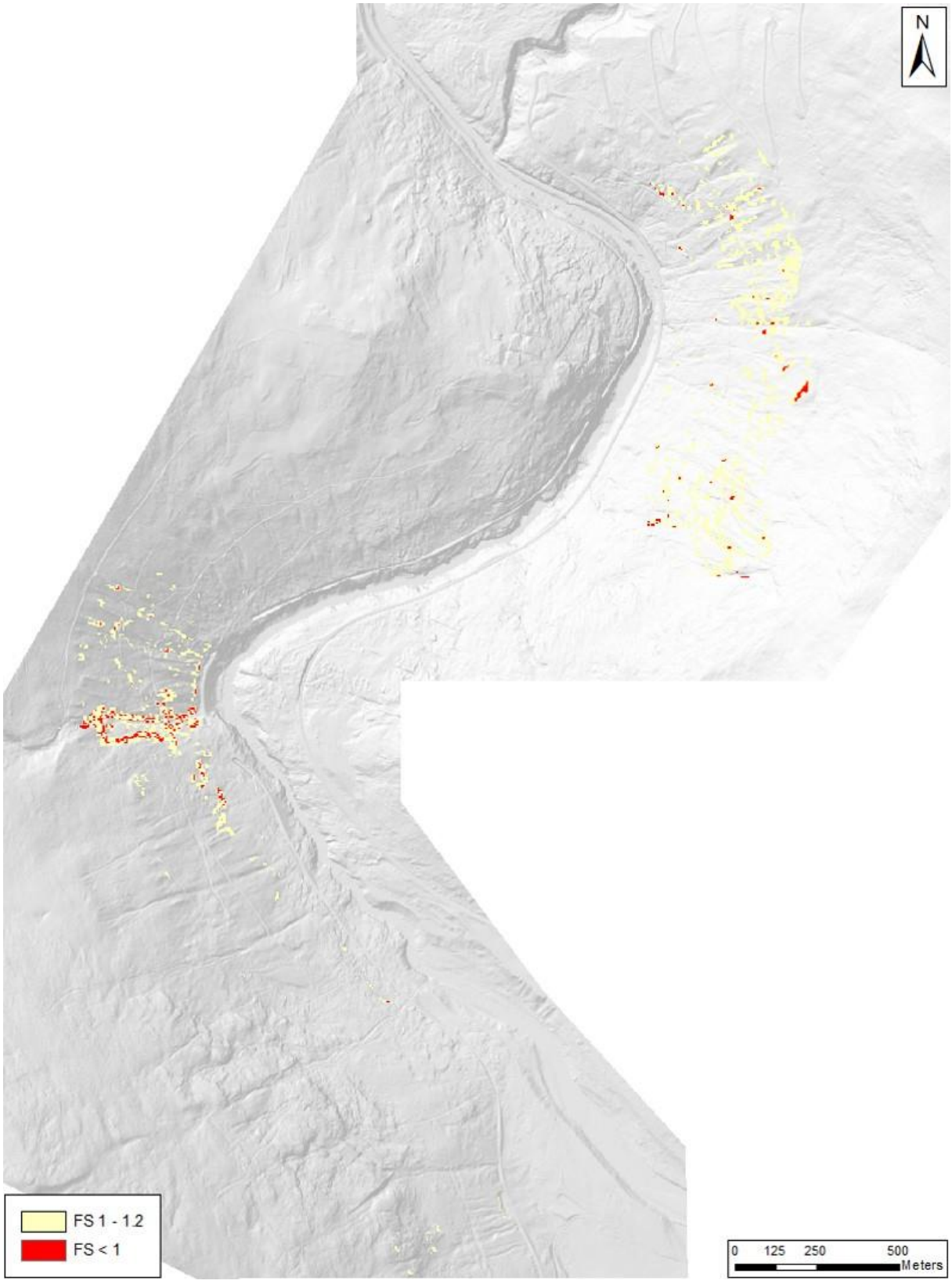

E8 – 24h precipitation event of 200-year recurrence interval, future climate

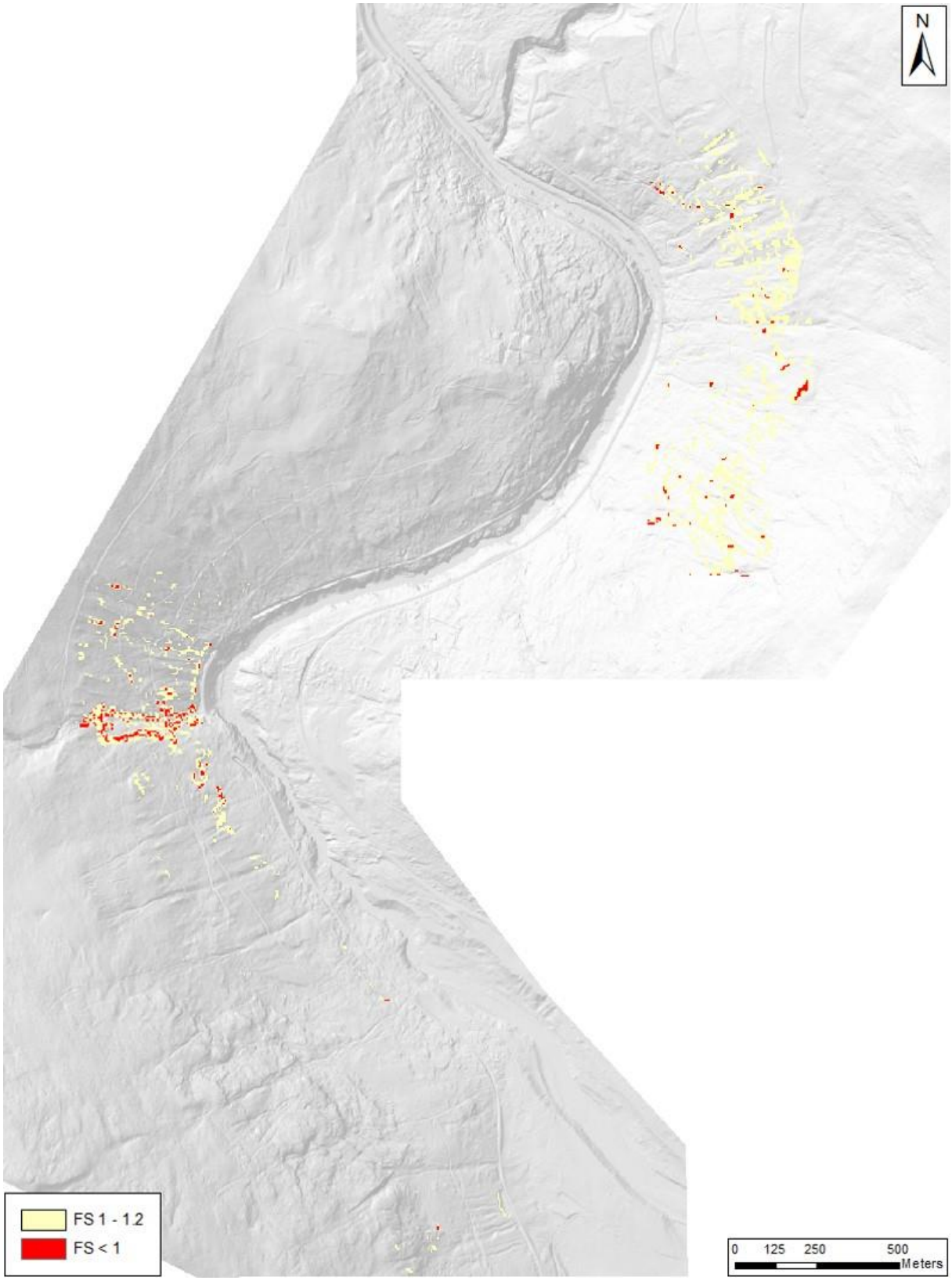

F) Link to digital maps and appendices:

https://onedrive.live.com/?id=37E0A41B9A040EE3%2113830&cid=37E0A41B9A040EE3